

# IPC/JEDEC-9301

2018 - December

## Numerical Analysis Guidelines for Microelectronics Packaging Design and Reliability

*An international standard developed by IPC*

*Association Connecting Electronics Industries*



---

## The Principles of Standardization

In May 1995 the IPC's Technical Activities Executive Committee (TAEC) adopted Principles of Standardization as a guiding principle of IPC's standardization efforts.

### Standards Should:

- Show relationship to Design for Manufacturability (DFM) and Design for the Environment (DFE)
- Minimize time to market
- Contain simple (simplified) language
- Just include spec information
- Focus on end product performance
- Include a feedback system on use and problems for future improvement

### Standards Should Not:

- Inhibit innovation
- Increase time-to-market
- Keep people out
- Increase cycle time
- Tell you how to make something
- Contain anything that cannot be defended with data

## Notice

IPC Standards and Publications are designed to serve the public interest through eliminating misunderstandings between manufacturers and purchasers, facilitating interchangeability and improvement of products, and assisting the purchaser in selecting and obtaining with minimum delay the proper product for his particular need. Existence of such Standards and Publications shall not in any respect preclude any member or nonmember of IPC from manufacturing or selling products not conforming to such Standards and Publication, nor shall the existence of such Standards and Publications preclude their voluntary use by those other than IPC members, whether the standard is to be used either domestically or internationally.

Recommended Standards and Publications are adopted by IPC without regard to whether their adoption may involve patents on articles, materials, or processes. By such action, IPC does not assume any liability to any patent owner, nor do they assume any obligation whatever to parties adopting the Recommended Standard or Publication. Users are also wholly responsible for protecting themselves against all claims of liabilities for patent infringement.

## IPC Position Statement on Specification Revision Change

It is the position of IPC's Technical Activities Executive Committee that the use and implementation of IPC publications is voluntary and is part of a relationship entered into by customer and supplier. When an IPC publication is updated and a new revision is published, it is the opinion of the TAEC that the use of the new revision as part of an existing relationship is not automatic unless required by the contract. The TAEC recommends the use of the latest revision. Adopted October 6, 1998

## Why is there a charge for this document?

Your purchase of this document contributes to the ongoing development of new and updated industry standards and publications. Standards allow manufacturers, customers, and suppliers to understand one another better. Standards allow manufacturers greater efficiencies when they can set up their processes to meet industry standards, allowing them to offer their customers lower costs.

IPC spends hundreds of thousands of dollars annually to support IPC's volunteers in the standards and publications development process. There are many rounds of drafts sent out for review and the committees spend hundreds of hours in review and development. IPC's staff attends and participates in committee activities, typesets and circulates document drafts, and follows all necessary procedures to qualify for ANSI approval.

IPC's membership dues have been kept low to allow as many companies as possible to participate. Therefore, the standards and publications revenue is necessary to complement dues revenue. The price schedule offers a 50% discount to IPC members. If your company buys IPC standards and publications, why not take advantage of this and the many other benefits of IPC membership as well? For more information on membership in IPC, please visit [www.ipc.org](http://www.ipc.org) or call 847/597-2809.

Thank you for your continued support.



**IPC/JEDEC-9301**



# **Numerical Analysis Guidelines for Microelectronics Packaging Design and Reliability**

Developed by the JEDEC Reliability Test Methods for Packaged Devices Committee (JC-14.1) and the SMT Attachment Reliability Test Methods Task Group (6-10d) of the Product Reliability Committee (6-10) of IPC

Users of this publication are encouraged to participate in the development of future revisions.

Contact:

IPC  
3000 Lakeside Drive, Suite 105N  
Bannockburn, Illinois  
60015-1249  
Tel 847 615.7100  
Fax 847 615.7105

This Page Intentionally Left Blank

## Acknowledgment

Members of the JEDEC Reliability Test Methods for Packaged Devices Committee (JC-14.1) and the SMT Attachment Reliability Test Methods Task Group (6-10d) of the IPC Product Reliability Committee (6-10) have worked together to develop this document. We would like to thank them for their dedication to this effort. Any document involving a complex technology draws material from a vast number of sources. While the principal members of the SMT Attachment Reliability Test Methods Task Group are shown below, it is not possible to include all of those who assisted in the evolution of this standard. To each of them, the members of JEDEC and IPC extend their gratitude.

<b>Product Reliability Committee</b>	<b>SMT Attachment Reliability Test Methods Task Group</b>	<b>Technical Liaison of the IPC Board of Directors</b>
Chair James Monarchio TTM Technologies	Chair Reza Ghaffarian Jet Propulsion Laboratory	Bob Neves Microtek Laboratories
Vice Chair Vasu Vasudevan Dell Inc.	Vice Chair Vasu Vasudevan Dell Inc.	
<b>SMT Attachment Reliability Test Methods Task Group</b>		
Mudasir Ahmad, Cisco Systems Inc	Reza Ghaffarian, Jet Propulsion Laboratory	Clarence Nichols, Gables Engineering, Inc.
Aileen Allen, Hewlett-Packard Inc.	Cynthia A. Gomez, Continental Temic SA de CV	David Oris, Gables Engineering, Inc
Dudi Amir, Intel Corporation	Allen Green, Acoustic Technology Group	Chandradip Patel, Schlumberger Well Services
Martin K. Anselm, Rochester Institute of Technology	Bill Hargin, Nan Ya Plastics Corporation	Jagadeesh Radhakrishnan, Intel Corporation
Michael Azarian, University of Maryland	Kayleen Helms, Intel Corporation	Gnyaneshwar Ramakrishna, Cisco Systems Inc.
Elizabeth Elias Benedetto, Hewlett-Packard Inc.	Gaston Hidalgo, Toyota Motor North America	Edda Rivera, Gables Engineering, Inc.
Nicole Butel, Broadcom Limited	Ife Hsu, Intel Corporation	Jose A. Sanchez, Gables Engineering, Inc.
William P. Cardinal, UTC Aerospace Systems	Christopher Hunt, Pireta	Martin Scionti, Raytheon Missile Systems
Beverley Christian, HDP User Group	Jeffrey ChangBing Lee, iST Integrated Service Technology	Jose Ma Servin-Olivares, Continental Temic SA de CV
Jean-Paul Clech, EPSI	Anna Lifton, Alpha Assembly Solutions	Russell S. Shepherd, NTS Anaheim
Gino Cochella, Northrop Grumman Aerospace Systems	Rene R. Martinez, Northrop Grumman Aerospace Systems	Julie Silk, Keysight Technologies
Richard J. Coyle, Nokia	Daniel McCormick, Naval Surface Warfare Center	Bhanu Sood, NASA Goddard Space Flight Center
William C. Dieffenbacher, BAE Systems	Steve Minich, Amphenol InterCon Systems	Jorge Suarez, Gables Engineering, Inc.
Harold O. Ellison, Quantum Corporation	Jim Mulvey, Lockheed Martin Corporation	Taylor J. Swanson, Rochester Institute of Technology
Gerd Fischer, NASA Goddard Space Flight Center	David R. Nelson, Raytheon Company	John Paul Thompson, FCI USA, Inc.
Dennis D. Fritz, SAIC	Keith G. Newman, AMD	
Enrico Galbiati, SEM Communication & GESTLABS Srl		
Phil Geng, Intel Corporation		

Kristen K. Troxel, Hewlett-Packard  
Inc.  
Vasu S. Vasudevan, Dell Inc.

Milena Vujosevic, Intel Corporation  
Michael Wolverton, Raytheon  
Systems Company

Fonda B. Wu, Raytheon Company  
Andy Zhang, Texas Instruments

---

**SPECIAL ACKNOWLEDGMENT**

JC-14.1 JEDEC Reliability Test Methods for Packaged Devices Committee

Ife Hsu, Intel Corporation

Mudasir Ahmad, Cisco Systems Inc

# Table of Contents

<b>1 SCOPE</b> .....	1	11.2.2 Stresses .....	14
1.1 Introduction .....	1	11.3 Volume Averaging .....	14
1.2 Purpose .....	1	11.4 Temperature Dependent Results .....	14
<b>2 APPLICABLE DOCUMENTS</b> .....	4	11.5 Correlation with Experimental Data .....	14
2.1 IPC .....	4	11.5.1 Nomenclature .....	14
2.2 ASTM .....	4	11.5.2 Experimental Statistical Analysis .....	15
<b>3 TERMS AND DEFINITIONS</b> .....	4	11.5.3 Comparison of Results .....	15
<b>4 RESULTS REPORTING</b> .....	5	<b>12 REFERENCES</b> .....	16
<b>5 BASIC ANALYSIS INFORMATION</b> .....	6	<b>13 APPENDICES</b> .....	17
5.1 Analysis Type .....	6	<b>APPENDIX A Material Property Modeling</b> .....	18
5.2 Physics Type .....	6	<b>APPENDIX B DMA/TMA Fitting Algorithms</b> .....	33
5.3 Software .....	7	<b>APPENDIX C Experimental Benchmarking Model Case Study (Thermomechanical Board Level Joint Reliability)</b> .....	38
5.3.1 Software Version .....	7	<b>APPENDIX D Warpage</b> .....	50
5.4 Analysis Files and Scripts .....	7	<b>APPENDIX E Experimental Benchmarking Model Case Study (Transient Bend Testing)</b> .....	52
<b>6 BASIC MODEL INFORMATION</b> .....	8		
6.1 Boundary Conditions .....	8		
6.2 Model Stackup Schematics .....	8		
6.3 Boundary Condition Schematics .....	8		
<b>7 MATERIAL PROPERTY INFORMATION</b> .....	10		
7.1 Material Properties .....	10		
7.2 Reference Temperature .....	10		
7.3 Temperature Dependent Properties .....	10		
<b>8 MESH INFORMATION</b> .....	10		
8.1 Mesh Selection and Information .....	10		
8.2 Mapped or Tetrahedral Mesh .....	10		
8.3 Dissimilar Meshes .....	11		
8.4 Mesh Sensitivity Analysis .....	11		
<b>9 LOADING INFORMATION</b> .....	11		
9.1 Ramped vs. Stepped Loading .....	11		
<b>10 SOLUTION INFORMATION</b> .....	12		
10.1 Operating System .....	12		
10.2 High Performance Computing (HPC) .....	12		
10.3 Hardware .....	12		
10.4 Solution Algorithms and Settings .....	13		
10.4.1 Time Steps .....	13		
10.4.2 Solution Time .....	13		
<b>11 POST PROCESSING</b> .....	13		
11.1 Post Processing .....	13		
11.2 Results Parameters .....	13		
11.2.1 Fatigue .....	13		
		<b>Figures</b>	
		Figure 1-1 Building Blocks of a Typical Finite Element Analysis Problem .....	2
		Figure 1-2 Expected Modular Structure of Numerical Analysis Reliability Guideline Documents .....	3
		Figure 6-1a Examples of Model Schematics .....	8
		Figure 6-1b Examples of Model Schematics .....	8
		Figure 6-1c Examples of Model Schematics .....	8
		Figure 6-2 Quarter Symmetric Model .....	8
		Figure 6-3 Symmetry Boundary Conditions Added .....	9
		Figure 6-4 Zoom in View of Symmetry Boundary Conditions .....	9
		Figure 6-5 Displacement Boundary Conditions to Constrain All Rigid Body Displacement .....	9
		Figure 8-1 Example of Multi-Point Constraint to "Tie" Dissimilar Mesh Regions .....	11
		Figure 8-2 Example of Mesh Sensitivity Analysis .....	11
		Figure 10-1 Computational Time vs. Number of Cores Used (PBGA 680 Solder Joint Model) .....	12
		Figure 10-2 Octant PBGA680 Solder Joint Reliability Model .....	12
		Figure 10-3 Example of Time Step Too Big to Capture Fluctuation in Loading History .....	13
		Figure A2-1a Isotropic and Kinematic Hardening Rules ...	21
		Figure A2-1b Isotropic and Kinematic Hardening Rules ...	21
		Figure A2-1c Isotropic and Kinematic Hardening Rules ...	21

Figure A2-2a	Examples of One-Dimensional Stress Strain Relationships .....	21	Figure A4-9b	Measurement and the Simulation of the Deflection Over Temperature of a Bi-material Beam Consisting of Molding Compound and Silicon. The Linear-elastic (LE) Model Clearly Overestimates the Deflection Whereas the LVE Model can Reproduce the Deflection Correctly .....	28
Figure A2-2b	Examples of One-Dimensional Stress Strain Relationships .....	21	Figure A4-10a	Schematic Representation of the Tests Until Failure: a) Tensile Test Until Failure, b) Tensile Test Until Failure with Relaxation Segments .....	29
Figure A2-2c	Examples of One-Dimensional Stress Strain Relationships .....	21	Figure 4-10b	Schematic Representation of the Tests Until Failure: a) Tensile Test Until Failure, b) Tensile Test Until Failure with Relaxation Segments .....	29
Figure A2-2d	Examples of One-Dimensional Stress Strain Relationships .....	21	Figure A4-11a	Results of the Tensile Tests Until Failure at Different Temperatures .....	30
Figure A3-1a	Characteristic Measurements of the Storage Modulus and the Thermal Expansion of a Thermosetting Polymer Over Temperature. ....	22	Figure A4-11b	Stress Relaxation of the Investigated Molding Compound .....	30
Figure A3-1b	Characteristic Measurements of the Storage Modulus and the Thermal Expansion of a Thermosetting Polymer Over Temperature. ....	22	Figure A4-12	Representation of the Bergstrom-Boyce Model .....	30
Figure A3-2a	Extraction of $T_g$ by Tangents from TMA Measurement. ....	23	Figure A4-13	Results of Experiment and Simulation of the Tensile Test Until Failure at 125 °C and the Load Rate of 1.0 mm/min .....	30
Figure A3-2b	Extraction of $T_g$ by Tangents from TMA Measurement. ....	23	Figure A4-14	Scheme of Curing Shrinkage During Polymerization Process of Molding Compound [7] .....	31
Figure A4-1a	Tri-linear (left) and Bi-linear (right) Interpolating Functions for Fitting of DMA/TMA Data Respectively .....	25	Figure A4-15	Constitutive Law for an Orthotropic Material .....	32
Figure A4-1b	Tri-linear (left) and Bi-linear (right) Interpolating Functions for Fitting of DMA/TMA Data Respectively .....	25	Figure C1-1a	Four Packages Selected for Case Study ....	38
Figure A4-2a	Example of Best Fit for DMA (left) and TMA (right) Data .....	25	Figure C1-1b	Four Packages Selected for Case Study ....	38
Figure A4-2b	Example of Best Fit for DMA (left) and TMA (right) Data .....	25	Figure C1-1c	Four Packages Selected for Case Study ....	38
Figure A4-3	Thermal Expansion Measurement of a Thermosetting Polymer and the Extraction of Instantaneous CTEs from Measured Thermal Strain Data .....	26	Figure C1-1d	Four Packages Selected for Case Study ....	38
Figure A4-4	Extracted Instantaneous CTE $\alpha_{th,inst}$ Over Temperature. The instantaneous CTE $\alpha_{th,inst}$ Changes at the Glass Temperature $T_g$ .....	26	Figure C1-2	Thermal Cycling Test Profiles .....	39
Figure A4-5	Extraction of the Secant CTE $\alpha_{th,secant}$ from Measured Thermal Strain Data for the Reference Temperature of 25 °C .....	26	Figure C1-3a	Different Model Type Schematics .....	40
Figure A4-6	Extracted Secant CTE $\alpha_{th,secant}$ Over Temperature for a Reference Temperature of 25 °C .....	27	Figure C1-3b	Different Model Type Schematics .....	40
Figure A4-7	Overview Viscoelastic Modeling .....	27	Figure C1-4a	Strip Model .....	41
Figure A4-8	Illustration of the Linear-Viscoelastic Material Modeling Approach Using the Generalized Maxwell Model Consisting of Several Spring-Damper Elements .....	28	Figure C1-4b	Strip Model .....	41
Figure A4-9a	Measurement and the Simulation of the Deflection Over Temperature of a Bi-material Beam Consisting of Molding Compound and Silicon. The Linear-elastic (LE) Model Clearly Overestimates the Deflection Whereas the LVE Model can Reproduce the Deflection Correctly .....	28	Figure C1-5	Example of Full Model Boundary Conditions for Component Level Temperature Cycling .....	41
			Figure C1-6a	Example of Boundary Conditions for Multichip Modules .....	42
			Figure C1-6b	Example of Boundary Conditions for Multichip Modules .....	42
			Figure C1-6c	Example of Boundary Conditions for Multichip Modules .....	42
			Figure C1-7a	Strip Model Boundary Conditions .....	43
			Figure C1-7b	Strip Model Boundary Conditions .....	43
			Figure C1-8	Critical Solder Joint Dimensions for Analysis .....	44
			Figure C1-9	CBGA400 Octant Model and Joint Mesh ....	45
			Figure D1-1a	Experiment vs. FEA Warpage Measurements Across Different Reference Planes .....	50



Figure D1-1b	Experiment vs. FEA Warpage Measurements Across Different Reference Planes .....	50	Figure E3-4a	Examples of the DIC Results Showing: (a) In-Plane, $U_x$ ; and (b) Out-of-Plane, $U_z$ , Displacement Components During the TB Testing of Bare-Aluminum Boards .....	62
Figure E-1	Typical System Manufacturing Process Flow .....	52	Figure E3-4b	Examples of the DIC Results Showing: (a) In-Plane, $U_x$ ; and (b) Out-of-Plane, $U_z$ , Displacement Components During the TB Testing of Bare-Aluminum Boards .....	62
Figure E1-2a	Typical Spherical Bend Test Set-Up .....	53	Figure E3-5	Finite Element TB Model of the Bare-Aluminum Board .....	63
Figure E1-2b	Typical Spherical Bend Test Set-Up .....	53	Figure E3-6	Comparison of the Force vs. Displacement Response from the Model and Experiment for a 32mil Thick Bare-Aluminum Board .....	64
Figure E2-1	A Typical Quarter Symmetric TB Analysis Model Created in Abaqus® CAE .....	54	Figure E3-7	Computational Model vs. Experimental Board Strains Comparison for the Strains on the Primary Board Side in a 32mil Thick Bare-Aluminum Board .....	64
Figure E2-2	Example of Solder Joint Mesh .....	55	Figure E3-8	Computational Model vs. Experimental Board Strains Comparison for the Strains on the Secondary Board Side in a 32mil Thick Bare-Aluminum Board .....	64
Figure E2-3	An Example of the Boundary Conditions in a Typical Quarter Symmetric TB Model ...	55	Figure E3-9	A Comparison of the Computational Model vs. DIC Experimental Results for the Board Displacements for a 32mil Thick Bare-Aluminum Board .....	65
Figure E2-4	A Schematic of the Post-Processed SJ Forces for a Given SJ Set in the Local Coordinate System .....	57	Figure E3-10	Comparison of the Force vs. Displacement Response from the Model and Experiment for a 62mil Thick Bare-Aluminum Board .....	65
Figure E2-5	Effect of Computational Model Element Type on the Board Strains and SJ Force ....	57	Figure E3-11a	Computational Model vs. Experimental Board Strains Comparison for the Strains on: (a) Primary Board Side; and (b) Secondary Board Side in a 62mil Thick Bare-Aluminum Board .....	66
Figure E2-6a	ETB Mesh Size Effect on Board Strains and SJ Force due to Variation in Mesh Size/Seed in the: (a) ETB Thickness Direction; and (b) ETB In-Plane Direction .....	58	Figure E3-11b	Computational Model vs. Experimental Board Strains Comparison for the Strains on: (a) Primary Board Side; and (b) Secondary Board Side in a 62mil Thick Bare-Aluminum Board .....	66
Figure E2-6b	ETB Mesh Size Effect on Board Strains and SJ Force due to Variation in Mesh Size/Seed in the: (a) ETB Thickness Direction; and (b) ETB In-Plane Direction .....	58	Figure E3-12	Comparison of the Force vs. Displacement Response from the Model and Experiment for a 62mil Thick Bare FR4 Board .....	66
Figure E2-7a	The Three Types of SJ Mesh Sizes/Seeds: (a) Coarse Mesh; (b) Medium Mesh; and (c) Fine Mesh .....	59	Figure E3-13	Comparison of the TB Model vs. Experimental Results for the Strains on the Primary Board Side for a 62mil Thick Bare FR4 Board .....	67
Figure E2-7b	The Three Types of SJ Mesh Sizes/Seeds: (a) Coarse Mesh; (b) Medium Mesh; and (c) Fine Mesh .....	59	Figure E3-14	BGA TV with the Board Strain Gauges Attached .....	67
Figure E2-7c	The Three Types of SJ Mesh Sizes/Seeds: (a) Coarse Mesh; (b) Medium Mesh; and (c) Fine Mesh .....	59	Figure E3-15	Comparison of the Force vs. Displacement Response from the Model and Experiment for BGA TV on a 40mil Thick ETB .....	68
Figure E2-8a	Package Mesh Size/Seed Effect on Board Strains and SJ Force Due to Change in Mesh Size/Seed in the: (a) Package Thickness Direction; and (b) Critical SJs .....	59	Figure E3-16a	Package Corner-to-Corner (SW, NW, NE and SE) Board Strain Comparison Between the Computational Model and Test Results: (a) $e_2$ Strain Component; and (b) $e_4$ Strain Component .....	69
Figure E2-8b	Package Mesh Size/Seed Effect on Board Strains and SJ Force Due to Change in Mesh Size/Seed in the: (a) Package Thickness Direction; and (b) Critical SJs .....	59	Figure E3-16b	Package Corner-to-Corner (SW, NW, NE and SE) Board Strain Comparison Between the Computational Model and Test Results: (a) $e_2$ Strain Component; and (b) $e_4$ Strain Component .....	69
Figure E2-9	Effect of Friction Coefficient on the Board Strains and SJ Forces .....	60	Figure E4-1	Board Level Test to Fail Data .....	70
Figure E3-1	A Typical TB Test Setup (Transient Bend Application of Quasi-Static DIC BKM, 2010) used for the Model Validation Process .....	61			
Figure E3-2a	Examples of (a) Schematic of the TB Test Set-up with STB (Shock Test Board); and (b) Position of the Strain-Gauges on the Primary Side of the Board .....	61			
Figure E3-2b	Examples of (a) Schematic of the TB Test Set-up with STB (Shock Test Board); and (b) Position of the Strain-Gauges on the Primary Side of the Board .....	61			
Figure E3-3	An Example of the Board-Strain Components ( $e_2$ , $e_4$ ) at Three of the Strain Gauges from the TB Testing of Bare-Aluminum Boards ...	62			

Figure E4-2	Model Calibration Board Level Test Data for 40mil Thick Board .....	70
Figure E5-1	Model Prediction Results for TV (pitch=0.4mm and board thickness=28mil) .....	71
Figure E9-1	SJ Loading Angle .....	77

### Tables

Table 4-1	Sample Final FEA Report Questionnaire .....	5	Table C1-7	Octant Model 1 Results and Comparison with Experimental Data .....	45
Table 5-1	Example of Physics, Loads and Degrees of Freedom .....	7	Table C1-8	Octant Model 2 Results and Comparison with Experimental Data .....	45
Table 11-1	Examples of Warpage and Fatigue Life Results Comparison Data .....	15	Table C1-9	Effect of "crplm" Command .....	47
Table A1-1	Typical Material Properties of Silicon .....	18	Table D1-1	Example of Warpage Results Comparison Data Across Different Reference Planes .....	51
Table A1-2	Typical CTE Properties of Silicon .....	19	Table E1-1	Parameters Defining Scope of Modeling Approach Applicability .....	53
Table A3-1	Recommended TMA Parameters .....	23	Table E2-1	Summary of the Finite-Element Mesh in the TB Model .....	54
Table A3-2	Recommended DMA Parameters .....	24	Table E2-2	Summary of the Contact Interactions in the TB Model .....	56
Table C1-1	Test Package Detail Information .....	38	Table E2-3	Summary of the TB Analysis Model Outputs .....	56
Table C1-2	Experimental Thermal Cycling Data .....	39	Table E2-4	Typical TB Analysis Model Run-Times .....	56
Table C1-3	Material Properties .....	39	Table E2-5	Details of the ETB Mesh Size/Seed Study ....	58
Table C1-4	3D Model Types and Tradeoffs .....	40	Table E2-6	Details of the Substrate Mesh Size/Seed Study .....	59
Table C1-5	Modeling Constants for Three Different Methodologies .....	43	Table E3-1	Summary of the TB Testing Used for Model Validation Purpose .....	60
Table C1-6	Strip Model Results and Comparison with Experimental Data .....	44	Table E5-1	Summary of Transient Bend Test Data for TV Used for Validation .....	70
			Table E5-2	Comparison Between Model and Experiment .....	71
			Table E5-3	General Reasons for Difference Between Model and Test Data .....	71

# Numerical Analysis Guidelines for Microelectronics Packaging Design and Reliability

---

## 1 SCOPE

**1.1 Introduction** This document is an effort to standardize and document some of the basic tenets of a typical Finite Element Analysis (FEA) model. The intent of this document is to help educate new designers (and in some cases even experienced designers) on the basic information and best practices that should be captured and provided to technical reviewers of the results of FEA data.

FEA has been used in the microelectronics industry for several decades. Numerical models offer several advantages in the design of microelectronics devices. If used correctly, they can provide guidance on:

1. Potential tradeoffs to be made in achieving the optimal design of microelectronic devices.
2. Performance and reliability of microelectronics devices will be evaluated by including the impact of multiple design, material, geometry, and process parameters.

With the exponential reduction in the cost of computing, numerical models can save significant time and expense because they can be used to reduce the number of iterations of experimental tests that may be needed to finalize and optimize a design. With ever increasing cost pressure, shrinking design margins and faster time to market, there is a need to rely more on numerical models rather than running multiple time consuming and expensive experiments.

However, to achieve all these benefits, numerical models must be used correctly. This involves setting up the problem correctly, obtaining the input parameters accurately, running the analysis properly and outputting and interpreting the results correctly.

There is considerable “tribal” knowledge across the industry where individual designers have their own best practices on how they run their models. However, there is a wide spectrum of knowledge proficiency. At one end, there are engineers who design and develop their own models, refined over decades of experience. At the other end of the spectrum, there are engineers who have very little experience, and use ad-hoc information to develop models that are incomplete and could result in even more expense and time-consuming losses if implemented incorrectly.

Across the industry, there is a need to standardize the basic information, terminology and methodologies used to develop these numerical models. While individual models can be quite complex and customized, some best practices could help make model comparison across different players in the microelectronics supply chain much easier and scalable. The basic structure of this document is outlined in the schematic in Figure 1-1.

**1.2 Purpose** FEA is versatile and is used to solve several complex problems in microelectronics. It is impossible to standardize all applications and flavors in which FEA is performed. This document is not intended to create device release requirements or to imply that simulation or design information is to be provided to customers as evidence for or as a condition of device suitability for any given application. It is expected that this document will be the first of a series of numerical analysis guideline documents. This will serve as a foundational document for other domain specific guidelines that delve deeper into best practices and guidelines for specific applications of FEA. The expected modular structure of the numerical analysis reliability guidelines documents is shown in Figure 1-2.

The objective of this document is to provide some guidelines for the basic information that should be provided when FEA is performed in most cases. Examples are provided for some select cases (illustrated as pattern filled topics in Figure 1-2) to help users understand why certain information should be captured and reported. In addition, some examples of best practices are provided, to help guide users on best practices that could be implemented to avoid loss of information or accuracy. The examples provided in this document are not meant to be exhaustive or all encompassing. They are meant to highlight examples of key aspects that need to be taken into account when an FEA analysis is set up and the results reported.

Several commercial FEA software are widely used across the industry. Due to the nature of the analysis, some recommendations may be specific to certain software and may be articulated in the context of a specific FEA software code. However, these recommendations are not exhaustive and do not imply endorsement of any one software over another.

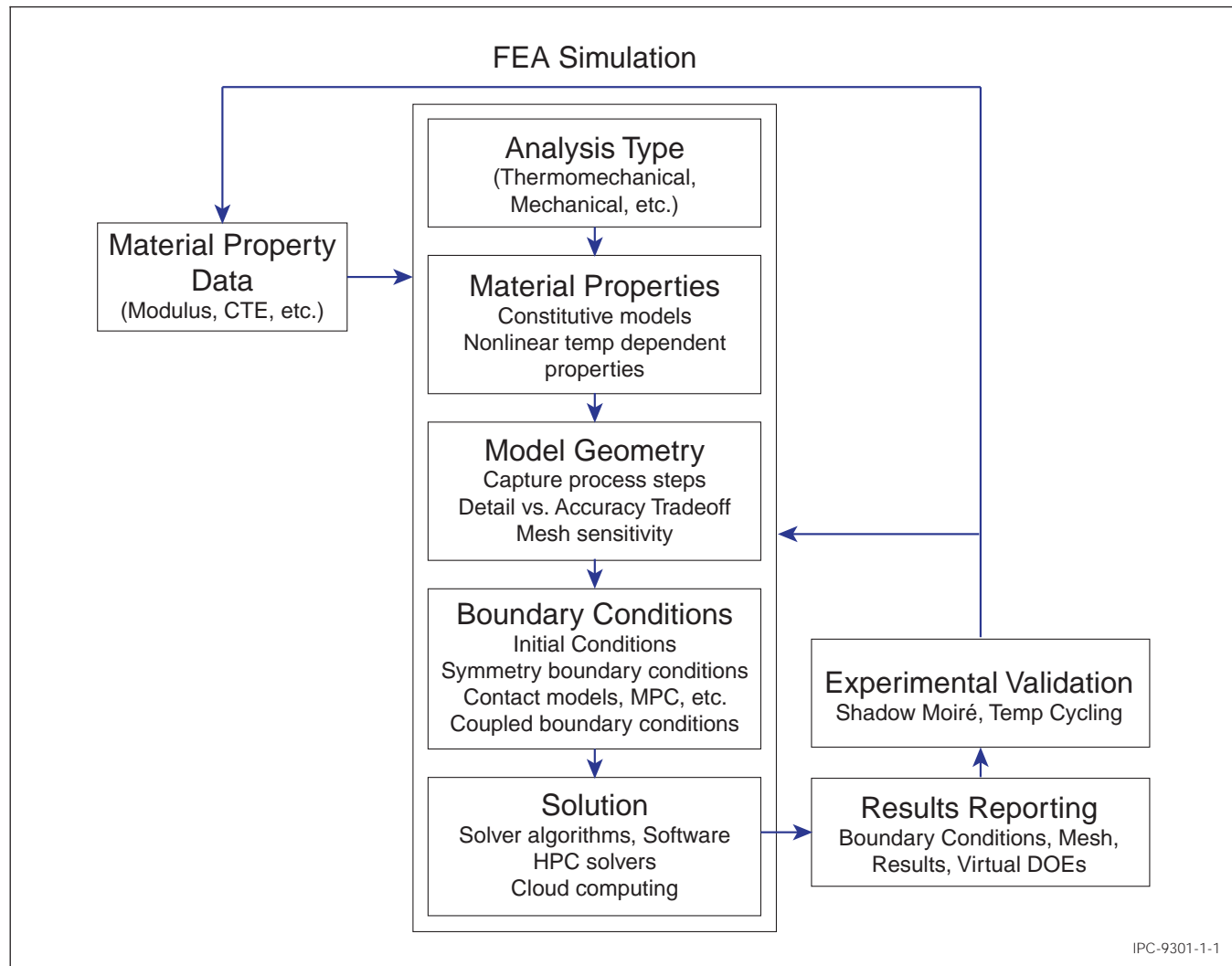


**Figure 1-1 Building Blocks of a Typical Finite Element Analysis Problem**

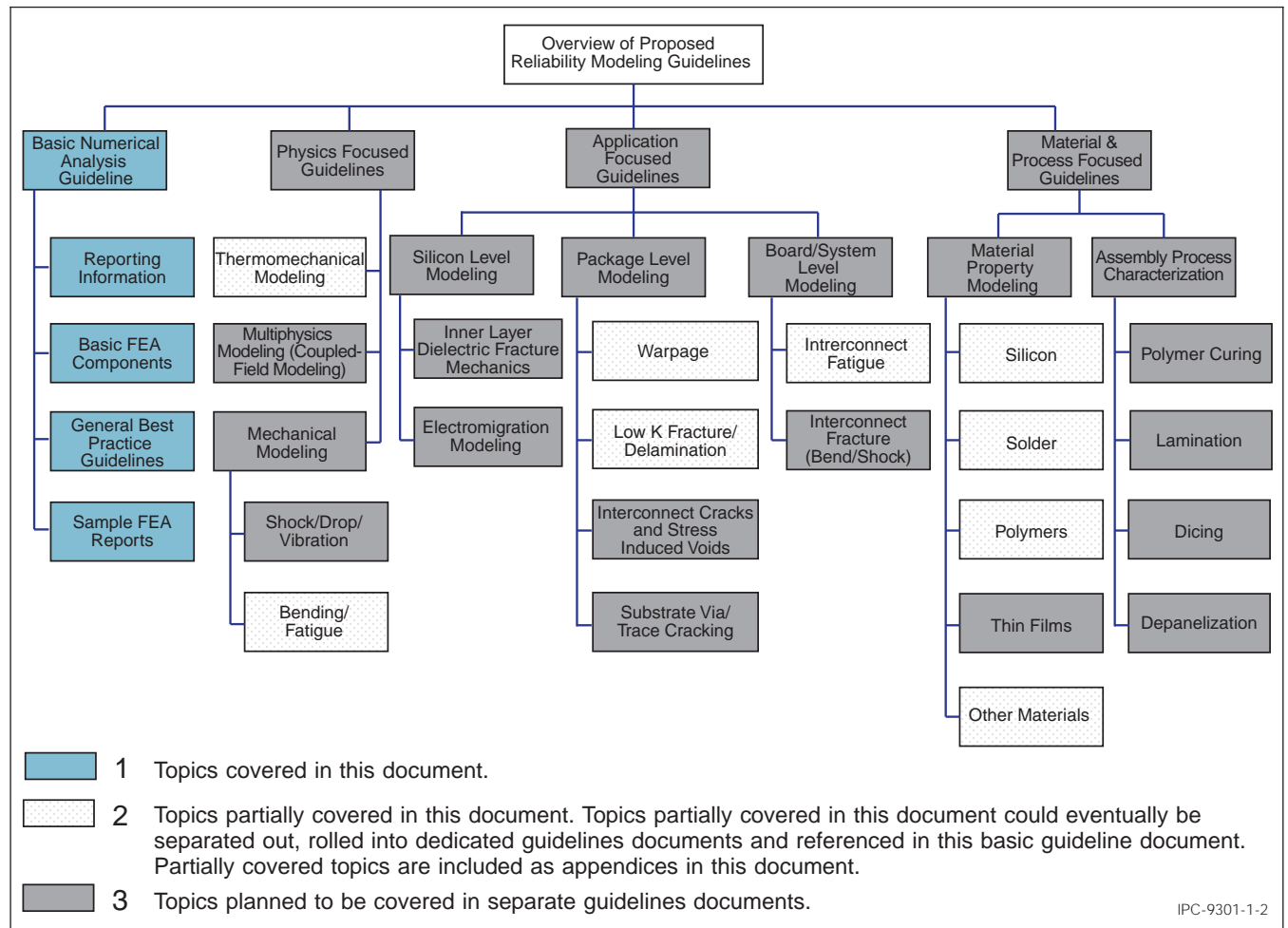


**Figure 1-2 Expected Modular Structure of Numerical Analysis Reliability Guideline Documents**

## 2 APPLICABLE DOCUMENTS

### 2.1 IPC<sup>1</sup>

**IPC-T-50** Terms and Definitions for Interconnecting and Packaging Electronic Circuits

**IPC/JEDEC-9707** Spherical Bend Test Method for Characterization of Board Level Interconnects

### 2.2 ASTM<sup>2</sup>

**ASTM B311-13** Standard Test Method for Density of Powder Metallurgy (PM) Materials Containing Less Than Two Percent Porosity

**ASTM B962-14** Standard Test Method for Density of Compacted or Sintered Powder Metallurgy (PM) Products using Archimedes' Principle

**ASTM D638-10** Standard Test Method for Tensile Properties of Plastics

**ASTM D696** Standard Test Method for Coefficient of Thermal Expansion of Plastics Between -30 °C and 30 °C with a Vitreous Silica Dilatometer

**ASTM D790** Standard Test Method for Flexural Properties of Unreinforced and Reinforced Plastics and Electrical Insulating Materials

**ASTM D5023** Standard Test Method for Plastics: Dynamic Mechanical Properties: in Flexure (Three-Point Bending)

**ASTM D5024** Standard Test Method for Plastics: Dynamic Mechanical Properties: In Compression

**ASTM D5026** Standard Test Method for Plastics: Dynamic Mechanical Properties: In Tension

**ASTM D5418** Standard Test Method for Plastics: Dynamic Mechanical Properties: In Flexure (Dual Cantilever Beam)

**ASTM D7028** Standard Test Method for Glass Transition Temperature (DMA T<sub>g</sub>) of Polymer Matrix Composites by Dynamic Mechanical Analysis (DMA)

**ASTM E132-04** Standard Method for Poisson's Ratio at Room Temperature

**ASTM E831** Standard Test Method for Linear Thermal Expansion of Solid Materials by Thermomechanical Analysis

**ASTM E1545** Standard Test Method for Assignment of the Glass Transition Temperature by Thermomechanical Analysis

**ASTM E1640** Standard Test Method for Assignment of the Glass Transition Temperature by Dynamic Mechanical Analysis

## 3 TERMS AND DEFINITIONS

The definition of all terms used herein **shall** be as specified in IPC-T-50.

---

1. [www.ipc.org](http://www.ipc.org)

2. [www.astm.org](http://www.astm.org)

#### 4 RESULTS REPORTING

To ensure that all pertinent and useful information is captured and communicated, a comprehensive final FEA report should be prepared and provided for all FEA analyses. The final FEA report provided should include details as outlined in all the applicable sections of this guideline. The details of each item are outlined in Table 4-1.

**Table-4-1 Sample Final FEA Report Questionnaire**

Parameter	Example	Value	Units	Description
<b>Basic Analysis Information</b>				
Analysis Type	Static, Transient etc.			
Physics Type	Mechanical Shock, Bend, Vibration, Thermomechanical, Multiphysics etc.			
Software	ANSYS® Mechanical, Multiphysics, ABAQUS®, COMSOL®, LS-DYNA®, etc.			
Software Version				
Analysis Script. If so, include in report	APDL, Log File, Model Files etc.			
<b>Basic Model Information</b>				
Model Category Levels	Silicon Level, Package Level, Board Level etc.			
Symmetry Conditions	Quarter, Octant etc.			
Schematic showing model stackup				
Geometric Information (Dimensions)				
Schematic showing boundary conditions	Show faces where constraints are set to zero. Include contour plots of high risk failure locations and plots of displacement from global/sub model if submodeling is used			
<b>Material Property Information</b>				
Reference Temperature			Celsius	
Temperature dependent properties used? Provide in report		Yes/No		
Glass Transition Temperature ( $T_g$ )	Materials 1, 2, 3 etc. Values per ASTM XXX		C	
Modulus below $T_g$	Materials 1, 2, 3 etc. Values per ASTM XXX		GPa, MPa	
Modulus above $T_g$	Materials 1, 2, 3 etc. Values per ASTM XXX		GPa, MPa	
CTE below $T_g$	Materials 1, 2, 3 etc. Values per ASTM XXX		ppm/C	
CTE above $T_g$	Materials 1, 2, 3 etc. Values per ASTM XXX		ppm/C	
Poisson's Ratio				
Viscoplastic Model & Constants	Materials 1, 2, 3 etc. Garofalo Creep, Anand Constants etc.			
Viscoelastic Model & Constants	Materials 1, 2, 3 etc. Maxwell Constants, Mooney Rivlin etc.			
Nonlinear Model & Constants	Materials 1, 2, 3 etc. Bilinear, Kinematic Hardening etc.			
<b>Mesh Information</b>				
Mapped or Tetrahedral?	Free or structured mesh			
Dissimilar Meshes? If so, specify interfaces	Different meshes joined with contact elements or constraint equations. Substrate/Substrate Interface			
Element Type	Provide the name and number of the element type used.			
Mesh Sensitivity Analysis?	Was effect of mesh density on results captured? If so, include results			
<b>Loading Information</b>				
Temperature dependent loading? If so, provide loading conditions	Temperature vs. Time data			
Ramped or Step Loading? If so, provide loading rate	The rate at which load is applied			

Parameter	Example	Value	Units	Description
Rate Dependent Loading? If so, provide loading rate	Force, Displacement, Energy applied as a function of time			
<b>Solution Information</b>				
Operating System	Win7, 8, IOS etc.			
Workstation or Cluster?				
High Performance Computing Used?	HPC licenses used?	Yes/No		
No. of Nodes Used (HPC)				
No. of Processors				
Processor Name	I7 etc.			
RAM Memory Size	96Gb, 128Gb, etc.			
Solution Algorithm	Sparse Solver, PCG, etc.			
Number of Load Steps				
Number of Time Steps				
Solution Time			Hours	
<b>Post Processing</b>				
Results Parameters	Warping, Fatigue Life, etc.			
Was volume averaging used? If so, provide specifics	Volume Averaging means averaging results over multiple elements. Show elements over which averaging was used	Yes/No		
Are the results temperature dependent? If so, provide at least 10 points over temperature	E.g. Reflow Profile, Thermal Cycling etc.	Yes/No		
Experimental Benchmark Data Available? Provide in report	Provide benchmark data to show correlation with model	Yes/No		
Experimental Calibration Data Available? Provide in report	Calibration data is used to derive the FEA model, whereas benchmark data is strictly for comparison purposes	Yes/No		
Tabulated Comparison of Results	Show percent difference between benchmark and model results			

## 5 BASIC ANALYSIS INFORMATION

**5.1 Analysis Type** Analysis type indicates the nature of the analysis performed. Static analysis is performed to analyze invariant solutions for the dependent variable(s) (which are typically displacements or temperatures). In static analysis, time derivatives of the dependent variable(s) are ignored.

Transient analysis, on the other hand, calculates the time-dependent response of the dependent variable(s). Consequently, inertial, damping and capacitance terms need to be included and impact the solution. A time integration technique is inherent in the finite element calculation. It should be noted that some FEA software (e.g., ANSYS®) uses the variable “time” to specify both actual time in a transient analysis and as a load index in static analysis.

It should be noted that time can also be modeled as discrete analysis steps, without the use of a transient method. In this simplified approach, some assumptions may be made, such as, for example, in the case of a thermally-cycled component. As thermal loads are applied in the form of load steps in lieu of a transient model, temperature variations across the component are assumed to be negligible.

Finally, modal analysis is used to calculate system natural frequencies and mode shapes under the presumption that the dependent variable has a solution which is harmonic in time. Modal structural analysis requires a mass matrix.

**5.2 Physics Type** Numerical analysis can be utilized to analyze several complex physical phenomena. It is important to document the underlying physics being modeled, because the type of physics dictates the types of boundary conditions, solution algorithms and loads that are applied to study the problem. Typical examples of physics type are shown in Table 5-1.

Since the underlying physics establish the framework for the analysis, it is important to explicitly state and explain the physics type being modeled.



**Table 5-1 Example of Physics, Loads and Degrees of Freedom**

Physics	Response	Loads	Degrees of Freedom
Mechanical Shock	Structural Deformation	Input G Excitation, Force, Displacement	Displacement
Mechanical Bend	Structural Deformation	Force, Displacement	Displacement
Mechanical Vibration	Structural Deformation	Force	Displacement
Thermomechanical	Temperature induced stress	Temperature	Displacement
Thermal-Electric (coupled field)	Thermal and Electric	Temperature, Current	Temperature, Voltage
Structural-Thermal-Electric (coupled field)	Structural, Thermal and Electrical Analysis	Force, Temperature and Current	Displacement, Temperature, Voltage

**5.3 Software** Several commercially available and proprietary codes can be used to perform numerical analysis. It is important to document the precise name of the software used, because variations in analysis settings and solution algorithms can vary significantly across software, which can impact results. Typical examples of software include (but are not limited to): ANSYS®, ABAQUS®, COMSOL®, LS- DYNA® etc.

Often, user defined functions are used to enhance the capabilities or simplify the analysis workflow within the commercially available software. If used, it should be explicitly stated that custom macros or user defined functions were used which could potentially impact the results and could not be replicated by anyone else that uses the same software. If non-commercial, proprietary software is used for the entire analysis, then it should be stated explicitly that “non-commercial, proprietary numerical analysis software” was used for performing the analysis.

**5.3.1 Software Version** Numerical analysis software is continuously updated, revised and modified as new solution algorithms are developed, errors are identified and new capabilities are added.

Variations in software versions can also result in markedly different results. Refer to the Appendix C, Section C1.3 for examples showing the effect of software version on analysis results.

Consequently, when reporting the software used for the analysis, the software version and release date should be explicitly included. For example: “ANSYS®, v15.0, 2014

**5.4 Analysis Files and Scripts** Numerical analysis software uses a wide variety of file types and structures. Even within the same software, several variations of file types can be used to perform the same analysis.

Often, numerical analysis is also performed using scripts, which are simple text files that store all the model building steps, analysis and post processing instructions. The scripts can be an excellent way to store information about the model because they show, line by line, each step taken to build the model and obtain results. Scripts can also be used for parametric analysis. Several macros can also be built using scripts and called as functions or libraries into other scripts to build the complete model.

A key benefit of scripts is their small file size. Since they only contain the model building instructions and not the actual model results, the scripts can be quite small. A user can easily run the script to generate the results for detailed review. Where possible, scripts can be shared in entirety for users and customers to review.

## 6 BASIC MODEL INFORMATION

**6.1 Boundary Conditions** The modeling approach and boundary conditions for the model can significantly impact the results obtained. The boundary conditions applied in the model should be clearly shown in the final report. For an example of boundary conditions applied to thermomechanical reliability, refer to Appendix C.

**6.2 Model Stackup Schematics** Schematic images should be included in the final report, illustrating the details of the model, mesh and the features included in the model. Examples of such schematic images are shown in Figure 6-1a, Figure 6-1b and Figure 6-1c.

**6.3 Boundary Condition Schematics** In the case of symmetric models, symmetric boundary conditions can be used. Figure 6-2 illustrates a quarter symmetric model. Symmetry boundary conditions are applied on both symmetric surfaces, as shown in Figure 6-3. From the zoomed in view in Figure 6-4, in the Y-Z cut plane, it can be seen that X displacement and Y, Z rotation degree of freedoms are constrained. In the case of 3D models where the node does not have a rotation of degree of freedom, only the X displacement boundary condition is in effect. The symmetric boundary condition on both Y-Z plane and X-Z plane constrains all the rigid body degrees of the freedoms, with the exception of the Z direction displacement. As seen in Figure 6-5, Z displacement was constrained on one node at the center corner of the model.

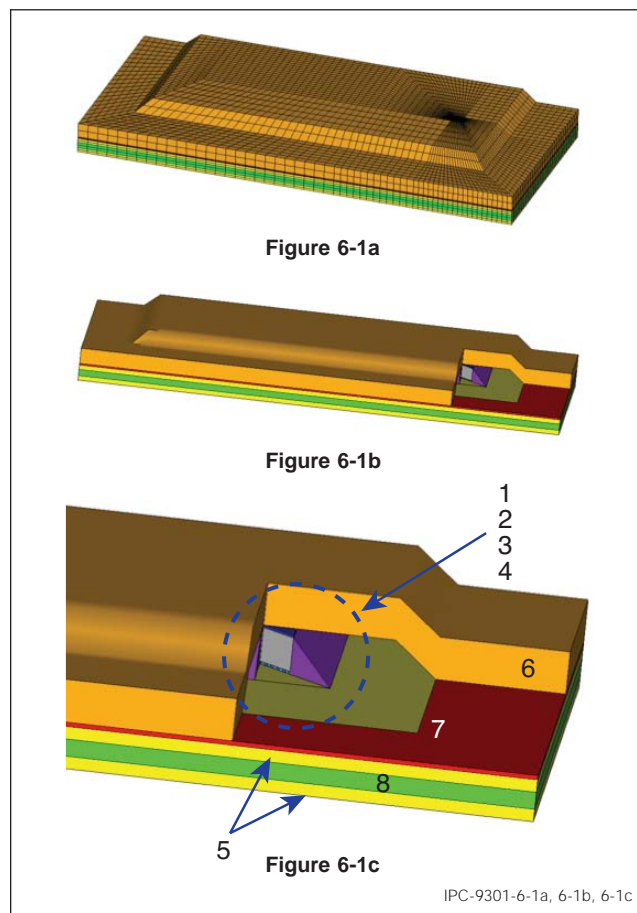


**Figure 6-1a, Figure 6-1b and Figure 6-1c Examples of Model Schematics**

- Note 1. Underfill (purple)
- Note 2. Silicon Die (gray)
- Note 3. Thermal Interface Material (blue)
- Note 4. Bumps
- Note 5. Upper and Lower Buildup Layers (yellow)
- Note 6. Lid
- Note 7. Lid Adhesive
- Note 8. Substrate Core (green)

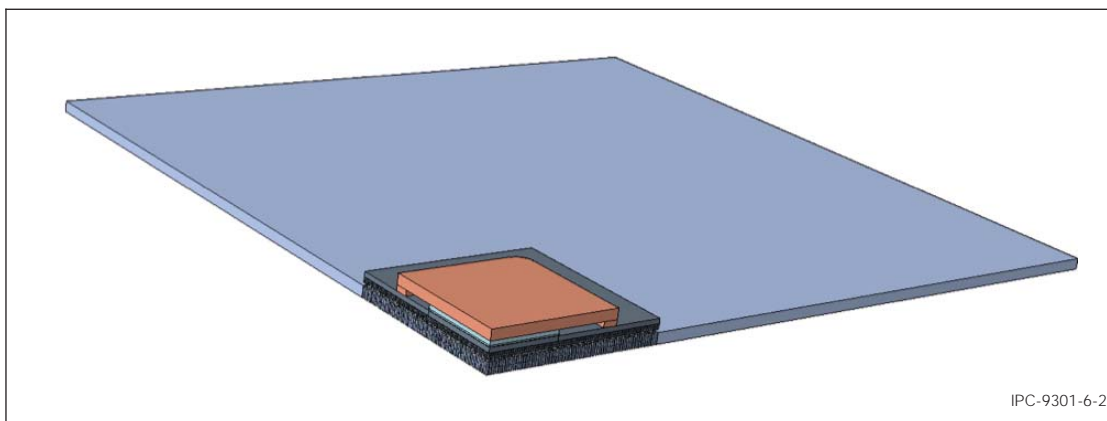


**Figure 6-2 Quarter Symmetric Model**

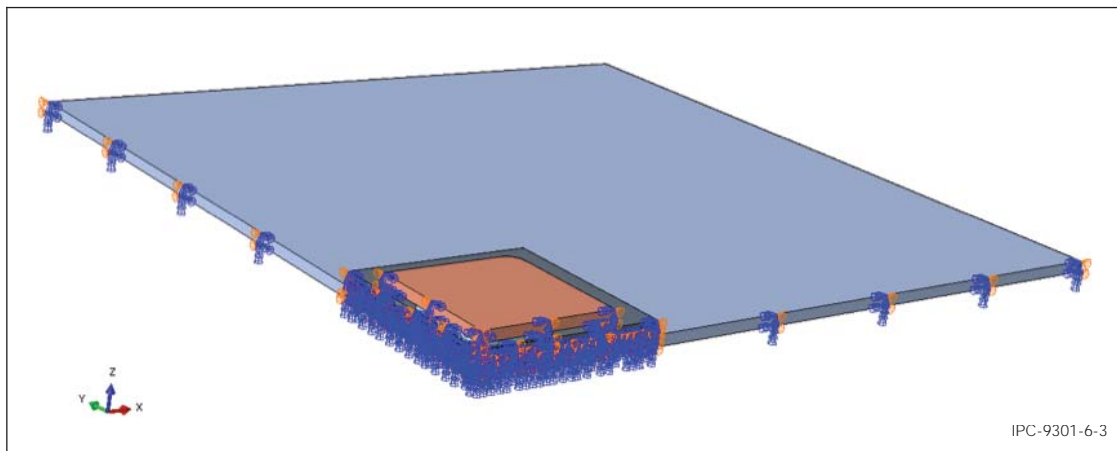


Figure 6-3 Symmetry Boundary Conditions Added

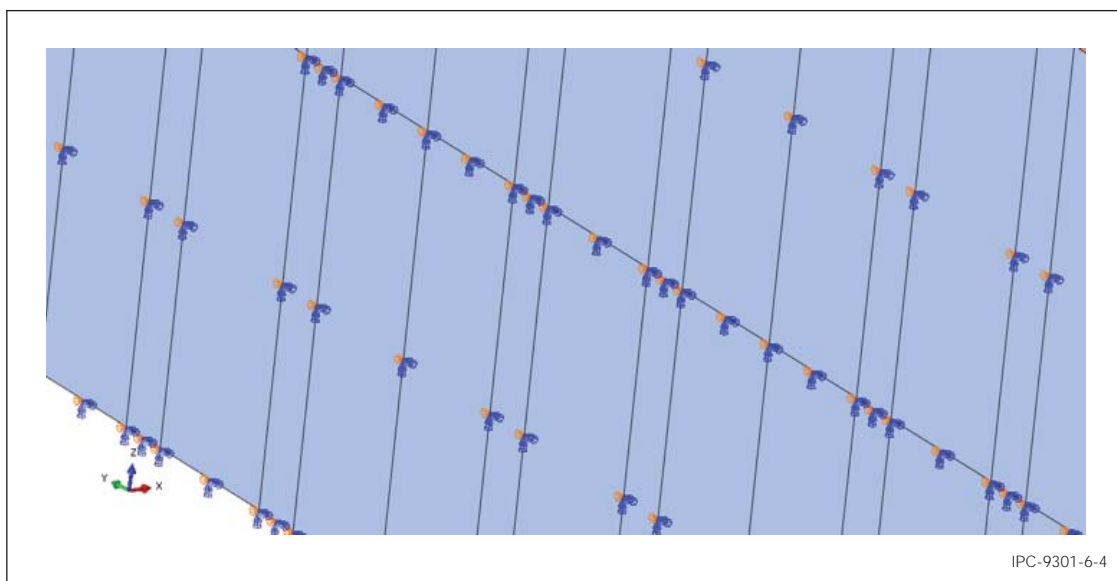


Figure 6-4 Zoom in View of Symmetry Boundary Conditions

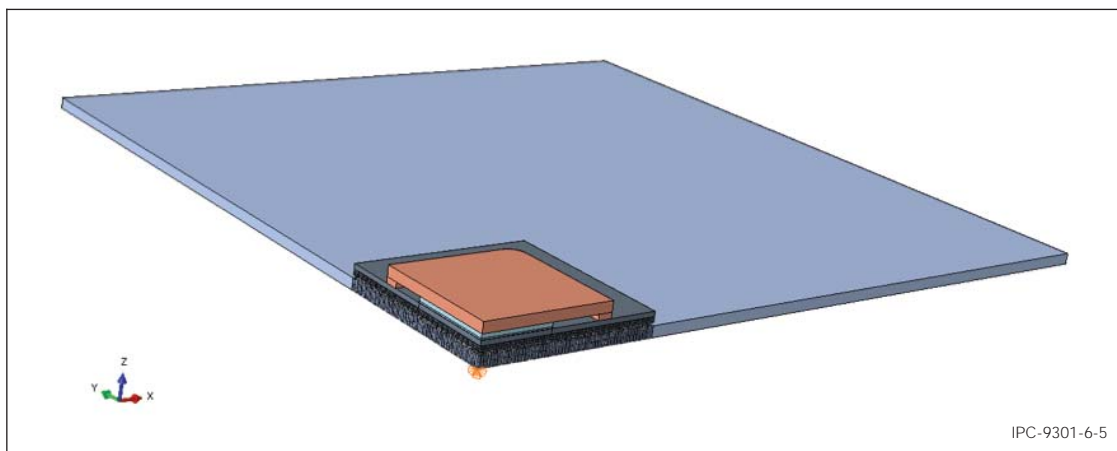


Figure 6-5 Displacement Boundary Conditions to Constrain All Rigid Body Displacement

## 7 MATERIAL PROPERTY INFORMATION

**7.1 Material Properties** Material properties can be used from known published literature and referenced properly. To ensure that the results predicted by the model are accurate and can be replicated by others; all material properties used in the model should be explicitly listed and the sources of the data explicitly referenced. For more specific guidelines on material properties for different material types, refer to Appendix A.

**7.2 Reference Temperature** The reference temperature is the temperature at which the material is considered to be at zero thermal strain. Generally, the reference temperature is the temperature that a material is “cured” or solidified between two different materials, e.g., a polymer cured after bonding between two materials. For solder joints, the reference temperature is the solidification temperature of the solder as the assembly is cooled from reflow to room temperature or lower. Most software packages provide two methods of specifying a reference temperature: global reference temperatures or reference temperatures specified as part of the material properties of each of the materials in the model.

Frequently, semiconductor assemblies may be modeled as having different reference temperatures for various constituents, but analyzed within a single linear analysis. Some analyses may benefit from the sequential assembly of a structure composed of subassemblies with different stress-free temperatures in multi-step nonlinear analysis. This procedure is sometimes described as element “birth or death” to signal the activation or de-activation of certain elements, simulating sequential assembly steps. If element “birth/death” is used, it should be explicitly stated in the final report.

**7.3 Temperature Dependent Properties** Temperature dependent properties need to span the range of temperatures the structure would be exposed to, in test conditions and use conditions. If temperature dependent properties are used, they should be explicitly reported in the final report, and tabulated data should be provided, outlining the properties at set temperature intervals.

## 8 MESH INFORMATION

**8.1 Mesh Selection and Information** A characteristic of the finite element method is that typically the numerical solution for dependent variables approaches the exact solution as the number of elements increases [1]. While dependent variables, such as displacements, approach the exact solution, derived results, such as stresses, may still deviate from the exact solution.

Consequently, the choice of mesh, both in terms of spatial discretization and element formulation, materially influences the accuracy and utility of a numerical solution. Definition of desirable meshing practices is a broad topic, which can be compounded by having different answers based on the nature of the problem to be solved. As a result, this document does not attempt to describe the attributes of “good” or “bad” meshes. It is presumed that the analyst is familiar with the theoretical background needed to define good meshes [e.g., [2] [3]] and performs convergence studies on a model to assure solution stability and correspondence to known analytic or experimental results. The transient bend discussion in Appendix D provides an excellent example of model tuning and validation through test.

Meshing is critical because it impacts the accuracy and sensitivity of a model. If a combination of meshing techniques and elements types are used, a picture of the whole model with the mesh should be provided. Detailed pictures should be shown of the mesh in high risk areas or critical locations. For example, if a model is focused on board level solder interconnect risk assessment, pictures of the solder joints mesh and the area around them should be shown.

The reason for element selection should be briefly discussed to explain what main physical phenomena was the target of the analysis and why this element type is capable of capturing it. For example, board or package bending is the main deformation factor for many failure mechanisms. In this case, element types with shear locking should be avoided, especially with limited layers in the thickness direction.

If multiple element types (e.g., shell and solid elements or linear and quadratic elements) are used in the same model, usually there will be deformation mismatch in the interfaces. These interfaces should be kept as far away from the points of interest as possible.

**8.2 Mapped or Tetrahedral Mesh** Generally, two different types of meshes are available, depending on the complexity of the geometry. Mapped meshes are more structured meshes with regularly or proportionately spaced elements, which are usually of the same shape. This method will generate higher mesh quality with uniform mesh size. When structured or mapped mesh cannot be achieved for complex geometry, “free meshing” can be adopted. This method may cause lower quality elements and discontinuities in the mesh. In general, effort should be made to use mapped meshes whenever possible.

Generally speaking, higher order shape functions will generate smoother results with lower element count. Linear brick elements have linear strain change from node to node, while tetrahedral elements have constant strain. So brick elements are suggested whenever possible.

**8.3 Dissimilar Meshes** Geometries with significant differences in feature size could require a large number of elements with mapped meshing. The higher the element count, the longer the computation time. In some instances, the computation time could become untenable as a result of the mesh. In such instances, different features could be meshed differently and then “joined” together by using contact elements or constraint equations.

If contact elements or “constraint equations” are used in the model to “join or tie” the dissimilar mesh elements together, the point of discontinuity at which the contact elements are set up should be kept as far away from the region(s) of interest as possible. An example of such an application is shown in Figure 8-1.

Moreover, care should be taken to ensure that the correct contact settings are used to minimize additional stiffness being introduced into the model due to the contact elements. The procedure used to tie dissimilar meshes affects accuracy. Methods that rely on constraint equations or contact elements enforced with penalty function or Lagrange multiplier techniques may permit geometric discontinuities at the contact surface. Alternately, when contacting surfaces only share certain nodes, the displacement of the unshared nodes are generally interpolated with the shape functions of the coarser mesh, unduly stiffening the finer mesh at the interface.

Most commercial FEA software allow for multiple contact behaviors, such as sliding, bonding etc. In situations where contact elements are used to join discontinuous meshes, bonding contact conditions are typically the best conditions to use. The contact or constraint conditions (sliding, bonding etc.) used in the models should be explicitly outlined in the report.

**8.4 Mesh Sensitivity Analysis** Complex geometries are particularly sensitive to the mesh used. Wherever possible, it is important to perform a mesh sensitivity analysis of the critical variables being studied (displacement, stress, strain energy density, creep etc.) to mesh density. Higher order node elements could be more sensitive than lower order node elements.

Tabulated results should be provided, showing the sensitivity of the key variables to mesh density. The results of at least three different meshes of varying densities should be analyzed and presented. Results provided without mesh sensitivity analysis can only be used for limited relative comparison purposes. An illustrative example of a mesh sensitivity analysis is outlined in Figure 8-2.

This example showed how creep strain energy density and creep strain range per cycle varied as function of number of elements used through the thickness of a thin layer (25-30µm) on the critical solder joint near the component pad interface. More elements through the thickness may increase the solution time significantly without improving the simulation results.

## 9 LOADING INFORMATION

**9.1 Ramped vs. Stepped Loading** How the load is applied in a problem depends on the problem being solved and the software being used. The loading rate is applicable specifically for nonlinear problems. Many software codes offer automated loading control to control the loading rate and achieve convergence. The convergence tolerance values can be adjusted for selected damage metrics (force, deformation, strain, L2 norm, etc.).

Loading type/rate will be important in cases where nonlinear time dependent material behavior is involved (e.g., viscoelastic, viscoplastic materials). Otherwise, the load type/rate is typically inconsequential to the end result (stress/strain/energy).

It should be clearly stated in the final report if non-default convergence tolerance values are used, and sensitivity analysis should be performed to understand the sensitivity of the convergence criteria on the solution results.

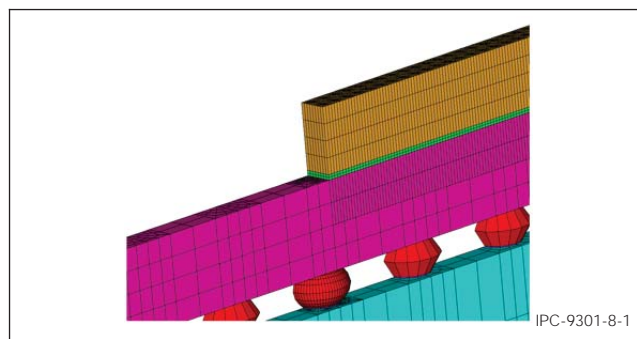


**Figure 8-1 Example of Multi-Point Constraint to “Tie” Dissimilar Mesh Regions**

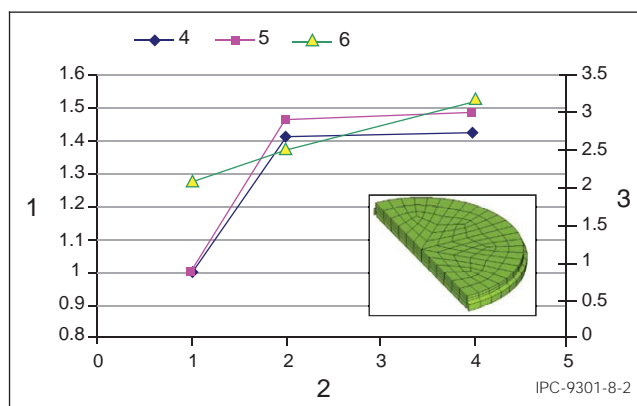


**Figure 8-2 Example of Mesh Sensitivity Analysis**

Note 1. Normalized Creep Strain/Energy Density  
 Note 2. Element Division Number  
 Note 3. Solving Time, Hour  
 Note 4. Cp str  
 Note 5. Cp eng den  
 Note 6. Solve time



## 10 SOLUTION INFORMATION

**10.1 Operating System** The operating system should not impact the results, but it is important to document the type of operating system used (e.g., Windows® 32bit, Windows® 64bit, REHL® etc.). Documenting the operating system helps in benchmarking the computation time required to run the analysis.

**10.2 High Performance Computing (HPC)** The advance of computing technologies makes High-Performance Computing more cost attractive and accessible for general purpose. By processing the information in parallel using multicore/multiprocessors, the total solution time could be significantly reduced. Figure 10-1 shows the total solution time in hours for a solder joint reliability model (Figure 10-2) as a function of the number of cores used for the analysis. In this particular benchmarking study case, the model consists of 249993 elements and 283871 nodes. The study was performed on clusters (each cluster node has 2 Intel® Xeon® Quad-core processors and 64GB RAM).

It is clear that the reduction in solution time is not linearly scalable to the number of CPUs/Cores used for the analysis. For this particular example, there is no benefit seen when the number of cores used is beyond 48. The reason for that is the available RAM from 6 cluster nodes (48 cores) is large enough to hold the entire model in memory, so the processor speed is becoming the gating item for further improvement. Furthermore, some software relies on the first node (master node), to “book keep” the information distributed among all CPUs/Cores, therefore more resources would be occupied for such a purpose instead of computation. There are a lot of factors that could impact the scalability of HPC performance. Listed below are the most common factors:

- The model size (total Degrees of Freedom (DOF), contact regions and current wave front width);
- Available physical memory (about 10GB RAM needed for 1 million DOFs);
- Problem nature (material nonlinearity prefers higher CPU clock frequency (higher mflops) over RAM size);
- Hardware efficiency (CPU clock frequency, and data bus speed);
- Software efficiency (ANSYS® recommends up to 8 cores for Shared Memory (SMP), and 32 cores for Distributed Memory Parallel (DMP));
- Interconnect speed (1000Mb/sec minimum interconnect speed recommended per ANSYS®);
- Scratch space location (in memory, SSD, HDD, NAS);
- Parallel processing type (SMP, distributed multiprocessor, GPU).

**10.3 Hardware Parameters** The hardware used to perform the analysis can impact the speed and performance of the analysis. In some cases, information about the hardware used can provide forensic insight on any potential problems/errors in the analysis. For instance, if an analysis takes 8 hours on a given hardware specification, but the same analysis takes 12 hours to run on different hardware, knowing the differences between the hardware can help determine the cause of the significant difference in analysis times.

The following key hardware parameters should be recorded and outlined:

1. Number of Processors/Cores used in the analysis
2. Memory (GB)

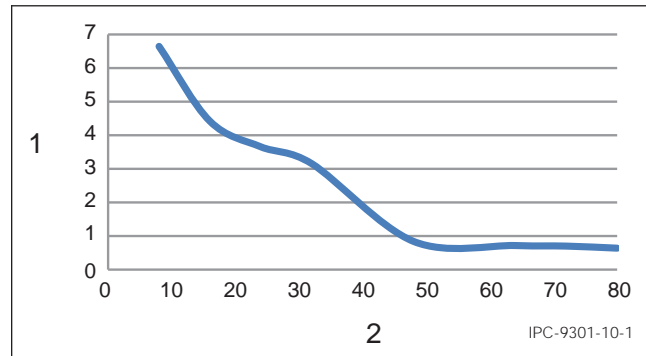


**Figure 10-1 Computational Time vs. Number of Cores Used (PBGA 680 Solder Joint Model)**

**Note 1.** Computational Time, Hour

**Note 2.** Number of CPU Cores

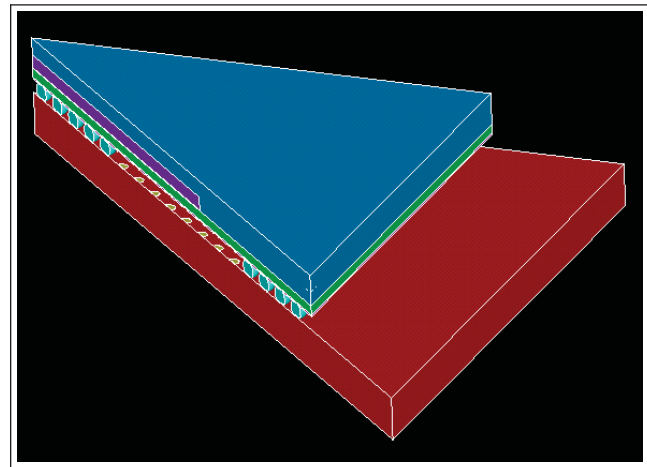


**Figure 10-2 Octant PBGA680 Solder Joint Reliability Model**

If using server cluster:

1. Number of nodes
2. Interconnect type between nodes e.g., FCoE, Infiniband® etc.
3. Typical interconnect speed between nodes

**10.4 Solution Algorithms and Settings** The algorithms and settings used depend on the software used for the analysis. Some best practices for some of the software commonly used in the industry for microelectronics modeling applications are provided in this section.

It is important to note that any software related recommendations should NOT be construed as endorsements of the use of the software in any way. These are only best practices consolidated from the general knowledge base of advanced users of software applications in the microelectronics industry. The user is encouraged to identify and develop similar best practices for the software they would be using for their applications.

**10.4.1 Time Steps** One condition that should be avoided is to allow the time increment to be much longer than the variations in loading history. Some FEA software allows users to input an amplitude time history profile to describe the loading history. Caution should be used to not let the time step become too big to capture some key changes in the loading step. One hypothetical example is shown in Figure 10-3. In this case, one possible solution is to manually setup stop points on the major turning points of the loading history.

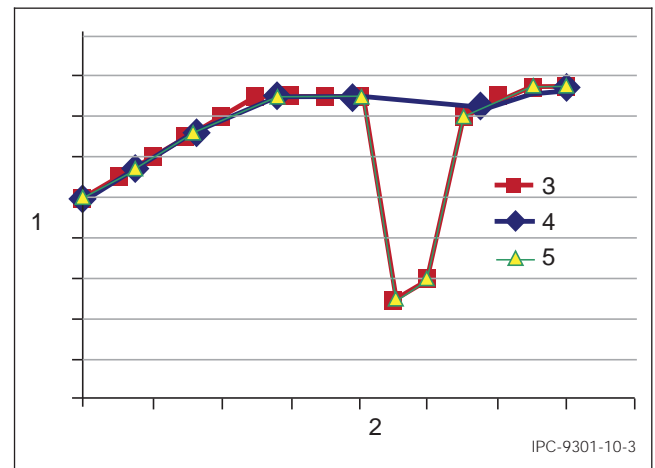


**Figure 10-3 Example of Time Step Too Big to Capture Fluctuation in Loading History**

**Note 1.** Load Level

**Note 2.** Time

**Note 3.** Loading Profile

**Note 4.** Time Step Too Big

**Note 5.** Reasonable Time Step

**10.4.2 Solution Time** The time taken by the simulation to solve and process should be included in the final report. Reporting solution times can help in understanding the degree of complexity of the model, and potentially help in debugging issues if the model is run at a different location. Differences in solution times can indicate potential convergence issues, boundary condition errors and even the type of material properties used. Temperature dependent, nonlinear material properties lead to time consuming models. Contact elements can also result in longer solution times. Errors in setting up the model are not easy to capture, but solution time can be a critical indicator of potential issues. The user can also review the solution output log (or “solve.out”) files to understand the causes of convergence issues.

## 11 POST PROCESSING

**11.1 Post Processing** Post processing involves analyzing the solution and extracting relevant results to be further analyzed for design decision making. Post processing in numerical modeling is not merely reviewing results. In some cases, the kind of post processing performed can significantly change the results output. For instance, displacement in finite element models is output as a nodal result. Stress on the other hand is frequently calculated at element integration points followed by extrapolation to the nodes with the element’s shape functions. Often averaging at contiguous element boundaries is used to produce aesthetically pleasing contour plots.

**11.2 Results Parameters** The following parameters are typically output from models and reported as results. The guidelines below highlight key practices when reporting these specific parameters.

**11.2.1 Fatigue** Fatigue life is an estimation of the number of cycles it will take for the structure to fail under cyclic loading. The cyclic loading could be thermal (as in thermal cycling) or mechanical (as in mechanical shock/drop). The structure in focus could be a solder joint, a trace or other structure.

The output of numerical models is never in terms of cycles. The output of numerical models is usually in the form of a damage metric (plastic work, strain energy density, creep strain, total strain etc.). The output metric should be explicitly identified and the metric values outlined.

The equations used to translate the damage metric into fatigue life (in cycles) should be explicitly stated and the transformed results included in the final report. For example, Darveaux's 4-constant model is commonly used in the microelectronics industry. [4]

**11.2.2 Stresses** In many instances, stresses and strains are compared when relative comparisons are required. A key challenge with finite element models is that the stresses or strains are extremely mesh density specific. That is because the formulation of elements that calculate stress (or strain) is based on a weighted residual within the entire element and, in some cases, because of permissible singular displacement fields. Further mesh refinement can result in markedly different stresses.

Comparisons of stresses in different loading/geometry scenarios should always be done with these two factors taken into consideration:

1. Only element output should be compared, not nodal stress output. Many commercial FEA software packages output stresses as nodal solutions, even though stresses are elemental solutions due to their dependence on area. Stress values and other derivative values are usually calculated at the integration point or the centroid of elements, depending on the element type. Nodal results are produced by averaging the stresses across the nodes of the element or extrapolated from the element, and averaged over the elements that share the same node. Element solutions (or Element Table solutions) should be used for comparisons.
2. The mesh density of the two scenarios being compared should be comparable. In addition, mesh sensitivity analysis should be performed as described in Section 8-3.

Volume averaging (as described in the next section) is also an effective technique to reduce the sensitivity of results on the mesh density.

**11.3 Volume Averaging** Finite element models inherently function by discretizing the domain into smaller elements. Consequently, the results depend significantly on the number of elements in a specific region of focus. Sharp corners, edges or regions of extremely high stress gradient could produce results that are so mesh dependent that they cannot be accurately quantified. This creates a "singularity," which can result in inordinately high stresses, strains, current density etc. in a small region. Any output parameter that is strongly dependent on area can be significantly impacted by singularities.

Volume averaging essentially distributes the results over a range of elements as opposed to using the output from a single element. The size variation of a single element can significantly skew results, whereas volume averaging the results over several elements tends to reduce the effect of the size of any single element. The volume averaging equation is:

$$E_{eff} = \frac{\sum VE}{\sum V}$$

Where E is the output parameter (stress, current density, strain energy density etc.) and V is the volume of the selected elements.

**11.4 Temperature Dependent Results** If temperature dependent material properties are used in the model, the results output of the model is also temperature dependent. The results extracted from the model should be at specified temperatures. For example, if stresses are extracted from the model, the stresses should be extracted at specific temperatures and those extraction temperature values should be included in the final report. Moreover, for any output parameters that are temperature dependent, the output parameters (such as stress, warpage etc.) should be reported for at least 2 distinct temperature values. Reporting results at two different temperatures facilitates a sanity check that can indicate whether the temperature dependent properties and boundary conditions have been correctly applied.

## 11.5 Correlation with Experimental Data

**11.5.1 Nomenclature** Numerical models are most effective when they are correlated well with experimental data. Correlating models with experimental data is a complex process, involving multiple stages with different semantics. To enable clear understanding, a nomenclature is outlined for each of the different steps involved in the correlation process:

1. **Validation:** This involves comparing parameters that are directly measured experimentally. For example, in monotonic bend tests, the experimentally measured strain and displacement for an applied force can be compared with model output data. To ensure good correlation, simpler, repeatable materials (like aluminum plates in monotonic bend testing) can be used for the experimental validation. The goal of validation is to confirm that the underlying physics of the model is



correct. Validation setups typically utilize simple, repeatable materials and geometries that closely capture the intended boundary conditions of the actual problem in focus.

2. **Calibration:** This involves using the numerical models to derive parameters that are not directly measurable in experiments and correlating them with model derived parameters. For example, determining the stress at which solder joints fail in monotonic bend tests. While PCB strain and displacement can be measured experimentally, the strain in the solder joint at which failure occurs cannot be measured experimentally. In this case, the solder joint strain output from the model for the same applied displacement and PCB strain can be correlated with the occurrence of failure. While the “true” strain in the solder joint is unknown, the model-derived joint strain can be “ascribed” to be the strain at which experimentally observed failure occurred. Experimental set ups should be first validated before they are used for correlation analysis.
3. **Benchmarking:** This involves comparing models that have been correlated with some experimental data with a *different* set of experimental data. It is imperative to ensure that the experimental data used to calibrate the numerical models is NOT the same data that is used to benchmark the models. After a model has been calibrated with select experimental data, the model should be compared with separate, independent experimental data to determine how well the model correlates with experimental data. The objective of benchmarking is to determine the versatility and range of applicability of the model. Only models that have been validated and calibrated should be used for benchmarking.
4. **Prediction/Extrapolation:** After completion of validation, calibration and benchmarking, the models are used to make predictions of future conditions (for which experimental data is not yet available) with a known range of accuracy. Only models that have been validated, calibrated and benchmarked should be used for prediction/extrapolation.

The final report should clearly show the experimental data used for calibration and the experimental data used for benchmarking the model. The final report should also indicate clearly when a model is used for prediction/extrapolation vs. benchmarking, correlation or validation.

**11.5.2 Experimental Statistical Analysis** Regardless of correlation stage, any experimental data used for correlation with models should be statistically analyzed before comparing with modeling data. All experiments have varying degrees of uncertainty due to variations in test set up, materials, test sample size, measurement data and failure thresholds. These uncertainties need to be accounted for in statistical terms before the experimental data can be compared with model output data. Refer to the appendix for an example on how statistical analysis is used to analyze experimental data before comparing with modeling data.

**11.5.3 Comparison of Results** The relevant result variables (e.g., warpage, fatigue, strain, stress etc.) should be reported in clear tabulated data. In addition, graphs and/or contour plots should be included to articulate the results of critical parameters (e.g., high stress and strain regions). If comparisons with experimental data are provided, the data should be clearly labeled to indicate validation, correlation, benchmarking or prediction data. Wherever applicable, differences between different model and/or experimental data should include percentage differences. An illustrative example of a reported results table is shown in Table 11-1.

**Table 11-1 Examples of Warpage and Fatigue Life Results Comparison Data**

Fatigue Life Results (Cycles)								
SN	Validation (Warpage, $\mu\text{m}$ )			Calibration (Plastic Work)	Benchmarking (Fatigue Life)			Prediction
	Model	Experiment	% Error	Model	Model	Experiment	% Error	Model

In addition to comparing with experimental data, benchmarked FEA models are also very effective in performing virtual Design of Experiments (DOEs) or Design of Simulation (DOS). Virtual DOEs (or DOS) can be used to run numerical models to determine the effect of various parameters on the design. For instance, to determine the effect of modulus or CTE of a certain substrate material on the warpage of a package, the CTE and modulus of the substrate could be incrementally changed and the resulting warpage derived from the FEA model.

Just as in experimental DOEs, the results output from virtual DOEs run with FEA models can be used to determine the optimal combination of modulus and CTE to achieve a target minimum warpage. Various statistical software can be used in conjunction with FEA software to build factorial DOE matrices and analyze the output from the FEA models. Refer to the Flexural Bend case study in the appendix for an example of the application of virtual DOEs.

## 12 REFERENCES

- [1] M.J. Turner, R.W. Clough, H. C. Martin and L. J. Topp, Stiffness and Deflection Analysis of Complex Structures, J. of Aero. Sci., 23 (9), 1956.
- [2] J. N. Reddy, An Introduction to the Finite Element Method, New York: McGraw-Hill 2nd ed., 1993.
- [3] R. D. Cook, D. S. Malkus and M. E. Plesha, Concepts and Applications of Finite Element Analysis, New York: Wiley, 3rd ed., 1989.
- [4] R. Darveaux, "Effect of Simulation Methodology on Solder Joint Crack Growth Correlation," in *Electronics Components Technology Conference*, 2000.
- [5] D. Kiener and others, "A further step towards an understanding of size-dependent crystal plasticity: In situ tension experiments of miniaturized single-crystal copper samples," *Acta Materialia*, vol. 56, no. 3, pp. 580-592, 2008.
- [6] D. Kiener and others, "Determination of Mechanical Properties of Copper at the Micron Scale," *Advanced Engineering Materials*, vol. 8, no. 11, pp. 1119-1125, 2006.
- [7] D. Kiener and others, "Overview on established and novel FIB based miniaturized mechanical testing using in-situ SEM," *International Journal of Materials Research*, vol. 100, no. 8, pp. 1074-1087, 2009.
- [8] G. Dehm and others, "Can micro-compression testing provide stress-strain data for thin films?: A comparative study using Cu, VN, TiN and W coatings," *Thin Solid Films*, vol. 518, no. 5, p. 1517-1521, 2009.
- [9] D. R. Askeland and P. P. Phulé, The science and engineering of materials (5th ed), Cengage Learning. p. 198. ISBN 978-0-534-55396-8., 2006.
- [10] M. A. Hopcroft, W. D. Nix and T. W. Kenny, "What is the Young's Modulus of Silicon?," *Jour. Microelectromech. Sys.*, vol. Vol. 19, no. No. 2, p. 229 - 238, 201.
- [11] Y. S. Touloukian, R. K. Kirby, R. E. Taylor and T. R. Lee, Thermophysical Properties of Matter, 14 volumes, 1970 - 1978.
- [12] F. P. Incropera and D. P. DeWitt, Fundamentals of Heat and Mass Transfer, Wiley, 1981.
- [13] ANSYS® *Mechanical Theory Reference*.
- [14] M. Motalab and others, "Creep Test Method for Determination of Anand Parameters for Lead Free Solders and their Variation with Aging," in *14th IEEE ITherm Conference*, 2014.
- [15] J. Eckermann and a. others, "Computational modelling of creep-based fatigue as a means of selecting lead-free solder alloys," in *14th IEEE International Conference on Thermal, Mechanical and Multi-Physics Simulation and Experiments in Microelectronics and Microsystems, EuroSime*, 2013.
- [16] D. Bhate and others, "Constitutive Behavior of Sn3.8Ag0.7Cu and Sn1.0Ag0.5Cu Alloys at Creep and Low Strain Rate Regimes," in *IEEE Transactions On Components And Packaging Technologies*, Vol. 31, No. 3, 2008.
- [17] K. Mysore and others, "Constitutive and Aging Behavior of Sn3.0Ag0.5Cu Solder Alloy," in *IEEE Transactions On Electronics Packaging Manufacturing*, Vol. 32, No. 4, 2009.
- [18] C. Norris and A. H. Landzberg, "Reliability of Controlled Collapse Interconnections," *IBM J. Res. Development*, vol. 13, p. 266 - 71, 1964.
- [19] J. Bergstrom, Large Strain Time-Dependent Behavior of Elastomeric Materials, Massachusetts Institute of Technology, 1999.
- [20] J. Bergström and M. C. Boyce, "Constitutive modelling of the large strain time-dependent behavior of elastomers," *Journal of the Mechanics and Physics of Solids*, vol. 46(5), pp. 931 - 954, 1998.
- [21] P. Gromala, J. Duerr, M. Dressler, K. Jansen, M. Hawryluk and J. de Vreugd, "Comprehensive material characterization and method of its validation by means of FEM simulation," in *EuroSimE*, Linz, Austria, 2011.
- [22] H. Shirangi, B. Wunderle, O. Wittler, H. Walter and B. Michel, "Modeling Cure Shrinkage and Viscoelasticity to Enhance the Numerical Methods for Predicting Delamination in Semiconductor Packages," in *EuroSimE*, Delft, The Netherlands, 2009.
- [23] K. Jansen, M. Hawryluk and P. Gromala, "Cure dependent characterisation of moulding compounds," in *EuroSimE*, Linz, Austria, 2011.
- [24] P. Gromala, S. Fischer, T. Zoller, A. Andreescu, J. Duerr, M. Rapp and J. Wilde, "Internal stress state measurements of the large molded electronic control units," in *EuroSimE*, Wroclaw, Poland, 2013.

- [25] W. Dauksher and J. Lau, "A Finite Element-Based Solder Joint Fatigue Life Prediction Methodology for Sn-Ag-Cu Ball Grid Array Packages," *IEEE TDMR*, vol. 9, no. 2, pp. 231-236, 2009.
- [26] T. Anderson, A. Barut and E. I. Guven, "Revisit of Life Prediction Models for Solder Joints," in *IEEE Electronics Components and Technology Conference*, 2000.
- [27] J. Lau and Y. Pao, *Solder Joint Reliability of BGA, CSP, Flip Chip, and Fine Pitch SMT Assemblies*, McGraw-Hill, 1997.
- [28] *Abaqus® User Manual*.
- [29] J. Pan, "Comparing Techniques for Temperature-Dependent Warpage Measurement," Forschung & Technologie, PLUS," 2007. [Online]. Available: [http://www.akrometrix.com/whitepapers/Comparing%20Techniques%20\(10-07\).pdf](http://www.akrometrix.com/whitepapers/Comparing%20Techniques%20(10-07).pdf).
- [30] ASTM-D790, D5023, D5024, D5026, D5418.
- [31] R. Han and others, "A Preliminary Solder Joint Life Prediction Model by Experiment and Simulation for Translation of Use Condition to Temperature Cycling Test Condition," in *Electronics Components and Technology Conference*, 2013.

### 13 APPENDICES

The appendix covers the following relevant topics:

Appendix A – Material Property Modeling

Appendix B – DMA/TMA Fitting Algorithms

Appendix C – Experimental Benchmarking Model Case Study (Thermomechanical Reliability)

Appendix D – Warpage

Appendix E – Modeling Methodology Development for BGA Risk Assessment in Board Flexure Tests

## APPENDIX A

### Material Property Modeling

#### A1 MATERIAL PROPERTIES AND CONSTITUTIVE MODELS

**A1.1 Material Properties and Constitutive Models** Material properties and the constitutive models used in numerical analysis are critical in ensuring that the problem is accurately captured and the results are meaningful. This section provides some basic guidelines on how to incorporate material properties based on the types of materials used. Material models can be quite complicated and application dependent. Only general guidelines and best practices are provided in this document. The recommendations provided in this guideline are for bulk materials and do not necessarily apply to thin films. Details on material characterization of thin films can be found in published literature. [5], [6], [7], [8]

**A1.2 Silicon** Silicon is one of the most pervasively used material across the microelectronics industry. To enable consistency, some basic silicon material properties are provided in this section.

**A1.2.1 Modulus** The elastic modulus of a material is defined as the resistance of the material to applied force. It can also be defined as the slope of the material's stress-strain curve in the elastic deformation region [9]. How the modulus of a material is measured can significantly impact the properties derived. For some more common materials like silicon, the baseline properties shown in Table A1-1 can be used. In the table, the crystal directions [100] and [110] are industry-standard designations for the two common wafer types. The crystal directions may not be parallel, but be rotated by 45° to the chip edges. For both wafer types, “x” and “y” are in the plane of the wafer and “z” is in the through-the-thickness direction.

**Table A1-1 Typical Material Properties of Silicon**

Elastic Properties for [100] p-type Si wafers									
	-200	-100	0	20	100	200	300	400	600
Ex, Ey, Ez	1.32E+11	1.31E+11	1.30E+11	1.30E+11	1.29E+11	1.28E+11	1.27E+11	1.26E+11	1.23E+11
Gyz, Gxz, Gxy	8.04E+10	8.00E+10	7.96E+10	7.95E+10	7.91E+10	7.85E+10	7.79E+10	7.71E+10	7.54E+10
vyx, vxy, vxz, vyz, vzy, vzx	0.2794	0.2789	0.2785	0.2784	0.2782	0.2779	0.2777	0.2775	0.2773
Elastic Properties for [110] p-type Si wafers									
Temp (°C)	-200	-100	0	20	100	200	300	400	600
Ex	1.71E+11	1.70E+11	1.69E+11	1.69E+11	1.68E+11	1.67E+11	1.65E+11	1.64E+11	1.60E+11
Ey	1.71E+11	1.70E+11	1.69E+11	1.69E+11	1.68E+11	1.67E+11	1.65E+11	1.64E+11	1.60E+11
Ez	1.32E+11	1.31E+11	1.30E+11	1.30E+11	1.29E+11	1.28E+11	1.27E+11	1.26E+11	1.23E+11
Gyz	8.04E+10	8.00E+10	7.96E+10	7.95E+10	7.91E+10	7.85E+10	7.79E+10	7.71E+10	7.54E+10
Gxz	8.04E+10	8.00E+10	7.96E+10	7.95E+10	7.91E+10	7.85E+10	7.79E+10	7.71E+10	7.54E+10
Gxy	5.14E+10	5.12E+10	5.09E+10	5.09E+10	5.06E+10	5.02E+10	4.98E+10	4.93E+10	4.80E+10
vyx	0.0635	0.063	0.0626	0.0625	0.0621	0.0616	0.0611	0.0605	0.0593
vxy	0.0635	0.063	0.0626	0.0625	0.0621	0.0616	0.0611	0.0605	0.0593
vxz	0.3631	0.3625	0.3619	0.3618	0.3614	0.3611	0.3609	0.3608	0.361
vyz	0.3631	0.3625	0.3619	0.3618	0.3614	0.3611	0.3609	0.3608	0.361
Vzy	0.2794	0.2789	0.2785	0.2784	0.2782	0.2779	0.2777	0.2775	0.2773
Vzx	0.2794	0.2789	0.2785	0.2784	0.2782	0.2779	0.2777	0.2775	0.2773

Elastic properties for p-type silicon are calculated for [100] and [110] wafers from the temperature- dependent stiffness coefficients [10]:

$$C_{11} = 165.6 \cdot (1 - \Delta T \cdot 73.25 \times 10^{-6} - \Delta T^2 \cdot 49.26 \times 10^{-9}) \text{ (GPa)}$$

$$C_{12} = 63.9 \cdot (1 - \Delta T \cdot 73.25 \times 10^{-6} - \Delta T^2 \cdot 49.26 \times 10^{-9}) \text{ (GPa)}$$

$$C_{44} = 79.5 \cdot (1 - \Delta T \cdot 73.25 \times 10^{-6} - \Delta T^2 \cdot 49.26 \times 10^{-9}) \text{ (GPa)}$$

where  $\Delta T$  is the temperature of interest (°C) minus the reference temperature, 25 °C.

**A1.2.2 Coefficient of Thermal Expansion (CTE)** Describes how the size of an object changes with a change in temperature. Specifically, it measures the fractional change in size per degree change in temperature at a constant pressure.

**Table A1-2 Typical CTE Properties of Silicon**

Select Thermo-Physical Properties of Silicon				
Temp (°C)	$\alpha(1/^\circ\text{C})$ (instantaneous)[11]	k (W/m°C) [11]	c (J/kg°C) [11]	$\rho(\text{kg/m}^3)$ [12]
-173	$-0.4 \times 10^{-6}$	884	259	
-123	$0.5 \times 10^{-6}$	409	429	
-73	$1.5 \times 10^{-6}$	264	557	
-23	$2.2 \times 10^{-6}$	191	646	
20	$2.6 \times 10^{-6}$	153	705	2330
127	$3.2 \times 10^{-6}$	99	785	
227	$3.5 \times 10^{-6}$	76	831	
327	$3.7 \times 10^{-6}$	62	852	
427	$3.9 \times 10^{-6}$	51	869	
527	$4.1 \times 10^{-6}$	42	886	
627	$4.3 \times 10^{-6}$	36	902	

## A2 SOLDER

**A2.1 Viscoplastic Models & Constants** Viscoplastic materials are materials whose deformation depends not just on the load that is applied, but also the rate at which the load is applied to the material. The rate dependency of the material can be captured with different models.

An example of a commonly used viscoplastic material is solder. Solder creeps, meaning it deforms under constant stress. To capture the deformation behavior of solder in models, especially to predict long term fatigue life and response to stress, solder is modeled as a viscoplastic material in finite element models. Different material property models can be used to capture viscoplastic behavior. Examples include Power Law Creep, Garofalo Creep viscoplastic models etc. as outlined below [13].

$$\text{Power Law Creep} \quad \dot{\epsilon} = A \exp\left(-\frac{Q}{RT}\right) \sigma^n \quad (1)$$

$$\text{Garofalo Creep} \quad \dot{\epsilon} = A \exp\left(-\frac{Q}{RT}\right) \sinh^n(\alpha\sigma) \quad (2)$$

Where A is a constant, Q is the activation energy, R is the universal gas constant and n is the stress exponent. These constants are usually empirical fits to experimental data. It is important to include the details of the material models and constants used in the analysis, in the final report.

**A2.2 Rate Dependent Plasticity** Rate dependent plasticity is the steady accumulation of plastic strain at constant stress. There are multiple constitutive models developed over the years to capture rate dependent plasticity. The most common ones are the Perzyna, Pierce and Anand Models.

In the Pierce and Perzyna models, rather than calculate creep and plasticity separately, inelastic strain is directly calculated. These models are typically used for very high strain rate applications (such as nonlinear deformation of metals in very high shock loading where the material plastically deforms). The equations for the Perzyna and Pierce models are respectively [13].

$$\dot{\epsilon}_{pl} = \gamma \left( \frac{\sigma}{\sigma_0} - 1 \right)^{1/m} \quad (\text{Perzyna})$$

$$\dot{\epsilon}_{pl} = \gamma \left( \left( \frac{\sigma}{\sigma_0} \right)^{1/m} - 1 \right) \quad (\text{Pierce})$$

Where:

$\dot{\epsilon}_{pl}$  = equivalent plastic strain rate  
 $m$  = strain rate hardening parameter  
 $\gamma$  = material viscosity parameter  
 $\sigma$  = equivalent stress  
 $\sigma_0$  = static yield stress of material

As  $\gamma$  tends to  $\infty$ , or  $m$  tends to zero or  $\dot{\epsilon}_{pl}$  tends to zero, the solution converges to the static (rate-independent) solution. [13] Another rate dependent model is the Anand Viscoplasticity model. This model is commonly used to model metals under high temperature conditions where the material deformation depends on strain rate, temperature, strain hardening and softening. It is a unified plasticity model that captures inelastic deformation from both the creep effect and rate dependent plasticity. The Anand model has been used in the industry to model lead-based solder joints for several years. Details of the constants used for lead-free solders can be found in several references [14], [15], [16], [17].

**A2.3 Rate Dependent Plasticity** Time-independent plasticity, or typically just “plasticity,” is a third common nonlinear constitutive characterization used for electronic packaging materials. Solders are frequently defined with plastic response and, as an example, fatigue criterion such as the Norris-Landzberg equation [18] are based on plasticity-induced damage.

The onset of plasticity occurs when a material’s elastic stress state becomes equivalent to a presumed yield function,  $f$ .  $f$  is typically taken to be a function of stress and formulated as  $f(I_1, I_2, I_3, k)$ , where the “I”s are the invariants of the stress tensor and  $k$  is constant. There is no change in plastic deformation as long as  $f < 0$  and plastic flow occurs when  $f = 0$ . Among the numerous yield surfaces, the von Mises and Tresca are perhaps the most common. Both follow Bridgman’s observation that plastic flow is independent of hydrostatic stress.

A flow rule will dictate the direction of plastic flow, once yielding occurs. For smooth yield surfaces, such as von Mises, or the smooth portions of faceted yield surfaces, such as Tresca, yielding occurs normal to the yield surface,  $f$ , at the point of loading:

$$d\epsilon_{ij}^{pl} = \Lambda \frac{\partial f}{\partial \sigma_{ij}}$$

where  $\Lambda$  is a constant of proportionality. At yield surface vertices, there are more than one limiting tangent plane and the direction of the plastic strain increment may depend on the loading vector. When a material exhibits perfect plasticity, yielding does not alter the stress state or the yield surface. Many materials are idealized as displaying hardening, which changes the yield surface after yield. The most frequently invoked hardening rules are isotropic and kinematic hardening. As shown in Figure A2-1a, Figure A2-1b, and Figure A2-1c, yielding causes a uniform expansion of the isotropic-hardening yield surface. In the case of kinematic hardening, the yield surface remains the same size and translates in stress space in response to yielding.

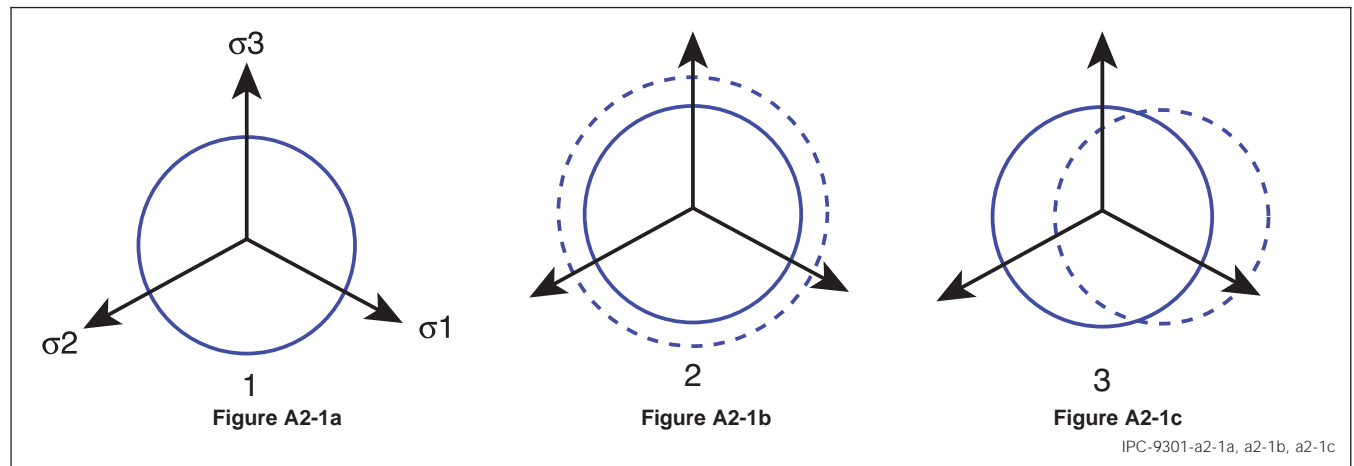


**Figure A2-1a, Figure A2-1b, and Figure A2-1c Isotropic and Kinematic Hardening Rules.**

**Note 1.** Projection of the von Mises Yield Surface on the  $\pi$  plane

**Note 2.** Isotropic Hardening

**Note 3.** Kinematic Hardening

**Note:** The solid circle is the initial yield surface and the dashed circles are the yield surfaces due to two hardening rules.

When performing an analysis with plasticity, a stress-strain curve is usually entered to define the constitutive response of the material where yielding is permitted. Figure A2-2a, Figure A2-2b, Figure A2-2c, and Figure A2-2d shows typical options. A perfectly elastic material may be defined with a single modulus (at a given temperature) and a linear relationship exists between stress and strain for this material. Elastic-perfect plasticity adds a yield point, beyond which stress remains constant as strain increases after yield. Hardening may be added to the elastic-perfectly plastic formulation by introducing a second (lower stiffness) relationship between stress and strain beyond yield. Complex hardening relationships may be created with the multilinear approach.

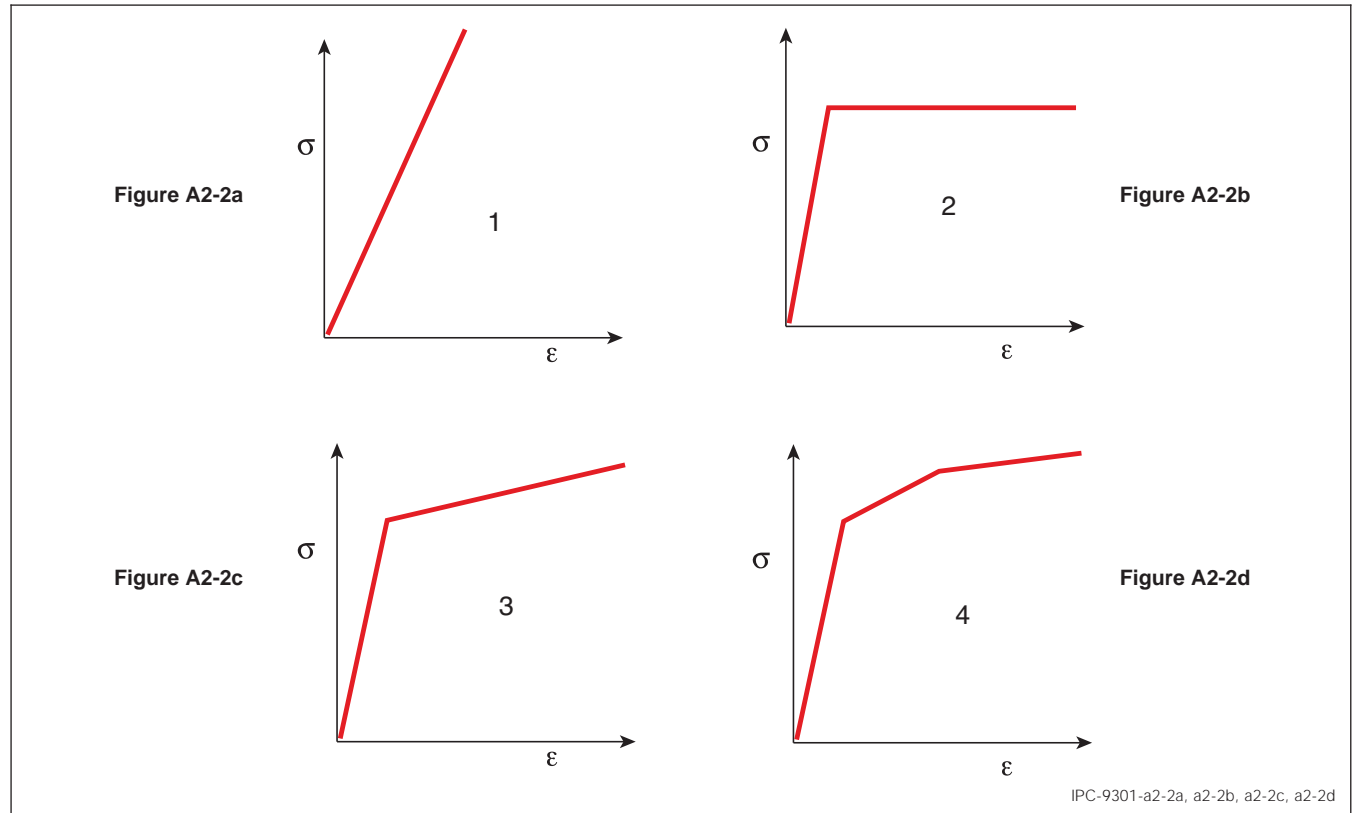


**Figure A2-2a, Figure A2-2b, Figure A2-2c, and Figure A2-2d Examples of One-Dimensional Stress Strain Relationships**

**Note 1.** Elastic

**Note 2.** Elastic-perfectly Plastic

**Note 3.** Elastic Plastic with Hardening

**Note 4.** Elastic Multi Linear Plastic Hardening



As with other nonlinear analyses, plasticity is path dependent, hence the solution requires precise definition of applied loads, and an iterative numerical solution. Piece-wise and iterative solutions are required to appropriately capture the stress-strain state within the model. FEA software generally provide default solution parameters, including load apportionment and convergence criteria. While these defaults can be helpful, they guarantee neither a correct nor a converged solution. The analyst must carefully consider and check the results of a nonlinear solution.

### A3 POLYMERS

**A3.1 Polymers** Thermosetting polymers are widely used in the packaging of electronic components, e.g., as molding compound, adhesive or underfill material.

The properties of thermosetting polymers change nonlinearly over temperature (see storage modulus and thermal expansion behavior over temperature in Figure A3-1a and Figure A3-1b). At low temperature, thermosetting polymers are in the “glassy” state. When sufficient amount of thermal energy is provided, the polymer chains become reorganized during the nonlinear “glass” transition. The state after transition is referred to as “rubbery” state.

The glass transition requires special efforts in modeling. Step-by-step, this section covers aspects of polymer material characterization, the thermal expansion modeling, the modeling of the viscoelasticity and the cure shrinkage modeling of thermosetting polymers.

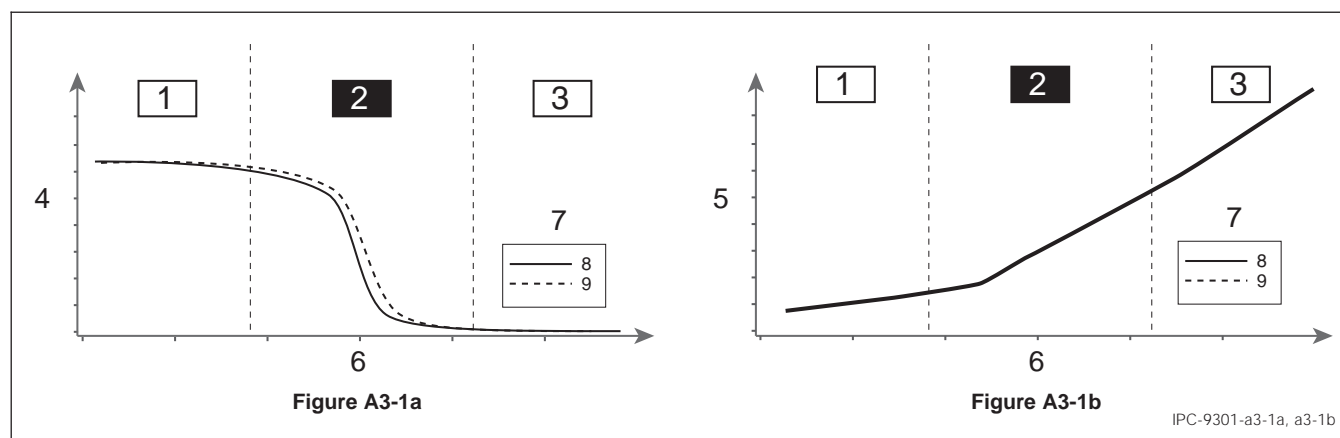


**Figure A3-1a and Figure A3-1b Characteristic Measurements of the Storage Modulus and the Thermal Expansion of a Thermosetting Polymer Over Temperature.**

**Note 1.** Glassy State  
**Note 2.** Glass Transition  
**Note 3.** Rubbery State  
**Note 4.** Storage Modulus  
**Note 5.** Thermal Strain  
**Note 6.** Temperature [°C]  
**Note 7.** DMA Frequency  
**Note 8.** 1 Hz  
**Note 9.** 10 Hz

**A3.1.1 Aspects of Polymer Material Characterization** When quantitative accuracy of the simulation results is required, the nonlinear nature of thermosetting polymers requires elaborate material characterization. The thermal expansion behavior of the polymers can be measured using a TMA (Thermo-Mechanical Analyzer). The viscoelastic behavior of polymers can be characterized using a DMA (Dynamic Mechanical Analyzer). The next subsections will briefly cover some aspects which need to be considered when thermosetting polymers are characterized.

**A3.1.1.1 Characterization of Thermal Expansion using TMA** The primary quantity measured in a TMA is the thermal strain of the specimen with respect to room temperature. The Coefficient of Thermal Expansion (CTE) values need to be subsequently derived from this data. Instantaneous/local CTEs (see ASTM D696 and ASTM E831) are derived for different temperature regions as they allow describing the thermal expansion over temperature independent of the reference temperature. The test parameters and sample preconditioning are recommended in Table 3-1:

Materials like thermosetting polymers which have domains with different instantaneous/local CTEs (see Figure A3-1a and Figure A3-1b) separated by (glass) transition regions need to be evaluated with care:

- The polymer needs to be heated at least once over its transition region before the actual measurement is taken (see ASTM E1545).
- The local CTEs shall not be evaluated with a safety margin away from the transition point and not in the vicinity of the transition region (see ASTM E831).



Table A3-1 Recommended TMA Parameters

TMA Test Parameters	Recommendation
Sample size dimensions	2 - 10 mm
Temperature Ramp Rate (deg C/min)	5 °C/min
Preload static force	Per machine supplier recommendation
Lowest temperature in measurement	20 °C below lowest temperature of interest (see ASTM E831)
Sample Preconditioning	As required for the considered simulation case
Temperature delta ΔT for determining a local CTE via tangents	50 °C (see ASTM E831)

- For an indication when the thermal expansion behavior changes, datasheets commonly report a “CTE1” for the glassy, a “CTE2” for rubbery state of thermosetting polymers and a glass transition temperature  $T_g$  although the actual glass transition takes place over a whole temperature range (see Figure A3-1a and Figure A3-1b). As it is impossible to derive a single characteristic temperature which represents a whole temperature range,  $T_g$  values reported for one polymer can differ significantly and also depend on which method was used for the extraction of  $T_g$  (e.g., TMA or DMA or others).
- The standard ASTM E1545 describes how the  $T_g$  can be extracted from a TMA measurement by the construction of two tangents for the glassy and rubbery states and their intersection. Figure A3-2a and Figure A3-2b shows two possibilities for the extraction of  $T_g$  which both conform to the standard, but lead to results which differ by more than 40 °C. Hence it is essential to explicitly state the method used to measure the  $T_g$  in the final report.

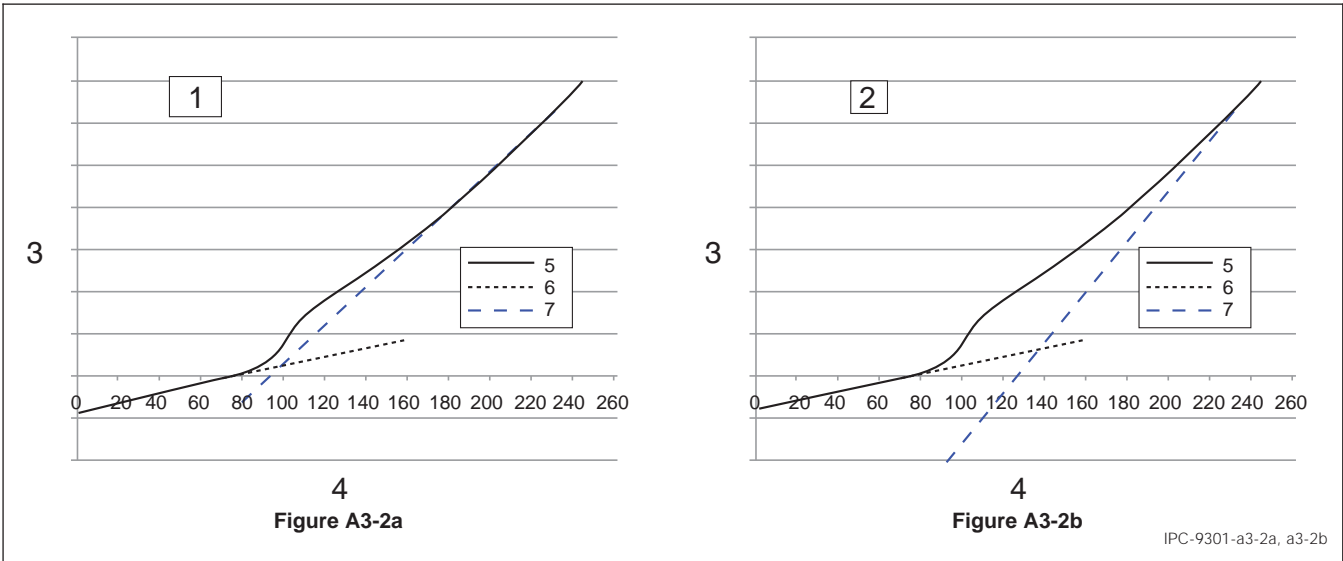


Figure A3-2a and Figure A3-2b Extraction of  $T_g$  by Tangents from TMA Measurement.

- Note 1:** Meaningful Example  $T_g = 98\text{ }^{\circ}\text{C}$
- Note 2:** Bad Example  $T_g = 140\text{ }^{\circ}\text{C}$
- Note 3:** Dimensional Change [ $\mu\text{m/m}$ ]
- Note 4:** Temperature [ $^{\circ}\text{C}$ ]
- Note 5:** TMA Measurement
- Note 6:** Tangent Below  $T_g$
- Note 7:** Tangent Above  $T_g$

**Note:** In the example on the left, the tangents are well-chosen and the intersection is close to the location of the glass transition region. In the example on the right, the tangent above  $T_g$  is far off leading to an intersection which is far away from the actual glass transition region and, thus, to an incorrectly reported  $T_g$ .

**A3.1.1.2 Characterization the Viscoelasticity using DMA** Visco-elastic material properties are usually derived from experimental tests like DMA. The machine settings and sample preparation can significantly impact the results of a DMA test. The following test parameters and sample preconditioning are recommended for performing DMA testing (Table A3-2).

The standards ASTM D7028 and E1640 describe the extraction of the glass transition temperature from DMA measurement “DMA  $T_g$ ”. This extraction is also based on the construction and intersection of tangents, but uses an approach different from the one described for TMA in ASTM E1545 and as a consequence, leads to different  $T_g$  values.

**Table A3-2 Recommended DMA Parameters**

DMA Test Parameters	Recommendation
Test Mode	Three Point Bending (3PB)
Sample Preconditioning	As required for the considered simulation case. e.g., 4h PMC + 24h bake at 125 °C
Temperature Ramp Rate (°C/min)	5 (could be lower for continuous sweep measurement with low frequencies)
Frequency for elastic properties (Hz)	1
Frequency range for viscoelastic properties (Hz)	0.01 to 50
Dynamic force control (method and value)	Amplitude control, 10µm
Preload dynamic force	Apply force to ensure amplitude >1µm
Temperature Range (min, max °C)	Equipment Specific (typical value: -55 - 260 °C)
*Length to thickness aspect ratio (Per ASTM D790)	Highest possible aspect ratio achievable given machine limits, but not less than “16:1”. Sample dimensions should be chosen in order to minimize side effects on measured Young’s modulus
*Max Strain Limit (Per ASTM D790)	5%

#### A4 DETERMINATION OF GLASS TRANSITION FROM DMA/TMA

**A4.1 DMA/TMA TESTING** The procedure described below allows determination of glass transition temperature from DMA/TMA measurements. It can be applied to data obtained under any test conditions, including standard ones, defined by ASTM D7028.

The fitting algorithm is based on least-squares optimization, which provides the best possible fit between DMA/TMA test data and tri-linear/bi-linear functions respectively. The glass transition temperature is defined as the intersection point of the first two lines.

The method offers several advantages:

- The application of least-squares optimization to measured data ensures that for the same data set fitted parameters will be the same. The  $T_g$  (defined as intersection of two lines) is very sensitive to how the lines are plotted
- The glass transition temperatures determined from DMA and TMA are often very similar. This is because the beginning of glass transition affects mechanical and thermal properties simultaneously
- It determines not only  $T_g$  in unique way, but also CTE1/CTE2 and  $E(T)$  as well

**A4.1.1 Method Description** Test data are interpolated by piecewise linear functions:

- DMA: tri-linear, four unknown parameters:  $T_g$ ,  $E(T_g)$ ,  $T_g^2$ ,  $E(T_g^2)$ . Four fixed parameters:  $T_{min}$ ,  $E(T_{min})$ ,  $T_{max}$ ,  $E(T_{max})$
- TMA: b-linear, four unknown parameters:  $T_g$ ,  $eth(T_g)$ ,  $eth(T_{min})$ ,  $eth(T_{max})$ . Two fixed parameters:  $T_{min}$ ,  $T_{max}$  Objective function of least-squares optimization (TMA):

$$\sum_{\text{Num. of temp. points}} [\epsilon_{measured}^{th}(Temp_i) - \epsilon_{bi-linear}^{th}(Temp_i)]^2 \rightarrow \min$$

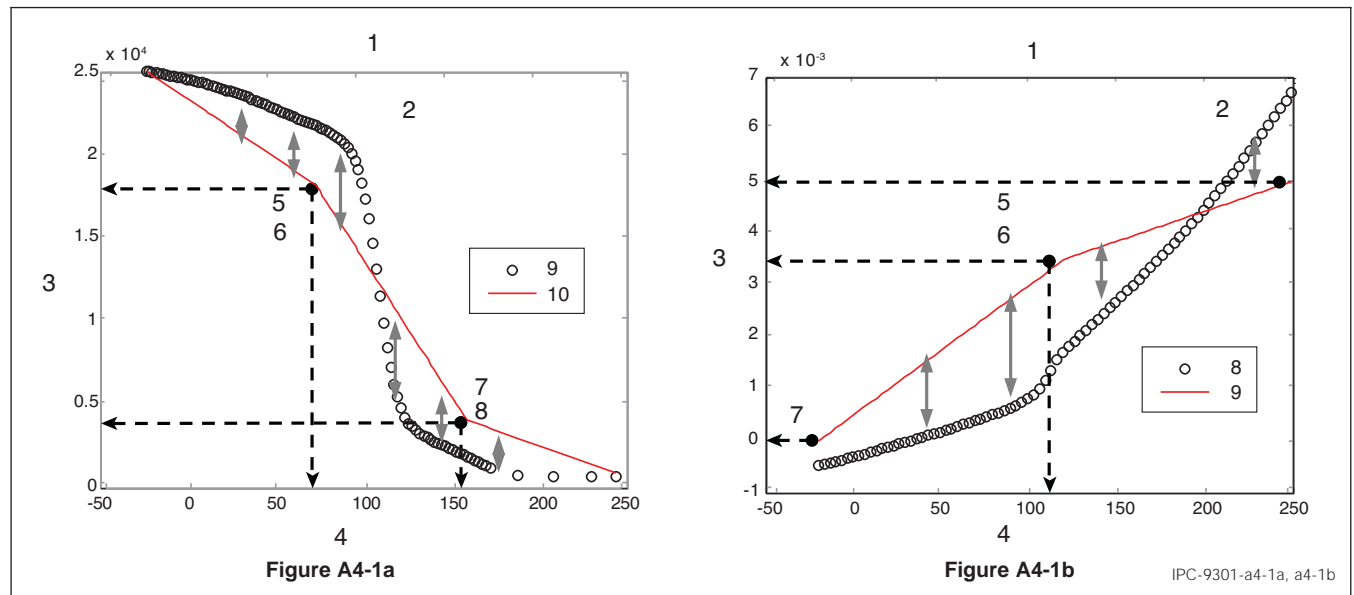


**Figure A4-1a and Figure A4-1b Tri-linear (left) and Bi-linear (right) Interpolating Functions for Fitting of DMA/TMA Data Respectively**

**Figure A4-1a:**

**Note 1.** DMA Least - Squares Fitting

**Note 2.**  $T_{(min)}$ ,  $T_{(max)}$ ,  $E(T_{min})$ ,  $E(T_{max})$  - are Fixed

**Note 3.** Storage Modulus [MPa]

**Note 4.** Temperature [°C]

**Note 5.** Var1:  $T_g$

**Note 6.** Var2:  $ET_g$

**Note 7.** Var3:  $T_g^2$

**Note 8.** Var4:  $E(T_g^2)$

**Note 9.** DMA Data

**Note 10.** Fitted

**Note:** Grey arrows illustrate deviation, which will be minimized

**Figure A4-1b:**

**Note 1.** TMA Least - Squares Fitting

**Note 2.**  $T_{min}$ ,  $T_{max}$  - are Fixed

**Note 3.** Thermal Strain

**Note 4.** Temperature [°C]

**Note 5.** Var1:  $T_g$

**Note 6.** Var2:  $eth(T_g)$

**Note 7.** Var3:  $eth(T_{gmin})$

**Note 8.** Var4:  $eth(T_{gmax})$

**Note 9.** TMA Data

**Note 10.** Fitted

Application of the procedure is demonstrated for one particular molding compound (Figure A4-2a and Figure A4-2b). Glass transition temperatures, determined from both data sets (DMA/TMA) are the same: 96 °C. This is expected from physics, because beginning of glass transition affects mechanical and thermal properties simultaneously.

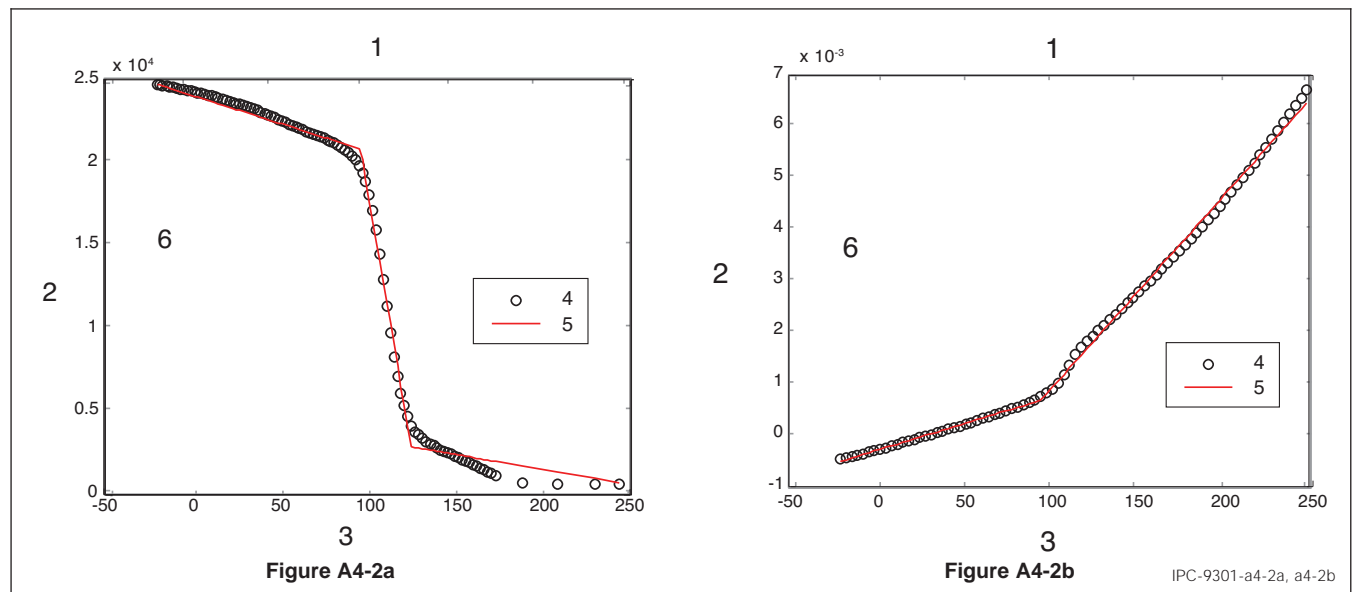


**Figure A4-2a and Figure A4-2b Example of Best Fit for DMA (left) and TMA (right) Data**

**Figure A4-2a:**

**Note 1.** DMA Least - Squares Fitting

**Note 2.** Storage Modulus [MPa]

**Note 3.** Temperature [°C]

**Note 4.** DMA Data

**Note 5.** Fitted

**Note 6.**  $T_g = 96$  °C  
 $E(-20$  °C) = 24760 MPa  
 $E(96$  °C) = 20856 MPa  
 $E(125$  °C) = 2863 MPa  
 $E(250$  °C) = 620 MPa

**Figure A4-2b:**

**Note 1.** TMA Least - Squares Fitting

**Note 2.** Thermal Strain

**Note 3.** Temperature [°C]

**Note 4.** TMA Data

**Note 5.** Fitted

**Note 6.**  $T_g = 96$  °C

CTE1 =  $1.03e-05$  1/k

CTE1 =  $1.03e-05$  1/k

**A4.1.2 Modeling the Thermal Expansion of Thermosetting Polymers** Depending on the FEA software used, different types of input for thermal expansion modeling are allowed:

- Thermal strain  $\epsilon_{th}$ , (e.g., THSX in ANSYS®)
- Instantaneous or local CTE  $\alpha_{th, inst}$  (e.g., CTEX in ANSYS®)
- Secant CTE  $\alpha_{th, secant}$  (e.g., ALPX in ANSYS®, “\*Expansion, Zero=” for secant CTE and reference definition in ABAQUS®)

As the CTE of thermosetting polymers changes with temperature, it is essential to understand the differences of the listed modeling options. In this section, the process of using the characteristic result of a thermal expansion measurement of a thermosetting polymer is outlined. The primary data obtained from a thermal expansion measurement is the change in length over temperature and thus, the thermal strain over temperature (see dashed line in Figure 4-1a and Figure A4-1b). If the FEA software allows for direct use of this data as input while automatically accounting for the reference temperature, no further action is required from the user.

If the instantaneous or local CTEs are to be used, the instantaneous CTEs  $\alpha_{th, inst, 1}$  and  $\alpha_{th, inst, 2}$  need to be extracted from the slope over a suitable temperature range as described in section A3.1.1.1. The resulting instantaneous CTE over temperature which then needs to be implemented in the FEA software is shown in Figure A4-4. The advantage of using instantaneous or local CTEs is that this type of thermal expansion modeling is independent of the reference temperature set for a material.

Most FEA simulation software use an upfront calculated secant CTE as it allows directly inferring the thermal expansion w.r.t. the reference temperature of a material. Figure A4-3 shows the extraction of the secant CTE  $\alpha_{th, secant}$  taking 25 °C as reference temperature. The secant CTE gives an effective value over regions of different instantaneous CTEs (Figure A4-5):

$$\alpha_{th, secant, Tref=25^{\circ}C} = \frac{\Delta\epsilon_{th, Tref=25^{\circ}C}}{\Delta T}$$

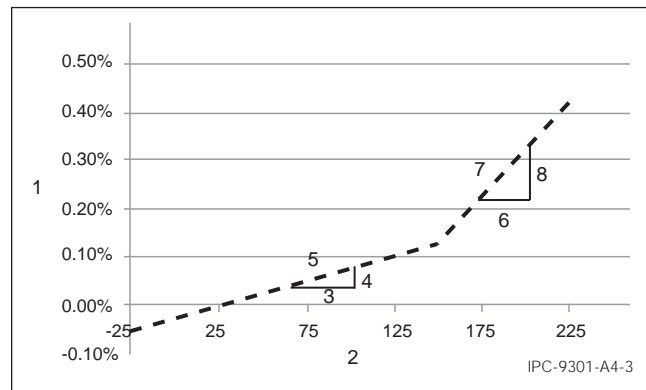


**Figure A4-3 Thermal Expansion Measurement of a Thermosetting Polymer and the Extraction of Instantaneous CTEs from Measured Thermal Strain Data**

- Note 1.** Thermal Strain  
**Note 2.** Temperature [°C]  
**Note 3.**  $\Delta T_1$   
**Note 4.**  $\Delta \epsilon_{th, 1}$   
**Note 5.**  $\alpha_{th, inst, 1}$   
**Note 6.**  $\Delta T_2$   
**Note 7.**  $\Delta \epsilon_{th, 1}$   
**Note 8.**  $\alpha_{th, inst, 2}$

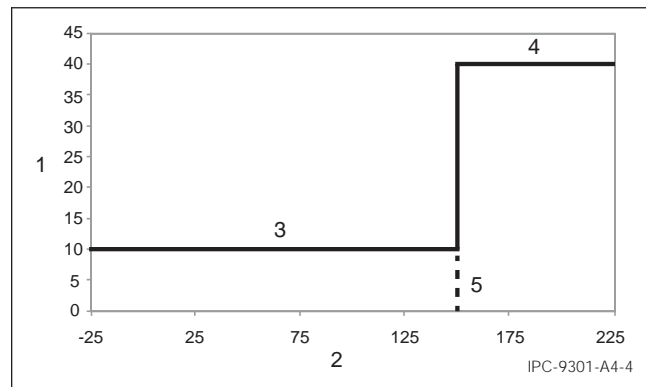


**Figure A4-4 Extracted Instantaneous CTE  $\alpha_{th, inst}$  Over Temperature. The instantaneous CTE  $\alpha_{th, inst}$  Changes at the Glass Temperature  $T_G$**

- Note 1.** Instantaneous CTE [ppm/°C]  
**Note 2.** Temperature [°C]  
**Note 3.**  $\alpha_{th, inst, 1}$   
**Note 4.**  $\alpha_{th, inst, 2}$   
**Note 5.**  $T_G$

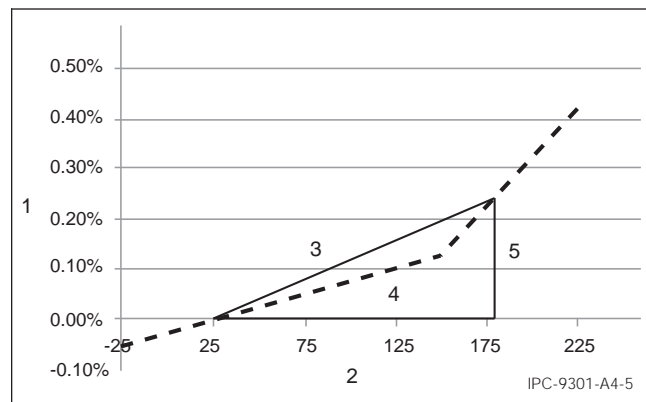


**Figure A4-5 Extraction of the Secant CTE  $\alpha_{th, secant}$  from Measured Thermal Strain Data for the Reference Temperature of 25 °C**

- Note 1.** Thermal Strain  
**Note 2.** Temperature [°C]  
**Note 3.**  $\alpha_{th, secant, Tref=25^{\circ}C}$   
**Note 4.**  $\Delta T$   
**Note 5.**  $\Delta \epsilon_{th, Tref=25^{\circ}C}$

As the secant CTE of the thermal expansion is now an effective CTE related to the reference temperature of 25 °C (in this illustrative example), the secant CTE over temperature is fundamentally different from the instantaneous CTE (see Figure A4-6).

Data sheets usually report instantaneous CTEs  $\alpha_{th,inst}$ , denoted as e.g., CTE, CTE1, CTE2 or ALPHA. These CTEs must not be confused with secant CTEs which have, as shown, a very different interpretation. Both secant and instantaneous input can lead to correct analysis result. The user should be familiar with the software available and use the correct settings. If uncertain, a test case can be used with simple structure to explore the whole temperature range.

**A4.1.3 Modeling the Viscoelasticity of Thermosetting Polymers** Analogous to the thermal expansion, the mechanical modulus also changes over temperature. The behavior during the glass transition is also nonlinear. Figure A4-7 shows which type of modeling is recommended for which case. The following modeling approaches are considered:

- LE: Linear elastic modeling
- LVE: Linear viscoelastic modeling
- NLVE: Nonlinear viscoelastic modeling

The following sections briefly cover material models which can be employed for LVE and NLVE modeling of molding compounds.

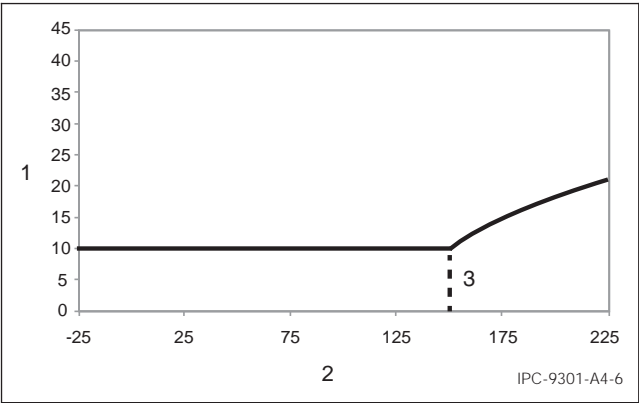


**Figure A4-6** Extracted Secant CTE  $\alpha_{th,secant}$  Over Temperature for a Reference Temperature of 25 °C

- Note 1.** Secant CTE [ppm/ °C]  
**Note 2.** Temperature [°C]  
**Note 3.**  $T_G$

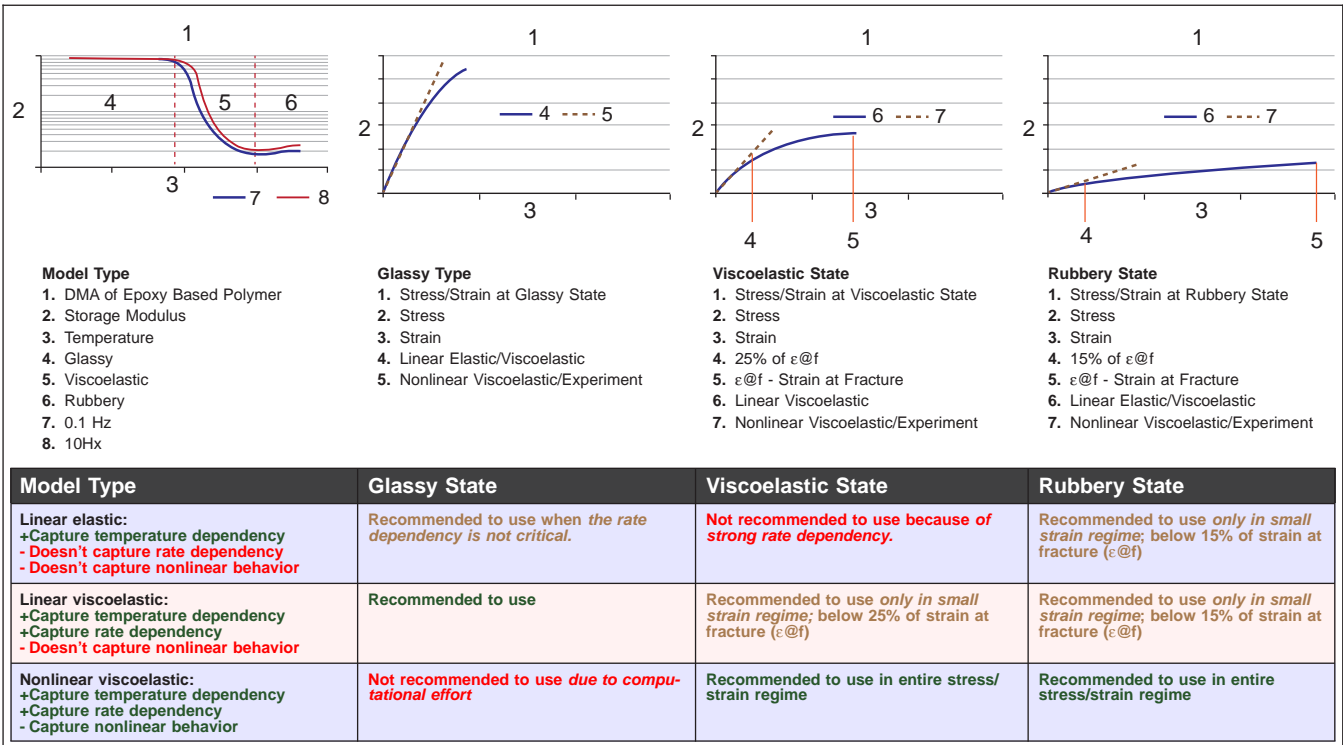


**Figure A4-7** Overview Viscoelastic Modeling

**A4.1.3.1 Linear Viscoelastic Modeling (LVE)** LVE modeling, which is only valid in the small strain regime, can be captured by various material models. A common LVE modeling approach is to use a compact model consisting of several spring-damper elements in parallel (see Figure A4-8). Each spring-damper element models an exponential decay with a respective magnitude and time constant. Consequently, the resulting relaxation of the material is formulated as a sum of exponential decays with respective magnitudes and time constants. This approach is also known as generalized Maxwell model or Prony series approach where the magnitudes and time constants are considered to as Prony pairs or parameters.

The viscoelastic response varies with temperature. For Prony series, the temperature dependence of the viscoelastic behavior can either be modeled by giving Prony series for different temperatures or by using a shift function [6]. In short, the procedure is as follows:

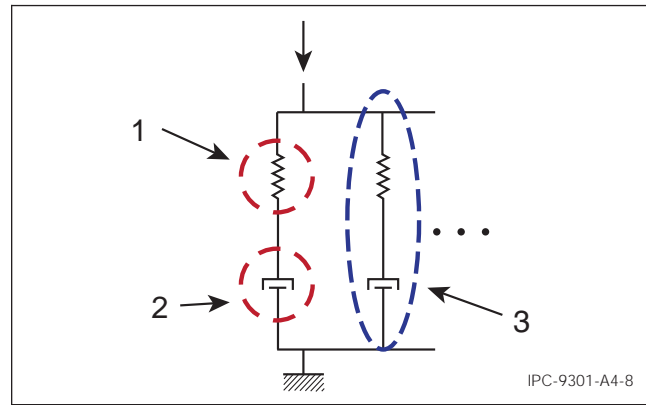


**Figure A4-8 Illustration of the Linear-Viscoelastic Material Modeling Approach Using the Generalized Maxwell Model Consisting of Several Spring-Damper Elements**

**Note 1.** Spring (elastic part)

**Note 2.** Damper (viscous viscous)

**Note 3.** One "Prony pair"

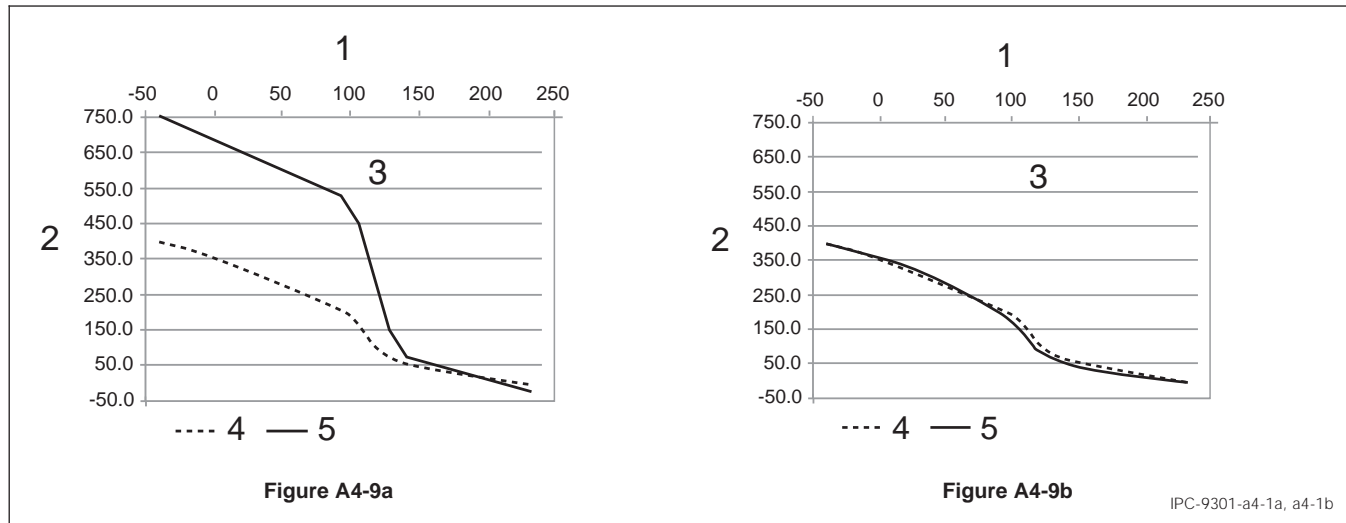


**Figure A4-9a and Figure A4-9b Measurement and the Simulation of the Deflection Over Temperature of a Bi-material Beam Consisting of Molding Compound and Silicon. The Linear-elastic (LE) Model Clearly Overestimates the Deflection Whereas the LVE Model can Reproduce the Deflection Correctly**

**Figure A4-9a**

**Note 1.** Temperature, °C

**Note 2.** Displacement, µm

**Note 3.** Linear Elastic Model

**Note 4.** Experiment

**Note 5.** Simulation

**Figure A4-9b**

**Note 1.** Temperature, °C

**Note 2.** Displacement, µm

**Note 3.** Visco-Elastic Model

**Note 4.** Experiment

**Note 5.** Simulation

1. Perform DMA measurements over temperature with different frequencies
2. Perform shifting of the measured data in order to generate a master curve and a shift curve
3. Fit the master curve using a Prony series and the shift curve using a suitable function (e.g., WLF)

To demonstrate the benefit of using LVE modeling instead of Linear-Elastic (LE) modeling with datasheet values, a bi-material beam consisting of silicon and molding compound was produced and its deflection over temperature both measured and simulated (Figure A4-9a and Figure A4-9b). In contrast to the LVE mode, the LE model clearly overestimates the deflection as it does not take the relaxation effects inside glass transition region into account. Consequently, the viscoelasticity of thermosetting polymers should be modeled wherever applicable.

**A4.1.3.2 Nonlinear Viscoelastic Modeling (NLVE)** The small strain assumption is not always valid. When thermosetting polymers are loaded in a relatively high stress/strain regime, they start behaving in a nonlinear way. This kind of behavior cannot be captured by LVE models. The nonlinear behavior, unlike most metals is caused by a crystalline scale dislocation. In the case of epoxy-based thermosetting polymers, plastic deformation is governed by a viscous, rate dependent behavior. This requires a different approach that can capture rate dependency, nonlinear stress/strain relationship and relaxation.

To investigate the nonlinear behavior of epoxy-based thermosets, the following two tests are recommended (Figure A4-10a and Figure A4-10b):

- Uniaxial, tensile stress test until failure (Figure A4-10 a)
- Uniaxial tensile stress with relaxation segments (Figure A4-10b)

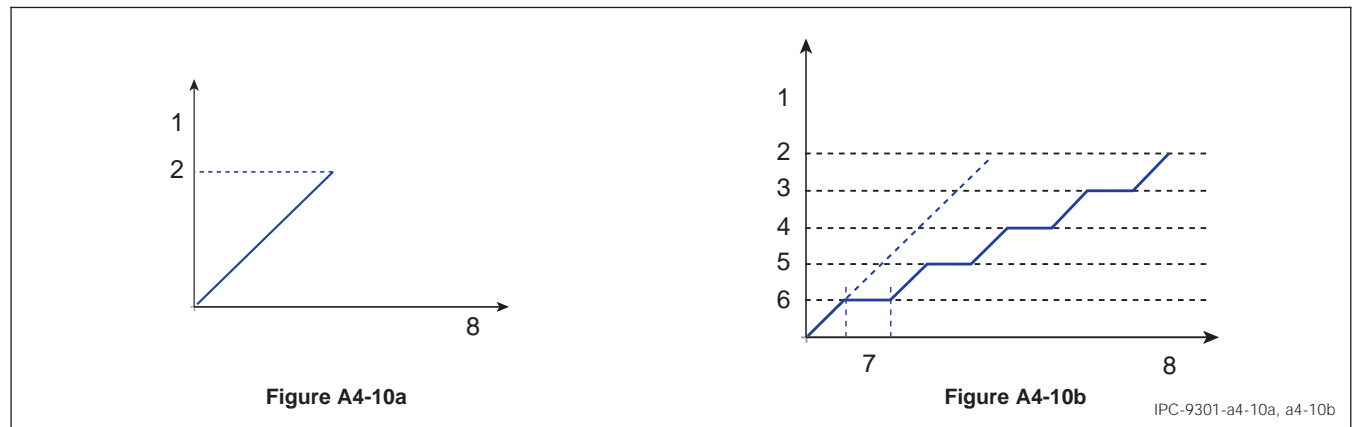


**Figure A4-10a and Figure 4-10b Schematic Representation of the Tests Until Failure: a) Tensile Test Until Failure, b) Tensile Test Until Failure with Relaxation Segments**

**Note 1.**  $\mu$  [mm]

**Note 2.**  $\mu_{\max}$

**Note 3.** 80%  $\mu_{\max}$

**Note 4.** 60%  $\mu_{\max}$

**Note 5.** 40%  $\mu_{\max}$

**Note 6.** 20%  $\mu_{\max}$

**Note 7.** 120 s

**Note 8.**  $T_{[min]}$

- These tests should be performed at different temperatures and with different strain rates. More tests should be done in the glass transition temperature region where time dependent effects play a significant role. The relaxation time strongly depends on the temperature. At low temperature, the relaxation time should be relatively large: recommended to be minimum 2 hours. At high temperature this time can be shortened to 15 minutes or even as low as 2 minutes. It is very important, especially at low temperature, to have a relatively long relaxation time. Otherwise, the relaxation behavior in simulations can be exaggerated due to relatively fast relaxation at the initial stage of the test.
- Figure A4-11a Depicts the mechanical response of a fully cured epoxy resin subjected to a tensile test until failure at different temperatures starting from room temperature up to 175 °C with a fixed loading rate of 1 mm/min. From the stress-strain curve, it is clear that there is a significant temperature effect on the mechanical behavior of the epoxy based molding compound. At 25 °C, the thermoset resin is capable of withstanding relatively high stress. When the temperature is increased, there is a decrease in the maximum stress at which the material fails.
- Figure A4-11b. Depicts the relaxation behavior of the investigated molding compound. At room temperature, the fully cured thermoset resin does not undergo much relaxation as compared to higher temperatures. For instance, at 25 °C, the stress relaxes by nearly 5%. But when the temperature is increased, the magnitude of stress relaxation is higher. At 100 °C, the stress relaxes by about 20%.



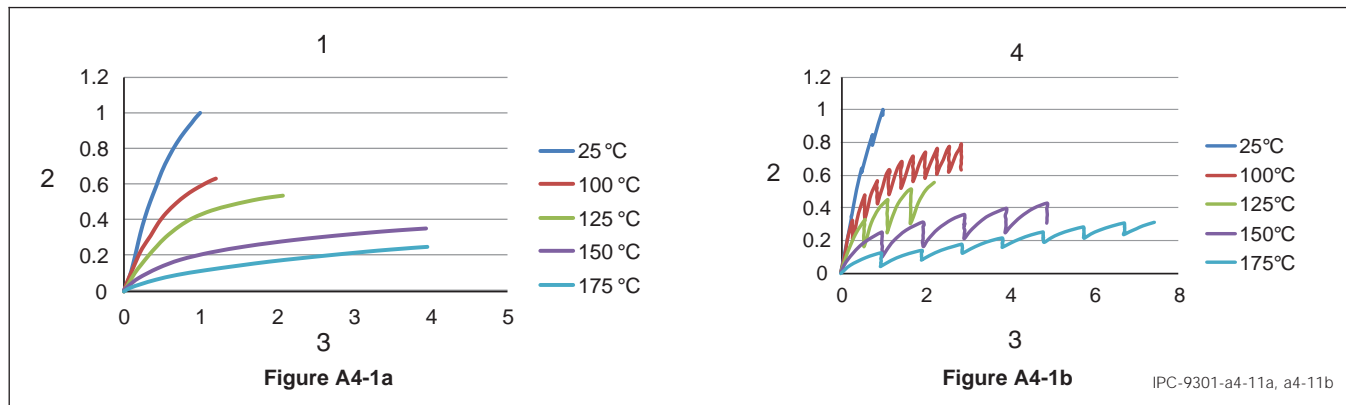


**Figure A4-11a Results of the Tensile Tests Until Failure at Different Temperatures**

**Figure A4-11b Stress Relaxation of the Investigated Molding Compound**

**Note 1.** Effect of the temperature at 1.0 mm/min

**Note 3.** Normalized Strain

**Note 2.** Normalized Stress [MPa]

**Note 4.** Relaxation Behaviour

To model the NLVE behavior of epoxy based thermosets, the material model needs to capture temperature dependency, time dependency, stress dependent relaxation, as well as nonlinear behavior. In commercially available FEA software, an example of such a model is the Bergstrom-Boyce model, which can be used to model all required physical behavior (e.g., time, temperature and strain dependency of the thermo-mechanical response of the material under tensile testing conditions)

Bergstrom [19], [20] proposed that the material response can be represented by two interacting macromolecular networks (Figure A4-12) the first network A, represents the equilibrium response, and it consists of a hyper-elastic element. The second network B, represents a time-dependent deviation from equilibrium. Network B consist of a spring element and a nonlinear, time-dependent element (dashpot) that acts to relieve the strain on the network with time.

There are two major differences between the LVE and NLVE material model. The first difference is the nonlinear behavior. Figure A4-13 shows results from the tensile test to failure at 125 °C LVE and NLVE material models. The LVE has only limited capability to predict behavior of the material correctly that is restricted to the low strain regime, which in this particular case is below 0.1%.

The second advantage of using NLVE is that NLVE can capture a stress dependent relaxation. Experimental results compared with the results from simulation utilizing stress at ultimate failure show that the LVE model results are exaggerated by a factor of 2.5. The NLVE model fits the experimental results very well in the entire stress strain regime.

**A4.1.4 Modeling the Cure Shrinkage of Thermosetting Polymers** Thermosetting polymers usually show volumetric shrinkage after application and/or curing at higher temperature. The driving process for the shrinkage is polymerization. The resulting shrinkage induces intrinsic deformation and

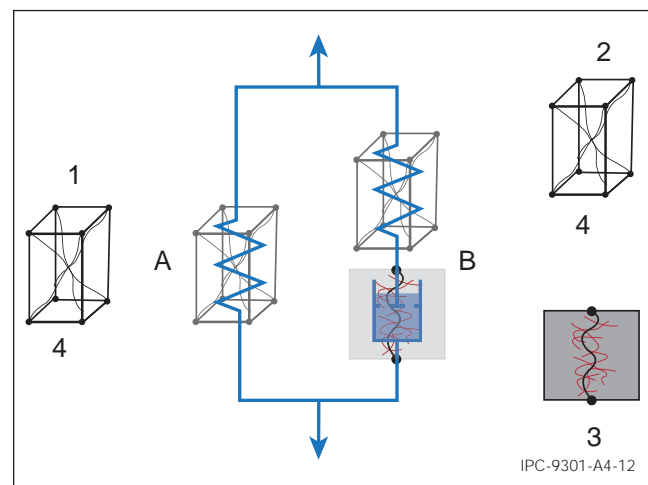


**Figure A4-12 Representation of the Bergstrom-Boyce Model**

**Note 1.** Equilibrium Response

**Note 2.** Time-Dependent Response

**Note 3.** Viscoelastic Flow Capture using a Reptation-Based Energy Representation

**Note 4.** 8-Chain Model

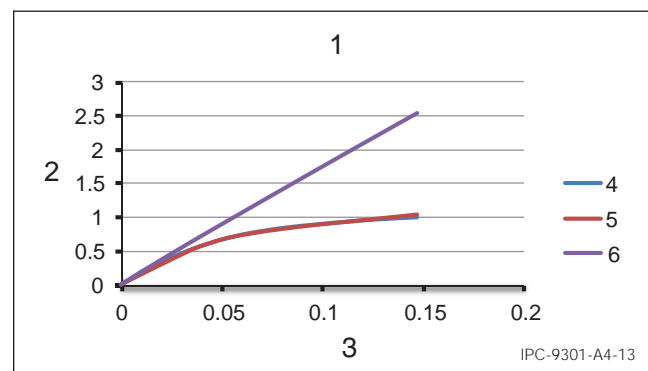


**Figure A4-13 Results of Experiment and Simulation of the Tensile Test Until Failure at 125 °C and the Load Rate of 1.0 mm/min**

**Note 1.** Molding Compound - Tensile Test until Failure @125 °C/load rate of 1.0 mm/min

**Note 3.** Displacement [mm]

**Note 4.** EXP

**Note 5.** NLVE

**Note 2.** Normalized Stress [MPa]

stresses in systems consisting of multiple materials and needs to be taken into account, e.g., for the accurate prediction of deformation over temperature.

In [21], the presence of cure shrinkage is illustrated by measuring the warpage of bi-material beam samples made of copper and molding compound over temperature. The samples show non-zero warpage at their assembly temperature of 175 °C. The scheme of cure shrinkage is outlined in Figure A4-14:

1. The uncured polymer has a defined initial volume at room temperature.
2. When heated, the  $T_{g1}$  of the uncured polymer is passed.
3. The curing temperature  $T_{cure}$  is reached and held for a defined time (usually >1hour).
4. During the dwell at  $T_{cure}$ , polymerization takes place resulting into volumetric shrinkage.
5. When cooled down, the  $T_{g2}$  of the cured polymer is passed. (Note that  $T_{g2}$  is higher than  $T_{g1}$ ).
6. At room temperature, the polymer has less volume than at (1).

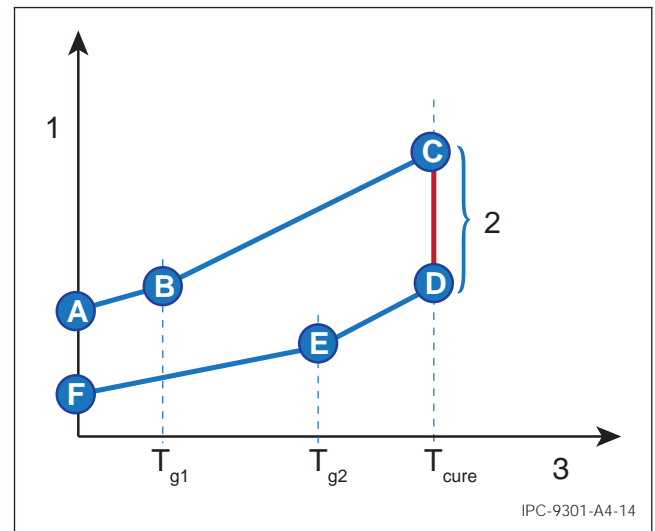


**Figure A4-14 Scheme of Curing Shrinkage During Polymerization Process of Molding Compound [7]**

**Note 1.** Volume

**Note 2.** Chemical Shrinkage

**Note 3.** Temperature

Only a fraction of the overall volumetric shrinkage induces intrinsic stresses and deformations in multi-material systems. This fraction is often referred to as effective cure shrinkage [7] and is the one which needs to be taken into account in simulation. Please refer to [22], [23], [24] for more details on the curing process and its impact on material properties.

Four approaches are commonly used to model the effective cure shrinkage in simulation:

- a. Pre-strain:** The effective cure shrinkage is applied as a negative pre-strain to the elements representing the molding compound.
- b. Shift of reference temperature:** The reference temperature of the molding compound material, i.e., the temperature where the molding compound has zero thermal strain is shifted to a higher temperature in order to account for the additional shrinkage. The temperature shift can be calculated from the effective shrinkage and the coefficient of thermal expansion above glass transition, also known as “CTE2”.
- c. Swelling:** Equations e.g., implemented for the simulation for swelling due to moisture are used to induce the effective cure shrinkage.
- d. Direct implementation:** Some FEM software allows for accounting directly for the cure shrinkage. Refer to the software technical documentation for software specific best practices. From a physics point of view and if the software used allows for it, it is recommended to use an approach which allows to separate chemical and thermal shrinkage from each other.

## A5 OTHER MATERIAL PROPERTIES

**A5.1 Poisson’s Ratio** The elongation of a member caused by an axial tensile force in the direction of the force is accompanied by contractions of the member in the transverse directions. Poisson’s ratio,  $\nu$  defines the ratio of the transverse strain to that in the axial direction:

$$\nu = - \frac{\text{transverse strain}}{\text{axial strain}}$$

Isotropic materials have a single Poisson’s ratio which is applicable to all loading cases. Orthotropic materials require the definition of 3 Poisson’s ratios corresponding to the 3 orthogonal material property axes.

The constitutive law for an orthotropic material is presented below (Figure A4-15). Since the compliance matrix is symmetric, the off-diagonal terms must be equivalent. As a result,  $\nu_{ij} = E_i * \nu_{ji} / E_j$  and only 3 unique Poisson’s ratios need to be defined.

$$\begin{Bmatrix} e_x \\ e_y \\ e_z \\ 2e_{yz} \\ 2e_{xz} \\ 2e_{xy} \end{Bmatrix} = \begin{bmatrix} \frac{1}{E_x} & \frac{-\nu_{yx}}{E_y} & \frac{-\nu_{zx}}{E_z} & 0 & 0 & 0 \\ \frac{-\nu_{xy}}{E_x} & \frac{1}{E_y} & \frac{-\nu_{zy}}{E_z} & 0 & 0 & 0 \\ \frac{-\nu_{xz}}{E_x} & \frac{-\nu_{yz}}{E_y} & \frac{1}{E_z} & 0 & 0 & 0 \\ 0 & 0 & 0 & \frac{1}{G_{yz}} & 0 & 0 \\ 0 & 0 & 0 & 0 & \frac{1}{G_{xz}} & 0 \\ 0 & 0 & 0 & 0 & 0 & \frac{1}{G_{xy}} \end{bmatrix} \begin{Bmatrix} \sigma_x \\ \sigma_y \\ \sigma_z \\ \sigma_{yz} \\ \sigma_{xz} \\ \sigma_{xy} \end{Bmatrix}$$

IPC-9301-A4-15

**Figure A4-15 Constitutive Law for an Orthotropic Material**

While test standards such as ASTM E132-04 and D638-10 specify procedures, the analyst needs to consider the source of the Poisson's ratio property and understand its interpretation by the finite element code. Different software requires input of Poisson's ratio differently. Refer to the software technical documentation for more details.

**A5.2 Density** The density of a material is a critical material property for transient or dynamic analysis. Examples include transient thermal simulations or mechanical shock/vibration simulations. While the density of some basic materials can be obtained from the literature, the density of composite materials (such as laminated printed circuit boards) is more difficult to obtain. Accurate, standard measurement of density is key to ensuring accurate models. Some relevant standards for density measurements are:

1. ASTM B962-14, Standard Test Method for Density of Compacted or Sintered Powder Metallurgy (PM) Products using Archimedes' Principle
2. ASTM B311-13, Standard Test Method for Density of Powder Metallurgy (PM) Materials Containing Less Than Two Percent Porosity

## APPENDIX B

### DMA/TMA Fitting Algorithms

**B1 DMA FITTING SCRIPT** The analysis script for performing the DMA fitting analysis is outlined in the following section.

" " "

Algorithm Author: Sergey ANANIEV

Contact: Infineon Technologies AG

Am Campeon 1-12

85579 Neubiberg

Email: Sergey.Ananiev@infineon.com

Python Script Authors: Tuhin Sinha and Max Cioban

Contact: IBM Systems - Hopewell Junction, NY

Email: tsinha@us.ibm.com and mcioban@us.ibm.com

Please install the required python libraries and distributions before running the script. Refer to the imported libraries below. It is recommended to use Anaconda utility as a python installer which installs all the necessary libraries by default (<https://www.continuum.io/downloads>)

We recommend installing Python 2.7®

Description:

- fits Storage Modulus  $E(T)$  from DMA data by tri-linear function
- 4 optimization parameters:  $T_g$ ,  $T_{gR}$ ,  $E(T_g)$ ,  $E(T_{gR})$
- $T_g$  is defined as intersection of first two lines
- $T_{min}$ ,  $T_{max}$  are defined by user (as a 'trusted' data window)
- $E(T_{min})$ ,  $E(T_{max})$  are taken directly from DMA data
- fitted  $E(T)$  is saved in 'DMA\_Fitting.txt'

" " "

```
import matplotlib.pyplot as plt
import pandas as pd
import numpy as np
from scipy.optimize import curve_fit
import os
nIter = 0
#%%
## Fitting function
def three_lines(x, a,b,c,d):
    global nIter
    data_size = len(x)
    nIter=nIter+1
    y = np.zeros(data_size)
    for i in range(data_size):
        if x.iloc[i] < c:
            y[i] = Emin + (a-Emin)/(c-Tmin)*(x.iloc[i]-Tmin)
        elif x.iloc[i] < d:
            y[i] = a+(b-a)/(d-c)*(x.iloc[i]-c)
        else:
            y[i] = b+(Emax-b)/(Tmax-d)*(x.iloc[i]-d)

    return y
#%% Set the work directory
```

```

dirPath='/Users/tsinha/Documents/Python Scripts/DMA_TMA_analysis'
os.chdir(dirPath)

#Read in data. Skips the first 61 rows in data file. Modify as needed.
DMA_data = pd.read_csv('dma.txt', sep= ' ' , header=61)
DMA_t = DMA_data[DMA_data.columns[1]] #temperature
DMA_e = DMA_data[DMA_data.columns[2]] #storage modulus
#%%
# Define datgTa window for fitting
Tmin = -20.0
Tmax = 250.0

#indices of data window
Tmin_id = np.argmax(DMA_t>Tmin)
Tmax_id = np.argmin(DMA_t<Tmax)

#data for optimization
DMA_t_optim = DMA_t[Tmin_id:Tmax_id]
DMA_e_optim = DMA_e[Tmin_id:Tmax_id]
Emin = DMA_e_optim.iloc[0]
Emax = DMA_e_optim.iloc[-1]
Tmin = DMA_t_optim.iloc[0]
Tmax = DMA_t_optim.iloc[-1]

#initial guess
fit0 = [18000, 4000, 75, 160]
Eg = fit0[0]
EgR = fit0[1]
Tg = fit0[2]
TgR = fit0[3]

#%% Fitting fuction
fit, cov = curve_fit(three_lines, DMA_t_optim, DMA_e_optim, fit0)
#
#%%Plotting
max_id = len(DMA_t_optim)
DMA_t_optim_red = DMA_t_optim[0:max_id:20] #reduce points for plotting
DMA_e_optim_red = DMA_e_optim[0:max_id:20] #reduce points for plotting
plt.plot(DMA_t_optim_red, DMA_e_optim_red,
ls='-',marker='o',markeredgecolor='black',\markerfacecolor='none')
plt.plot(DMA_t_optim, three_lines(DMA_t_optim, *fit), 'r-')
plt.annotate('Tg='+str(round(fit[2],2))+ '$\degree$C',xy=(-45,15000),fontsize=10,)
plt.annotate('E ('+str(round(Tmin,0))+ '$\degree$C)='+str(round(Emin,2))+ ' MPa',xy=(-45,13000),fontsize=10,)
plt.annotate('E ('+str(round(fit[2],2))+ '$\degree$C)='+str(round(fit[0],2))+ ' MPa',xy=(-45,11000),fontsize=10,)
plt.annotate('E ('+str(round(fit[3],2))+ '$\degree$C)='+str(round(fit[1],2))+ ' MPa',xy=(-45,9000),fontsize=10,)
plt.annotate('E ('+str(round(Tmax,0))+ '$\degree$C)='+str(round(Emax,2))+ ' MPa',xy=(-45,7000),fontsize=10,)
plt.xlabel('Temperature [C]', fontsize=12)
plt.ylabel('Storage Modulus [MPa]', fontsize=12)
plt.title('DMA least-squares fitting', fontsize=16)
plt.ylim(ymin=0,ymax=25000)
plt.xlim(xmin=-50,xmax=250)
plt.legend(['DMA Data','DMA Fitted'])
plt.savefig('DMA_fitting.jpg',dpi=300)
plt.show()

```

```
###Export fitted DMA parameters
OutFile=open('DMA_fitted.txt','w')
OutFile.write('OPTIMIZATION RESULTS'+'\n')
OutFile.write('Tmin'+'\t'+ 'Tg'+'\t'+ 'TgR'+'\t'+ 'Tmax'+'\t'+ 'E(Tmin)'+'\t'+\
'E(Tg)'+'\t'+ 'E(TgR)'+'\t'+ 'E(Tmax)'+'\n')
OutFile.write(str(round(Tmin,2))+'\t'+str(round(fit[2],2))+'\t'+str(round(fit[3],2))+\
'\t'+str(round(Tmax,2))+'\t'+\
str(round(Emin,2))+'\t'+str(round(fit[0],2))+'\t'+str(round(fit[1],2))+'\t'+str(round\
(Emax,2)))
OutFile.close()
```

**B2 TMA FITTING SCRIPT** The analysis script for performing the TMA fitting analysis is outlined in the following section.

"""

Algorithm Author: Sergey ANANIEV

Contact: Infineon Technologies AG  
Am Campeon 1-12  
85579 Neubiberg  
Email: Sergey.Ananiev@infineon.com

Python Script Authors: Tuhin Sinha and Max Cioban

Contact: IBM Systems - Hopewell Junction, NY  
Email: tsinha@us.ibm.com and mcioban@us.ibm.com

Please install the required python libraries and distributions before running the script. Refer to the imported libraries below. It is recommended to use Anaconda utility as a python installer which installs all the necessary libraries by default (<https://www.continuum.io/downloads>)

We recommend installing Python 2.7@

Description:

- fits thermal strains from TMA data by bi-linear function
- 4 optimization parameters: Tg, ETH(Tg), ETH(Tmin), ETH(Tmax)
- Tg is defined as intersection of fitted lines
- CTE1/2 are defined as first derivation of fitted lines
- Tmin, Tmax are defined by user (as a "trusted" data window)
- CTEs are saved in "TMA\_Fitting.txt"

"""

```
import matplotlib.pyplot as plt
```

```
import pandas as pd
```

```
import numpy as np
```

```
from scipy.optimize import curve_fit
```

```
import os
```

```
###
```

```
##Fitting Function
```

```
def two_lines(x, a, b, c, d):
```

```
    data_size = len(x)
```

```
    y = np.zeros(data_size)
```

```
    for i in range(data_size):
```

```
        if x.iloc[i] < d:
```

```
            y[i] = a + (c - a)/(d-Tmin)*(x.iloc[i]-Tmin);
```

```
        else:
```

```
            y[i] = c + (b - c)/(Tmax - d)*(x.iloc[i] - d);
```

```
    return y
```

```
### Set work directory
```

```
dirPath='C:\DMA_TMA_least-squares_ananiev'
```

```
os.chdir(dirPath)
```

```
#Read in data. Skips the first 46 rows in data file. Modify as needed.
```

```
TMA_text = pd.read_csv('tma.txt', sep= " ", nrows = 45)
```

```
TMA_data = pd.read_csv('tma.txt', sep= " ", header=46)
```

```
TMA_t = TMA_data[TMA_data.columns[1]] #temperature
```

```
TMA_line = pd.Series.to_string(TMA_text.iloc[12])
```

```
TMA_length = float(filter(unicode.isdigit, TMA_line))/100 #convert mm to um
```

```
TMA_e = TMA_data[TMA_data.columns[2]]/TMA_length #storage modulus
```

```
###
```



```

# Define datgTa window for fitting
Tmin = -20.0
Tmax = 250.0

#indices of data window
Tmin_id = np.argmax(TMA_t>Tmin)
Tmax_id = np.argmin(TMA_t<Tmax)

#data for optimization
TMA_t_optim = TMA_t[Tmin_id:Tmax_id]
TMA_e_optim = TMA_e[Tmin_id:Tmax_id]
ETHmin = TMA_e_optim.iloc[0]
ETHmax = TMA_e_optim.iloc[-1]
Tmin = TMA_t_optim.iloc[0]
Tmax = TMA_t_optim.iloc[-1]

#Initial guess
fit0=[0.0e-3, 5e-03, 3.5e-3, 120]
ETHmin = fit0[0]
ETHmax = fit0[1]
ETHg = fit0[2]
Tg = fit0[3]

# Fitting Function & CTE Calculations
fit, cov = curve_fit(two_lines, TMA_t_optim, TMA_e_optim, fit0)
CTE1 = (fit[2]-fit[0])/(fit[3]-Tmin)
CTE2 = (fit[1]-fit[2])/(Tmax-fit[3])

# Plotting
max_id = len(TMA_t_optim)
TMA_t_optim_red = TMA_t_optim[0:max_id:20] #reduce points for plotting
TMA_e_optim_red = TMA_e_optim[0:max_id:20]
plt.plot(TMA_t_optim_red, TMA_e_optim_red, 'o', TMA_t_optim, two_lines(TMA_t_optim, *fit), 'r-')
plt.annotate('Tg='+str(round(fit[3],2))+ '$\degree$C',xy=(-25,.004),fontsize=15,)
plt.annotate('CTE1='+str(round(CTE1,7))+ ' 1/K',xy=(-25,.0035),fontsize=15,)
plt.annotate('CTE2='+str(round(CTE2,7))+ ' 1/K',xy=(-25,.003),fontsize=15,)
plt.xlabel('Temperature [C]', fontsize=12)
plt.ylabel('Thermal Strain []', fontsize=12)
plt.title('TMA least-squares fitting', fontsize=16)
plt.ticklabel_format(style='sci', axis='y', scilimits=(0,0))
plt.legend(['TMA Data', 'TMA Fitted'], loc=4)
plt.savefig('TMA_fitting.jpg',dpi=300)
plt.show()

# Export fitted TMA parameters
OutFile=open('TMA_fitted.txt','w')
OutFile.write('OPTIMIZATION RESULTS'+'\n')
OutFile.write('Tmin'+'\t'+Tg+'\t'+Tmax+'\t'+CTE1+'\t'+CTE2+'\n')
OutFile.write(str(round(Tmin,2))+'\t'+str(round(fit[3],2))+'\t'+str(round(Tmax,2))+'\t'+str(round(CTE1,7))+'\t'+\
str(round(CTE2,7)))
OutFile.close()

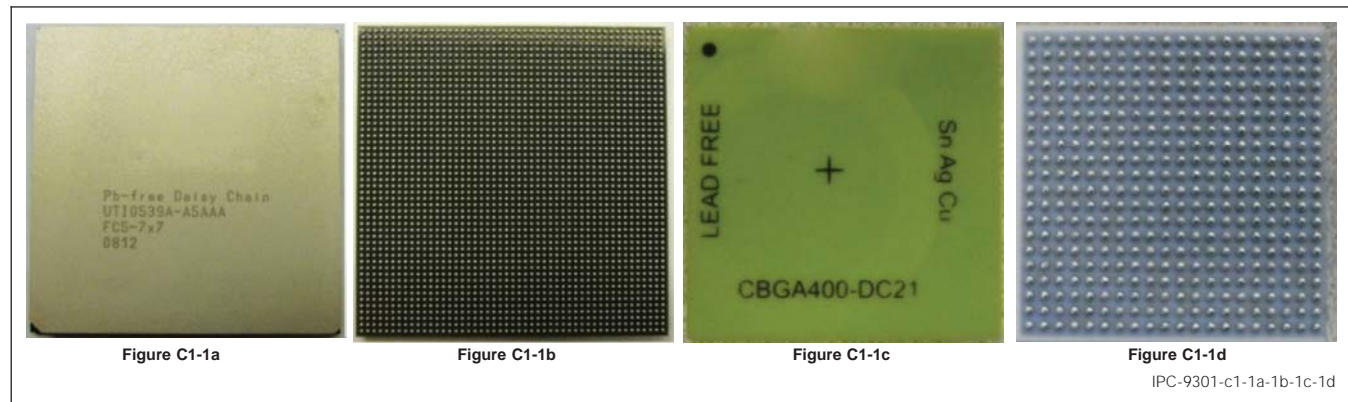
```

## APPENDIX C

### Experimental Benchmarking Model Case Study (Thermomechanical Board Level Joint Reliability)

#### C1 EXPERIMENTAL BENCHMARKING

**C1.1 Benchmarking Case Study** Tests of two organic (45mm FCBGA 1849 and 50mm FCBGA2401) and one ceramic (27mm CBGA400) package were selected for use in the study. These package types generally represent the extremes, both in terms of materials and fatigue lives, of large networking packages. These packages are shown in the figures below (Figure C1-1a, Figure C1-1b, Figure C1-1c, and Figure C1-1d) and a description of the relevant geometric attributes is presented in Table C-1.



**Figures C1-1a, C1-1b, C1-1c and C1-1d** Four Packages Selected for Case Study

**Table C1-1** Test Package Detail Information

Package type	FCBGA 2401	FCBGA 1849	CBGA 400
Package dimension (mm)	50x50	45x45	27x27
Substrate material	Organic 2-2-2 build-up	Organic	Ceramic
Substrate thickness (mm)	1.1	1.1	1
Die dimension (LxWxT) (mm)	22.27x22.27x0.765	17.3x17.3x0.725	None
BGA ball map	full array	full array	full array
BGA pitch (mm)	1	1	1.27
BGA ball size (mm)	0.6	0.6	0.75
BGA standoff (mm)	0.43	0.45	0.53
Substrate pad size (mm) Solder Mask Defined	0.4	0.53	0.65
PCB pad size (mm) Non Solder Mask Defined	0.56	0.56	0.56
Stiffener dimension (mm)	0.8 thick/5 width	0.66 thick/9 width	None
Lid thickness (mm)	0.5	1 (assumed)	None

All packages were assembled on High T<sub>g</sub> FR-4 (Isola 370HR) PCB with Pb-free OSP pad finish. The board thickness and layer count were: 23.622 mm (0.093 in.)/8 layers, and 3.302 (130 in.)/16 layers.

The assembled boards then went through temperature cycling under 2 profiles (Figure C1-2):

- Profile 1: standard IPC 0/100 °C profile with 40 minutes per cycle (10 minutes dwell and 10 minutes ramp);
- Profile 2: modified 0/100 °C profile to include mini-cycle effect with 90 minutes per cycle, the profile was modified based on the first standard profile by adding 10 mini cycles on hot dwell (10 °C swing and 5° C/min ramp)

Table C1-2 summarizes the experimental matrix and characteristic lives of the tested parts as influenced by the thermal profiles and PCB thickness. As can be seen in the table, the experimental setup can provide insight to the individual effects of package type, PCB thickness and thermal environment.

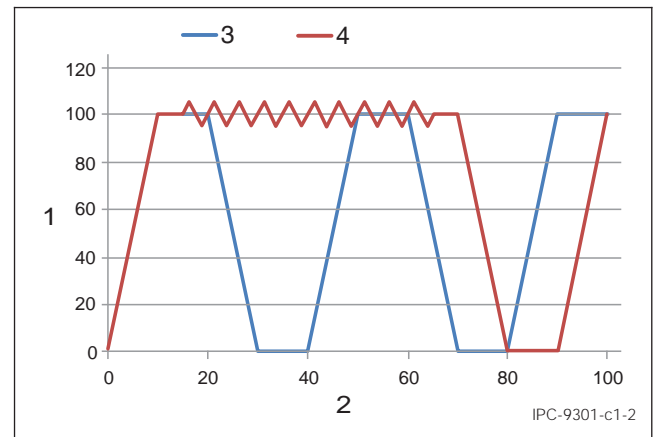


**Figure C1-2 Thermal Cycling Test Profiles**

**Note 1.** Temperature, Degree

**Note 2.** Time, minutes

**Note 3.** Std Profile

**Note 4.** Mini Cycle Profile

**Table C1-2 Experimental Thermal Cycling Data**

2p Weibull Characteristic Life (cycles)	Profile 1	Profile 2	PCB Thickness (mils)
FCBGA 2401	4769	—	130
FCBGA 1849	4867	—	130
FCBGA 1849	8683	—	93
CBGA 400	1508	790	93

For the tested packages, linear elastic properties were used in all subsequently discussed models (Table C1-3). These properties are accurate for the specific packages tested and representative of those for many similar packages. A note indicates where properties differ among models.

**Table C1-3 Material Properties**

Material	Young's Modulus, GPa	CTE, ppm/C	Poisson's Ratio
Ceramic substrate	300	6.7	0.21
Organic substrate	23	16.9	0.2
Underfill (T <sub>g</sub> =70C)	8.5	36	0.3
	0.04	120	
Lid adhesive (T <sub>g</sub> =49C)	9.3	39	0.3
	0.4	162	
TIM	0.00023	232	
Lid/stiffener	120	17	0.3
PCB (Octant 1 model)	16	17.7	0.11
PCB (Strip model)	27	18	0.39
Silicon	167	2.54	0.28
Copper (Octant 1 model)	128	17	0.34
Electroplated Copper (Strip model)	76	17	0.35

C1.1 MODELING APPROACHES AND BOUNDARY CONDITIONS

**C1.1.1 Model Type Tradeoffs** An example of the tradeoffs of each model type, boundary conditions and a comparison between the different modeling approaches is shown in Table C1-4 and Figure C1-3a and Figure C1-3b.

Table C1-4 3D Model Types and Tradeoffs

Model Types	Pros	Cons
2D Model (Note: in electronic packaging cases, model of cross section should use plane strain)	<ul style="list-style-type: none"><li>• Computationally inexpensive</li><li>• Easily scalable from Ball Grid Array (BGA) to die level interconnects</li></ul>	<ul style="list-style-type: none"><li>• Accuracy may be limited by geometric simplification</li><li>• Cannot capture 3D corner effects</li><li>• Cannot capture 3D geometry (like lid corner)</li></ul>
3D Strip Model (Note: in electronic packaging cases, generalized plane strain boundary conditions should be applied on strip surface)	<ul style="list-style-type: none"><li>• Computationally inexpensive</li><li>• Easily scalable from BGA to die level interconnects</li></ul>	<ul style="list-style-type: none"><li>• Accuracy may be limited by geometric simplification</li><li>• Cannot capture 3D corner effects</li><li>• Cannot capture 3D geometry (like lid corner)</li></ul>
Slice Model	<ul style="list-style-type: none"><li>• Computationally inexpensive</li><li>• Can easily be scaled from BGAs to die level interconnects</li></ul>	<ul style="list-style-type: none"><li>• Does not capture BGA behavior in the center of the die or substrate</li></ul>
Octant, Quarter, or Half Symmetry	<ul style="list-style-type: none"><li>• Captures BGA fatigue and warpage</li><li>• Accurate for geometrically symmetric packages and boundary conditions</li></ul>	<ul style="list-style-type: none"><li>• Computationally expensive</li><li>• Difficult to scale into die level interconnects due to computation expense</li></ul>
Global-Local Model	<ul style="list-style-type: none"><li>• Computationally hybrid between full octant and slice</li><li>• Useful for zooming into high stress areas that are relatively independent of remaining geometry</li><li>• Finer meshing can be used locally</li><li>• Can zoom into finer geometry</li></ul>	<ul style="list-style-type: none"><li>• Cumbersome and prone to error</li><li>• Extra measures need to be taken to ensure that the deformation field is continuous between global and local model.</li><li>• Differences between linear properties used in global model vs. nonlinear properties used in local model could yield unusual results</li></ul>
Full Package Model	<ul style="list-style-type: none"><li>• Capture BGA shear and warpage</li><li>• Accurate for non-symmetric packages and boundary conditions</li></ul>	<ul style="list-style-type: none"><li>• Computationally expensive</li></ul>

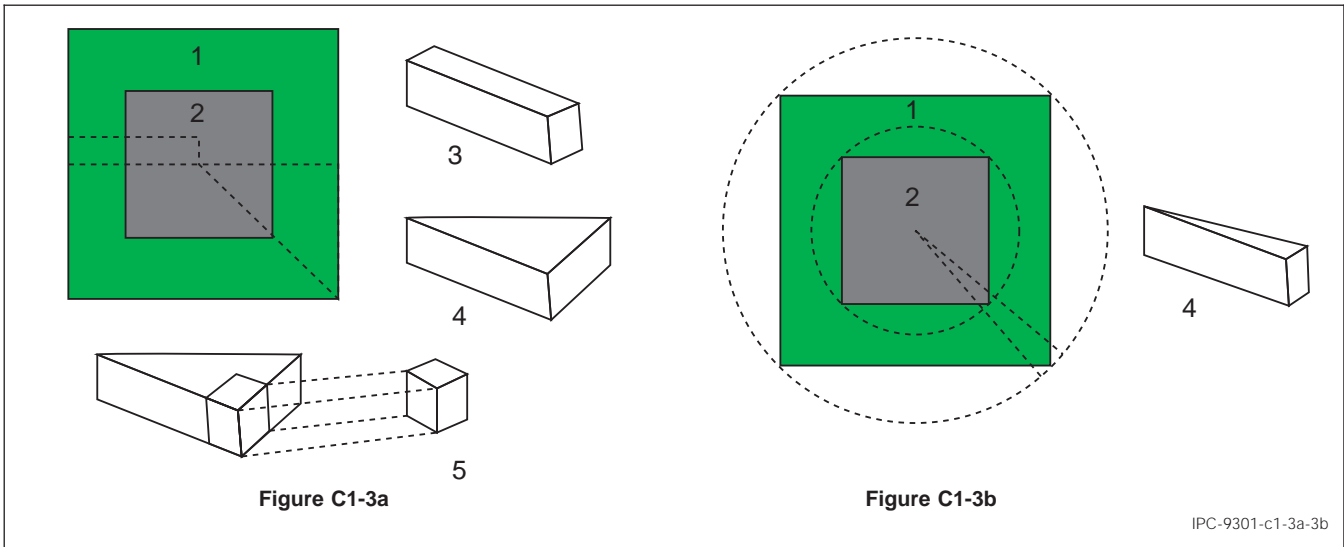


Figure C1-3a and Figure C1-3b Different Model Type Schematics

- Note 1.** Substrate

**Note 2.** Die

**Note 3.** Strip
- Note 4.** Octant

**Note 5.** Global Life

**Note 6.** Slice

The examples that follow highlight select boundary conditions choices for electronic packages. The considerations discussed are equally applicable to models of other length scales, e.g., the die or device level. Figure C1-4a and Figure C1-4b shows examples of a strip model. In this case, the model is constructed to examine solder ball fatigue life. The model runs from the center of the package along a diagonal to a package corner and includes the underlying printed circuit board. Strip models may be constructed along package mid-planes, diagonals or any similar planes of interest.

Since the nodes on Cut Plane A are on a symmetry surface, the in-plane translations of these nodes are restrained (y displacement set equal to 0 in the local coordinate system shown). Along Cut Plane B, boundary conditions may establish a state of plane strain, plane stress or generalized plain strain in the thickness (y) direction. Plane stress boundary conditions dictate that the nodes on Cut Plane B are not restrained in the y direction and plane strain boundary conditions occur when the y translations on Cut Plane B are restrained. In some cases, plane stress and plane strain boundary conditions may be considered to produce extremes of either displacement or stress.

Generalized plane strain boundary conditions reflect a compromise between the aforementioned treatments of Cut Plane B. In this case, a set of constraint equations are applied to all the nodes on Cut Plane B. These constraint equations dictate that the y displacements of all nodes on Cut Plane B are equal. The result is that Cut Plane B may translate in y yet remains parallel to Cut Plane A. As a result of this treatment, model y stresses are closer to those in a full package simulation when compared with plane stress or plane strain boundary condition results.

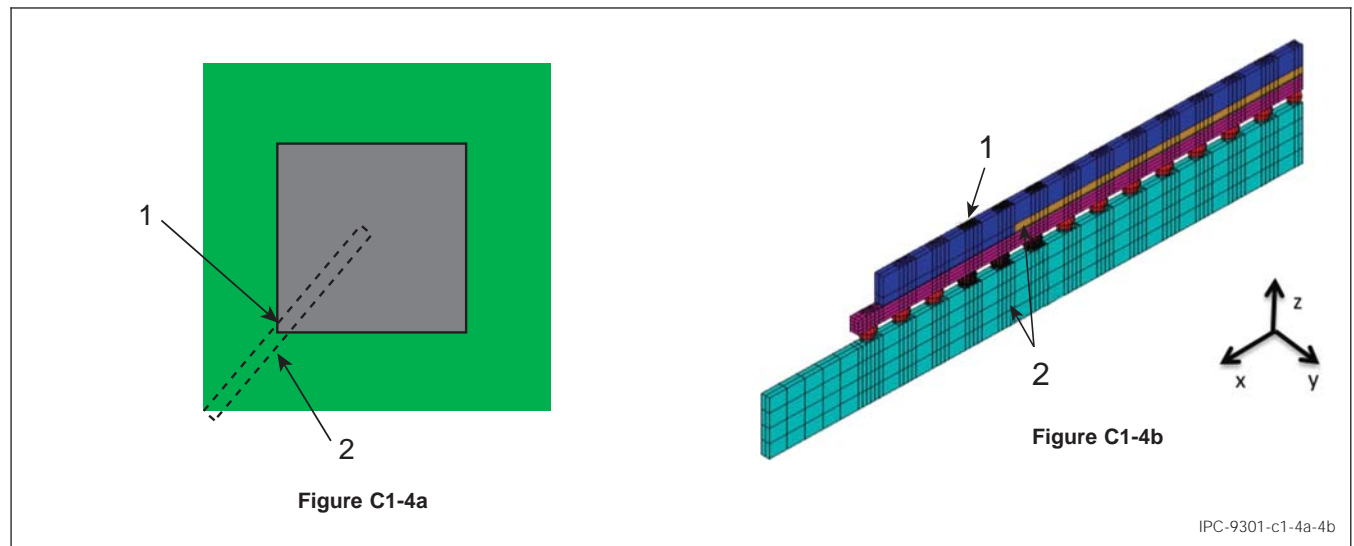


**Figure C1-4a and Figure C1-4b Strip Model**

**Note 1.** Cut Plane A

**Note 2.** Cut Plane B

Other than symmetric boundary conditions, the other boundary conditions will depend on real loading conditions in the field. For example, in the case of component level thermal cycling where the test board has no constraints in the thermal chamber, only rigid body displacement needs to be constrained. One example is shown in Figure C1-5. In this example, since the nodes do not have rotational degrees of freedom, 6 translational boundary conditions are used to constrain the 6 rigid body degrees of freedom.

Many multichip modules (including 2.5D TSV devices) are non-symmetric: multiple memory devices are placed around a silicon chip as close together as possible.

In such cases, conventional symmetry boundary conditions cannot be utilized. The location where rigid body motion is constrained is not necessarily in the center. The following key principles should be utilized in applying the boundary conditions in non-symmetric designs:

1. St. Venant's principle: the boundary conditions should be applied as far away from the region of interest as possible.
2. Utilize the "distance from neutral point" principle: when two structures of different coefficient of thermal expansion value are bonded together, the displacement is highest the furthest away from the center of the structures. Consequently,

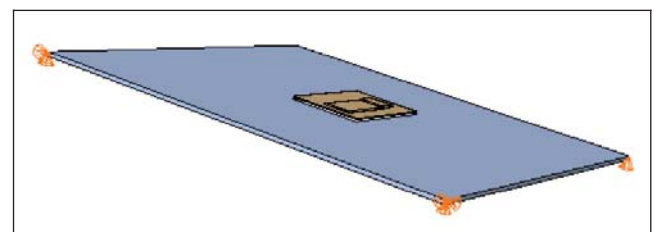


**Figure C1-5 Example of Full Model Boundary Conditions for Component Level Temperature Cycling**

zero displacement boundary conditions could be applied at the center of such structures. Coupled displacement boundary conditions could be applied at the center of the structures as well, to capture localized displacement without necessarily forcing a zero displacement (Figure C1-6a, Figure C1-6b, and Figure C1-6c).

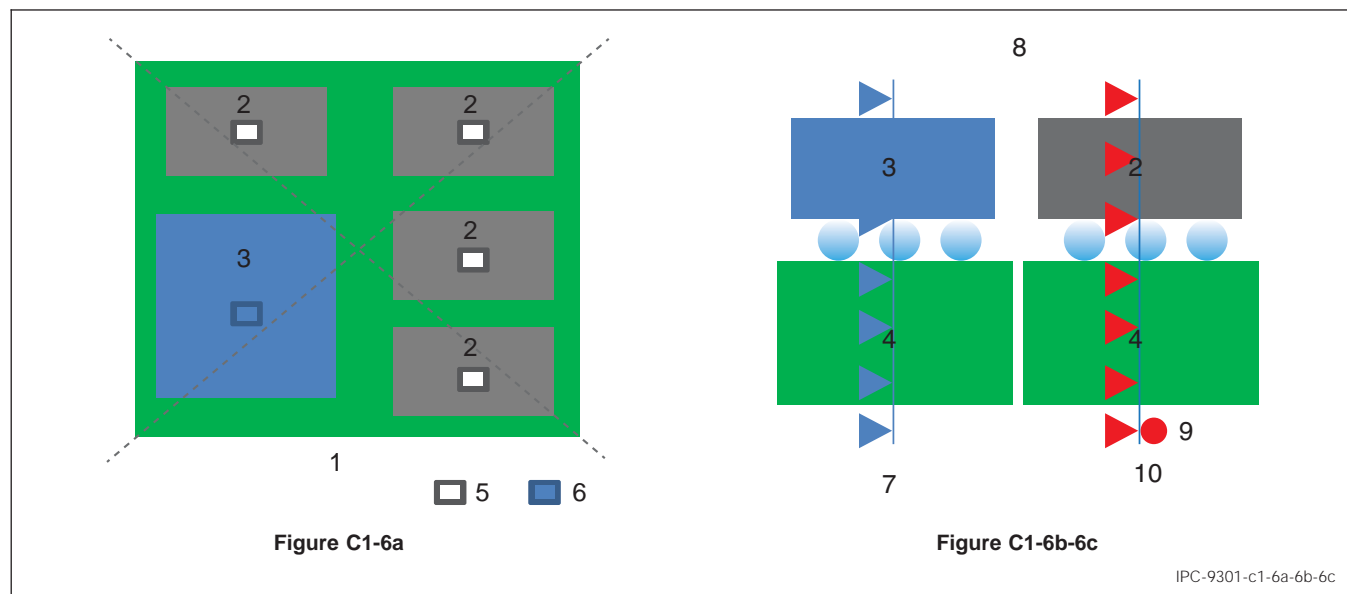


**Figure C1-6a, Figure C1-6b, and Figure C1-6c Example of Boundary Conditions for Multichip Modules**

- |   |   |
|---|---|
| <b>Node 1.</b> Plan View                                      | <b>Node 7.</b> Fixed Nodes, Fixed Displacement = 0  |
| <b>Node 2.</b> Memory   | <b>Node 8.</b> Side View  |
| <b>Node 3.</b> Silicon Die                                    | <b>Node 9.</b> Master Node  |
| <b>Node 4.</b> Substrate                                      | <b>Node 10.</b> Coupled Nodes: Displacement is Equal to that of Master Node but is not Specified or 0 |
| <b>Node 5.</b> Fixed UX UY UZ at 2 Nodes in Center of Silicon |   |
| <b>Node 6.</b> Coupled Nodes at Center of Memories            |   |

#### **Example of Model Type Selection – Best Practices for Board Level Models:**

The first step in selecting the appropriate model is to outline the goal of the modeling.

1. If the objective of the model is strictly to evaluate the relative difference in fatigue life between two package designs of the same package type, then the Strip model or the Slice model would suffice. These models have shown a very good predictive capability for a new package within a specific package type when data already exists for that package type. [25] 2D models that can capture the key difference of the structures can also be used.
2. If the objective of the model is to determine the weakest BGA joint and to quantify how weak it is in absolute terms, then the Octant Symmetry model or full model of all the BGA joints is preferred. Symmetric selection will depend on package and test condition set up.
3. If the objective is to understand chip/package interaction and the impact of die level interconnects on BGA fatigue or vice versa, then the Slice model is preferred. However, the Slice model is a bit difficult to build, and if only qualitative differences are needed, then the Strip model can be used.
4. If the absolute fatigue life of a specific BGA package is required, then the Octant Symmetry or full model are preferred.



## C1.2 THREE MODELING APPROACHES

**C1.2.1 Modeling Approaches** The strip and two octant modeling methodologies are presented and explored. While the methods were developed independently, they share common attributes such as the Morrow failure criterion, the use of a hyperbolic creep model and common solution steps. However, there are important differences in the creep constitutive and fatigue life parameters between specific modeling details. These differences are outlined in Table C1-5.

**Table C1-5 Modeling Constants for Three Different Methodologies**

	Term	Strip Model	Octant Model 1	Octant Model 2
Creep Equation Constants	c1 (1/s)	500000	1.3672	277984
	c1 (1/MPa)	0.01	0.1189	0.02447
	c1 (-)	5	4.0120	6.41
	c4 (K)	5800	6479.4	6500
Morrow Constants	n	1.6 <sup>1</sup>	0.398 <sup>2</sup>	1 <sup>3</sup>
	A (cycles*MPa <sup>n</sup> )	Varies <sup>1</sup>	754 <sup>2</sup>	151 <sup>3</sup>

**Note 1.** n=1.6 common to all package types. "A" differs by package type, assembly site, etc. Must be obtained for a package of interest by modeling a similar package. Typical values of A are 900-3000 for CBGA, 100-400 for PBGA and ~2000 for WLCSP

**Note 2.** Constants benchmarked on ceramic packages

**Note 3.** Benchmarked against fine-pitch organic packages

While models dedicated to a specific package and having significant supporting data combined with tight manufacturing controls can produce very accurate solder ball fatigue predictions, typical "general purpose" models may be expected to have a predictive accuracy within a range as broad as  $\pm 30 - 50\%$ . Studies have shown much greater error is easily possible with a general-purpose model. [26] It is important to note that, as done here, fatigue life benchmarking is usually done with the characteristic life (62.3%) or mean life of experimental Weibull fatigue life data. Consequently, the predicted fatigue life from these models should be translated into the characteristic life or mean life, not the 1% or 0.1% failure free life of packages. Use of the models to predict other cumulative failure rates, such as 1% or 0.1%, require the Weibull slope parameter,  $\beta$ . Ideally,  $\beta$  in the modeled environment would be the same as that for the tested part. It is common practice to choose a conservative  $\beta$  having a value of ~5-6 for added confidence that projections to low failure rates are conservative.

**C1.2.1.1 Strip Model** The strip model methodology employs a three-dimensional slice that runs along a diagonal from the center of the package through a package corner and has a width of one half the diagonal BGA pitch. Symmetry boundary conditions are applied to one cutting plane and a plane strain condition is enforced on the other cut surface. All elements are 8-node hexahedron and a typical model is shown in Figures C1-7a and C1-7b.

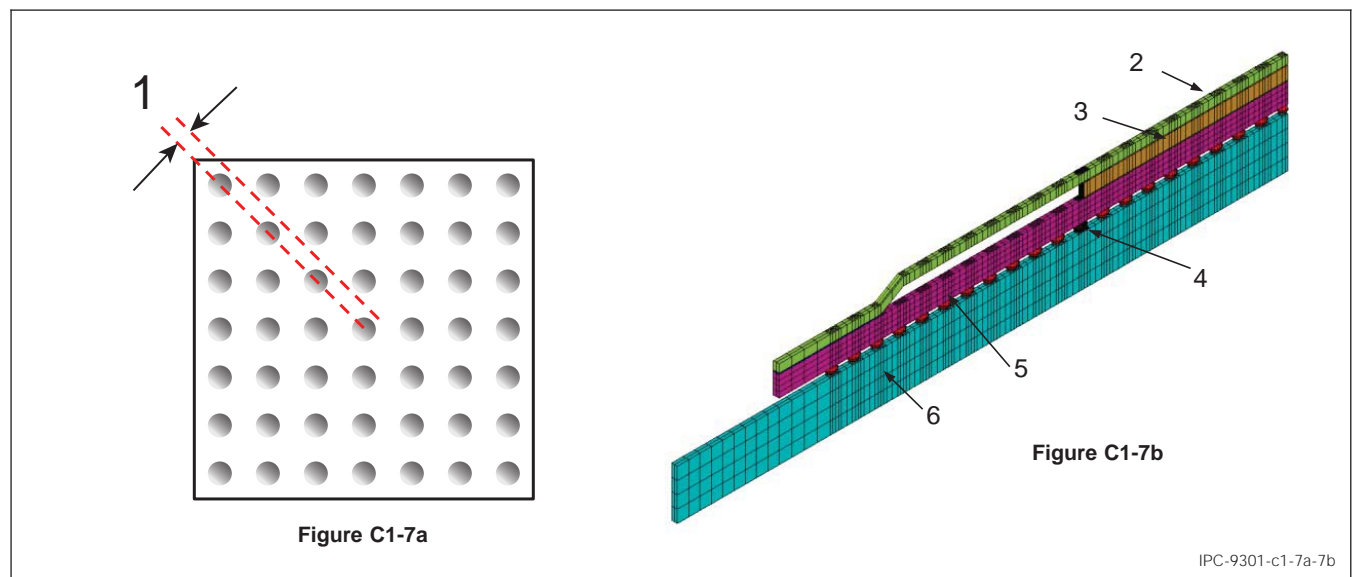


**Figure C1-7a and Figure C1-7b Strip Model Boundary Conditions**

**Note 1.** Modeled Geometry

**Note 2.** Lid

**Note 3.** Die

**Note 4.** Refined mesh solder ball

**Note 5.** Substrate

**Note 6.** PCB



The failure metric is the maximum change in creep strain energy density in any single solder ball element. Due to this criterion, and the existence of re-entrant geometry and multi-material interfaces at the locations of solder crack initiation (the BGA corners) particular concern must be applied to the solder ball mesh where results are examined. Critical failure locations are taken to be the four corner elements numbered 1-4 in as shown in Figure C1-8. These elements used in results reporting are 15µm thick and span 5-6° along the solder ball's circumference.

For the case where the failure location is known a-priori, the refined-mesh BGA is only required where failures are expected or of interest. As a computational efficiency, the remaining BGAs need only provide the proper stiffness, hence may be coarsely meshed. In general, the lateral extent of the modeled PCB is 20% greater than that of the package.

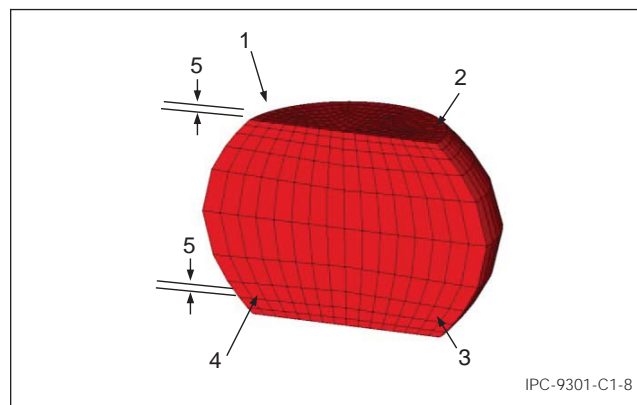


**Figure C1-8 Critical Solder Joint Dimensions for Analysis**

**Notes 1- 4.** Critical failure locations

**Note 5.** 15 µm

The strip model methodology is based on the greatest change in creep strain energy density in the third thermal cycle among each of the 4 corner elements of the refined mesh solder balls. For these models, the creep strain energy change per cycle is usually stabilized by the third cycle; see [27] for empirical and simulation examples. The exponent of 1.6 was developed from and is applied to element-averaged results.

The strip model results (Table C1-6) demonstrate two means of applying the relative life prediction methodology. For the CBGA, there are two empirical results. In this case, models are made which capture the CBGA subject to Profile 1 and Profile 2. The predicted life under Profile 2 is obtained with knowledge of the life under Profile 1 through  $N_2 = N_1(\Delta W_1 / \Delta W_2)^{1.6}$  where the subscripts 1 and 2 indicate the respective thermal profiles.

**Table C1-6 Strip Model Results and Comparison with Experimental Data**

Strip model results								
Package Type		ATC profile	PCB Thickness (mils)	SED Per Cycle (MPa)	Predicted Mean Life Cycles	Measured 2P Weibull Mean Life	% Error	Comment
CBGA	400	Profile 1	93	1.37	1509	1509	NA	Baseline
		Profile 2	93	1.47	1348	790	-70.6	Prediction
FCBGA	2401	Profile 1	130	0.131	6014	4796	-25.4	A=234
FCBGA	1849	Profile 1	93	0.119	7071	8683	18.6	A=234
FCBGA	1849	Profile 1	130	0.151	4778	4867	1.83	A=234

In a slightly different application, the 2401 and 1849 FCBGA data are used to demonstrate the development of the constant A for packages of this type, based on the FCBGA data. Here all packages are modeled and a least squares analysis determines A, the amplitude term in the predictive equation  $Nf = A/\Delta W^{1.6}$ . When a life prediction is needed for a new FCBGA with similar attributes, this relationship with A = 234 may be applied directly. A comparison of the model predicted and experimental fatigue life values indicates remarkably close correlation for the Profile 1 cases. The large error is seen in the prediction for Profile 2 is attributed to benchmarking the model against significantly different Profile 1. Similar trend can also be seen for Octant Models.

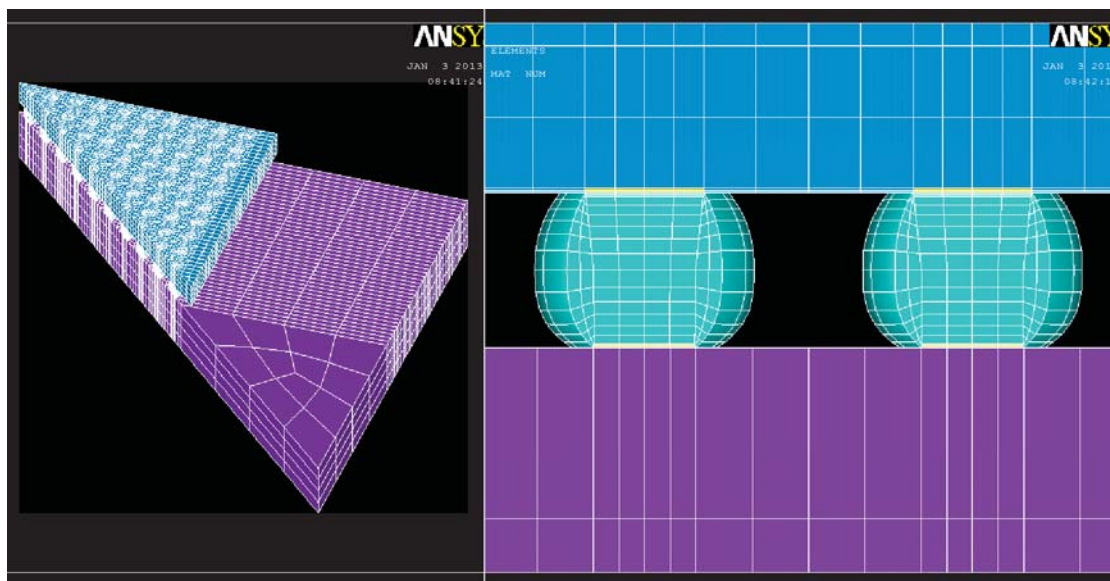
**C1.2.1.2 Octant Model 1** The model uses solid 185, at least 8 elements in lateral of the joint, and 16 elements around the peripheral of the joint. The top half of the solder joint is used to extract the average creep strain energy density. The results are shown in Table C1-7.

The model uses solid 185, at least 8 elements in lateral of the joint, and 16 elements around the peripheral of the joint (Figure C1-9). The top half of the solder joint is used to extract the average creep strain energy density. The results are shown in Table C1-7.

Given that this is not a benchmarking case (the model predicts absolute values as opposed to values derived from a benchmark), the predicted results are close. Typically, for absolute life prediction, values within 50% of experimental data are expected. The results for Profile 2 have higher error as expected because the model was benchmarked against Profile 1. The trends in fatigue life are also consisted with the experimental data.

**Table C1-7 Octant Model 1 Results and Comparison with Experimental Data**

Package Type	ATC Profile	PCB Thickness (mils)	SED Per Cycle (MPa)	Predicted Mean Life (Cycles)	Measured 2P Weibull Mean Life	% Error
CBGA 400	Profile 1	93	0.1308	1694	1509	-12.3
FCBGA 2401	Profile 2	93	0.1508	1556	790	-96.9
FCBGA 2401	Profile 1	130	0.035	2862	4796	40.32

**Figure C1-9 CBGA400 Octant Model and Joint Mesh**

**C1.2.1.3 Octant Model 2** All geometric details are captured except for exact trace details on die and substrate. A global-local modeling approach is used where joints at multiple locations are modeled with details joint geometry. A volume averaging technique is used to extract SED values for 25μm thick layers of solder interfacing with substrate and board pads. These layers have 2 elements across the thickness to further avoid singularity issues.

A comparison between the simulated and experimental data shows close correlation in most cases (Table C1-8). In this case, the lognormal mean life is used, as opposed to Weibull 2P life. The trends in life are similar to those predicted by the experimental data.

**Table C1-8 Octant Model 2 Results and Comparison with Experimental Data**

Octant Model 2 Results								
Package Type		ATC profile	PCB thickness (mils)	SED Per Cycle (MPa)	Predicted Mean Life Cycles	Measured Lognormal Mean Life (50%)	% Error	Comment
CBGA	400	Profile 1	93	0.2653	569	1416	59.8	
		Profile 2	93	0.2914	518	729	28.94	
FCBGA	2401	Profile 1	130	0.0255	5911	4474	-32.1	Supplier 1 Board Properties
				0.0365	4141		7.44	Supplier 2 Board Properties

Summary:

The results of all three cases show that while the constants used and the precise equations or methodology are not consistent, the error between predicted and measured life is similar and the trends predicted by the simulations are consistent with the experimental data.

### C1.3 SOFTWARE SPECIFIC BEST PRACTICES

**C1.3.1 ANSYS®** ANSYS® is a general-purpose finite element code with broad acceptance in multiple industry sectors. In general, ANSYS® versions 14 or later are recommended. The following presents a solution algorithm for performing BGA solder joint thermomechanical fatigue analysis in ANSYS®. Specific commands are presented and a sensitivity study examines select element formulation and creep convergence parameters. This material may be viewed as an example of the pre-work expected in developing and testing an analysis methodology.

There are two ways of implementing solder creep constitutive equation in ANSYS®; a) by using implicit creep model - TBOPT = 8, or b) by using Anand's viscoplastic deformation model while setting hardening/softening constant  $h_0$  as zero. While the SOLID185 element is generally used for implementing creep model, Anand's viscoplastic model were previously implemented in older (pre-version 14) versions of ANSYS® using VISCO107 elements. Since studies [16] have shown a difference between VISCO107 and SOLID185 results and since the new versions of ANSYS® do not provide documentation for VISCO107 elements, the use of SOLID185 with implicit creep is recommended. Suggested ANSYS® input and solution commands are listed below in the ANSYS® format.

**C1.3.2 In the pre-preprocessor (/Prep7)** This defines the SAC creep constitutive properties

```
TB, CREEP, MAT #, 1, , 8           ! generalized Garofalo, MAT# is the
                                   number associated with SAC solder

TBTEMP, 273

TBDATA, 1, 500000, 10e-9, 5, 5802 ! this is the input for the creep
                                   properties used in the strip model ;
                                   ! can be changed to that for the octant
                                   models as appropriate
```

**C1.3.3 Solution phase (/Solution)**

```
TREF, use high temp dwell
NLGEOM, ON
RATE, ON                               !implicit creep
SOLCON, ON
EQSLV, SPARSE
CRPLIM, blank or 3, 1                 !implicit creep
OUTRES, ALL, , -15                    !stores results evenly within loadstep

for each main loadstep (ramp, dwell):
KBC, #                               !#=0 for ramp or kbc, 1 for dwells
BFE, all, temp, , VALUE               ! tunif will step on first load step
                                   regardless of kbc

DELTIM, .01, .001, .05*total load step time
```

Since the model includes creep, 2 or 3 thermal cycles are simulated with the expectation that creep response per cycle stabilizes shortly after the first cycle. TUNIF may be used in place of BFE if the analyst recognizes that TUNIF will step the first load step regardless of the KBC value.

Postprocessing is performed in /Post26 for last full cycle. The discussion of each model will include postprocessing details.

The models have two subtle differences in formulation and solution. All models are constructed in ANSYS® using 8 node hexahedral elements. This is element type 185 and has a default selective reduced (B-bar) integration. Since the selective reduced integration does not restrict bending-induced shear locking, the enhanced natural strain option is sometimes used. This option, flagged by keyopt 2 = 2, introduces internal degrees of freedom which inhibit shear locking.

All models use the implicit creep analysis formulation as defined by the ANSYS® command CRPLIM,,1. In this default state, the amount of creep per time step is not limited. Concerns regarding the degree of creep per time step have motivated replacing the blank field in the command with a numerical value which sets the maximum ratio of the von-Mises creep strain within a time step. This is often set to CRPLIM,3,1 where 3 is the aforementioned maximum ratio. Should the ratio exceed, in this case 3, the time step is bisected.

In order to investigate these options, a Ceramic Ball Grid Array (CBGA) 400 ball model was run with the type 185 element and creep limit permutations. As shown in the rows for the type 185 elements in Table C1-9, the critical element creep strain

energy densities are normalized to that for the element type 185 with no creep limits and the standard temperature profile. For all cases, the ratio of the creep strain energy density in the mini-cycle thermal profile to that in the standard profile is approximately 1.07. Consequently, life predictions for the two thermal profiles will be in proportion to  $1.07^N$  for the examined model formulations. The results demonstrate that (for the cases examined) there will be no or minimal difference in solder joint fatigue life predictions providing the choice of creep limit ratio and element formulation are consistently applied.

**Table C1-9 Effect of “crplm” Command**

		400 CBGA		
		Std profile	Mini-cycle profile	Ratio (Mini/Std)
crplm,,1	et,1,185	1.00	1.07	1.07
crplm,3,1	et,1,185	1.00	1.07	1.07
crplm,,1	et,1,185,,2	0.91	0.97	1.07
crplm,3,1	et,1,185,,2	0.91	0.97	1.07
crplm,,1	et,1,186	1.16		
crplm,,1	et,1,186,,1	1.27		

ANSYS® supports a higher-order version of the type 185 element. This is type 186, which is a 20 node serendipity hexahedra. The last two lines of the table present the normalized creep strain energy density from the model using element type 186. The default formulation is reduced integration and setting keyopt 2 = 1 forces full stiffness matrix integration. As may be expected with the greater node density, the calculated creep strain energy density is higher for the models employing type 186 elements. Solution times were significantly longer (approximately 4x) for models with type 186 elements when compared to those with type 185 elements.

Since the convergence of nonlinear problems is often a function of integration point density rather than the number of nodes, the analyst may need to consider convergence as a key criterion in the choice of lower versus higher order elements.

**C1.3.4 Poisson Ratio Implementation for Orthotropic Materials in ANSYS®** ANSYS® provides two definitions for Poisson’s ratio as specified on the MP command. As defined for the compliance matrix (see Section C1.3.1), the terms  $v_{xy}$ ,  $v_{yz}$  and  $v_{zx}$  are entered as “major” Poisson’s ratios with the input commands “MP, PRXY,” “MP, PRYZ” and “MP, PRXZ”. The “minor” values  $v_{yx}$ ,  $v_{zy}$  and  $v_{zx}$  are applied with “MP, NUXY,” “MP, NUYZ” and “MP, NUXZ”. The terms major and minor arise from the assumption that  $E_x$  is larger than  $E_y$ , hence  $v_{xy}$  (PRXY) is larger than  $v_{yx}$  (NUXY).

When using ANSYS®, it is important to understand the derivation of Poisson’s ratio data being input into a model and the implementation within the code. In the simplest case, incorrect input causes the off-diagonal terms in the compliance matrix to be incorrect. In the extreme, improper input for Poisson’s ratio and Young’s modulus will destroy the necessary positive definite characteristic of the compliance matrix.

**C1.3.5 Cure Shrinkage Implementation in ANSYS®** Implementation of cure shrinkage via shift of the reference temperature at ANSYS® is accomplished as follows:

*MP, REFT, mat\_number\_molding, T\_reference+Delta\_T\_shrinkage*

The shifted reference temperature should be applied to the molding compound material only and not as a global reference temperature to the full model.

## C1.4 ABAQUS®

**C1.4.1 ABAQUS® Commercial FEA Software** ABAQUS® is a widely used commercial FEA software. ABAQUS® provided a graphic user interface called ABAQUS® CAE (Computer Aided Engineering) that provided most functions provided by the solver. Users can further customize the FEA model in the text input file (.inp file) before it is submitted to the solver.

ABAQUS® provided two solvers for solid mechanics FEA modeling: ABAQUS®/Standard and ABAQUS®/Explicit. ABAQUS®/Standard is typically used for most issues related to electronic packaging including dynamic type of models. The run times of ABAQUS®/Explicit strongly depend on the smallest element size. The wide variation in element sizes in most electronic packaging models mean the run speeds are relatively slow with ABAQUS®/Explicit.

Newer version of ABAQUS® (version 6 as of 2015) use an object-oriented approach to arrange models to facilitate re-use of parts, materials, etc. In the .inp file, the parts are usually defined immediately after the header of the file.

```

*Heading
*Preprint, echo=NO, model=NO, history=NO, contact=NO
** PARTS
*Part, name=PARTEXAMPLE
*Node
...
*Element, type=C3D20R
...
*Nset, nset=ALL, generate
...
** Section: MATERIAL1
*Solid Section, elset=ALL, material= SnAg,
*End Part

```

In this example, the 3D 20 nodes quartic brick element with reduced integration points C3D20R is used to avoid shear locking. Different materials are assigned to different regions of the part. The definition of the material property is defined in the “\*material” section of the .inp file. With parts defined, each part will be arranged in the assembly with shift or rotation if needed.

```

** ASSEMBLY
*Assembly, name=Assembly
*Instance, name=INST1, part=PARTEXAMPLE
*End Instance
*End Assembly

```

Materials are defined after the assembly section. A user defined creep law will be used as example of materials.

```

*Material, name = SnAg
*Creep, law=USER
*Elastic
48500., 0.36, 218.
32590., 0.36, 490.
*Expansion
2e-05,

```

Initial conditions, such as initial boundary condition and initial temperature, can be defined before the first step. Boundary conditions, temperature loading and other loads can be modified in each step. The output request is also handled in the steps.

```

** BOUNDARY CONDITIONS
** Name: FIX123 Type: Displacement/Rotation
*Boundary
FIX123, 1, 1
FIX123, 2, 2
FIX123, 3, 3
** PREDEFINED FIELDS
** Name: T_ALL Type: Temperature
*Initial Conditions, type=TEMPERATURE
INST1.ALL, 373.
** -----
** STEP: RampDown
*Step, name= RampDown, amplitude=RAMP, inc=1000
*Visco, cetol=0.01 [17]
30., 300., 0.003, 300.

```

```
**
** PREDEFINED FIELDS
** Name: ALL Type: Temperature
*Temperature
INST1.ALL, 218.
** OUTPUT REQUESTS
*Restart, write, frequency=0
** FIELD OUTPUT: SOLDER_BRD
*Output, field, frequency=9999
*Element Output, elset= INST1.ALL, directions=YES
ELEDEN, E, S
*Output, history, frequency=0
*End Step
```

In the above example, a “visco” step is used to capture the time dependent deformation of solder material. If automatic time increment is used, the user needs to define creep strain tolerance per increment “cetol”. A sensitivity study should be performed on this value to achieve convergence.

A temperature ramp is applied to the whole model, and several outputs are requested. The creep strain energy density output “ECDDEN” is a subset of variable “ELEDEN” or element energy density. They are requested as well as strain “E” and stress “S”.

The .inp file can then be submitted to the solver with command line or from the CAE. CAE can also post process the result file. ABAQUS® provides a scripting environment to customize and automate the modeling building and post processing. The solver also accepts customization by user subroutines. More details are available in [28].



## APPENDIX D

### Warpage

#### D1 WARPAGE

**D1.1 Warpage** Warpage is a displacement output. Nodal results should be used to output warpage from numerical models. Care should be taken when comparing model output warpage and experimental (Moiré or DIC) measurements. Moiré or DIC measurements typically assume a reference plane that is derived from a least squared fit of the measured data points. On the other hand, the warpage data output from numerical models is based on an absolute reference scale.

For quarter symmetric and octant models, if all the rigid body motions are constrained correctly, then the predicted deformation and the best plane fit results will be the same. However, if the planed of interest is not along the symmetry axes, to make an accurate comparison, either the experimental data or the modeling data will need to be “rotated” to match the same reference plane. To rotate the data, the experimental data could be translated from a least squares fit to a global reference plane. The final report should explicitly state if the experimental data has been transformed (or not) before comparisons were made with the numerical model.

A hypothetical example of the effect of reference plane transformation on comparison of results is illustrated in Figure D1-1a and Figure D1-1b and Table D1-1. The structure modeled is an asymmetric multi-chip module as illustrated in Figure C1-6a, Figure C1-6b, and Figure C1-6c. Figure D1-1a shows a comparison of the experimentally measured warpage with the FEA model predicted warpage, with global coordinates used in the FEA model. Figure D1-1b shows the same data with the FEA model translated into the same reference plane as the experimental data (a least squares fit reference plane, indicated by the dotted trend line). In this hypothetical case, the translated results match closer to the experimental data after reference plane translation

However, that is not always the case. In some cases, the translated FEA results may not necessarily match better with the experimental data. Regardless of the degree of match, results should always be compared against the same reference plane as the one used in the experimental data. “The problem in comparing results across techniques lies in the definition of the coplanarity gauge. Coplanarity is the difference between the highest and lowest displacement values in the full-field data set, with respect to a least-squares fit reference plane. As a result, it is extremely sensitive to statistical extrema in the data set.” [29]

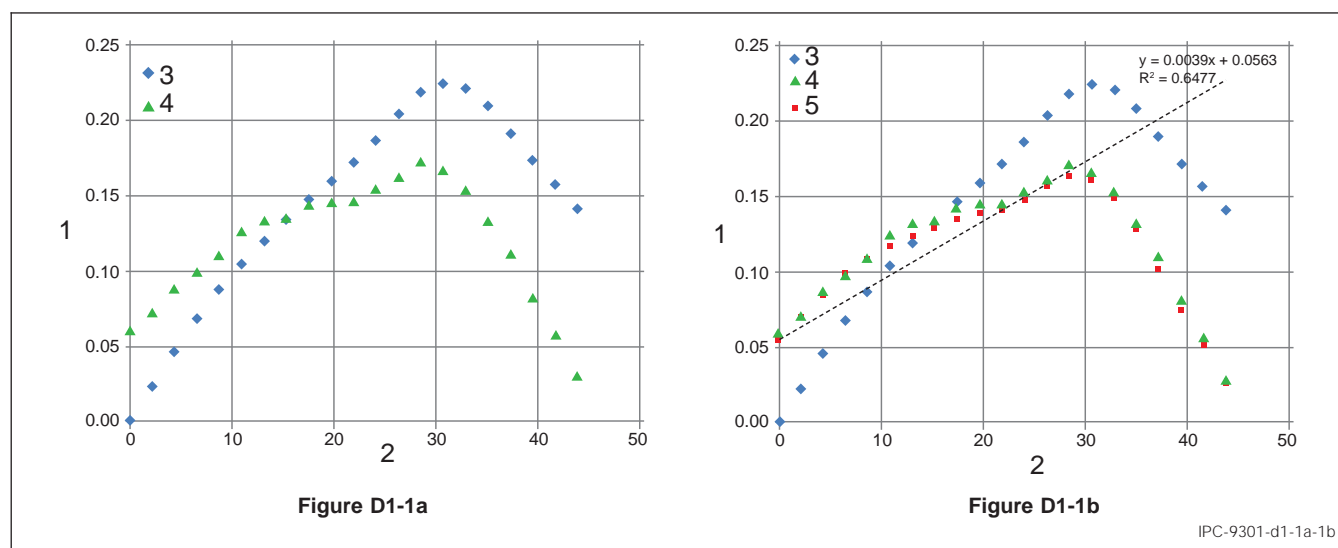


**Figure D1-1a and Figure D1-1b Experiment vs. FEA Warpage Measurements Across Different Reference Planes**

**Note 1.** Warpage (mm)

**Note 2.** Distance (mm)

**Note 3.** FEA Results - Global Coordinates (mm)

**Note 4.** Measured Warpage (mm)

**Note 5.** Model Results - Least Square Plane (mm)



**Table D1-1 Example of Warpage Results Comparison Data Across Different Reference Planes**

	Experimental Moiré Data	Numerical Model Results		
Distance (mm)	Measured Warpage (mm)	FEA Results (Global Coordinates) (mm)	Least Square Fit Reference Plane	Model Results (Least Square Plane) (mm)
Min (mm)	0.030	0.000		0.027
Max (mm)	0.172	0.225		0.164
Coplanarity (mm)	0.142	0.225		0.137
% Difference	–	57.93%		-3.695%

## APPENDIX E

### Experimental Benchmarking Model Case Study (Transient Bend Testing)

#### E1 INTRODUCTION

**E1.1 Introduction** The objective of this section is to demonstrate the level of detail and approach needed to develop predictive modeling methodology that can potentially replace some of the experimental data collection. The focus is on how one goes from understanding of the physics, to defining appropriate mathematical formulation, its numerical implementation, and most importantly on the steps that need to be taken to make a methodology fully predictive.

To explain a modeling methodology, a specific test needed to be selected as an example. The example selected here was a test already done in the industry for certain types of risk assessment. It is not the intent of this document to recommend a specific experimental approach, or to give preference to one approach over any other. The intent is to demonstrate how for a selected test, a methodology needs to be developed for modeling based risk assessment. The steps outlined here can therefore be applied on any test of interest.

**E1.1.1 Risk Assessment Example Problem Background** Board Level Interconnects of soldered assemblies are exposed to failure risks due to printed circuit board (PCB) flexure during different stages of the system assembly, testing and handling (board assembly, In-circuit testing (ICT), functional tests, system assembly and system packaging. A typical system manufacturing process flow is displayed in Figure E1-1.

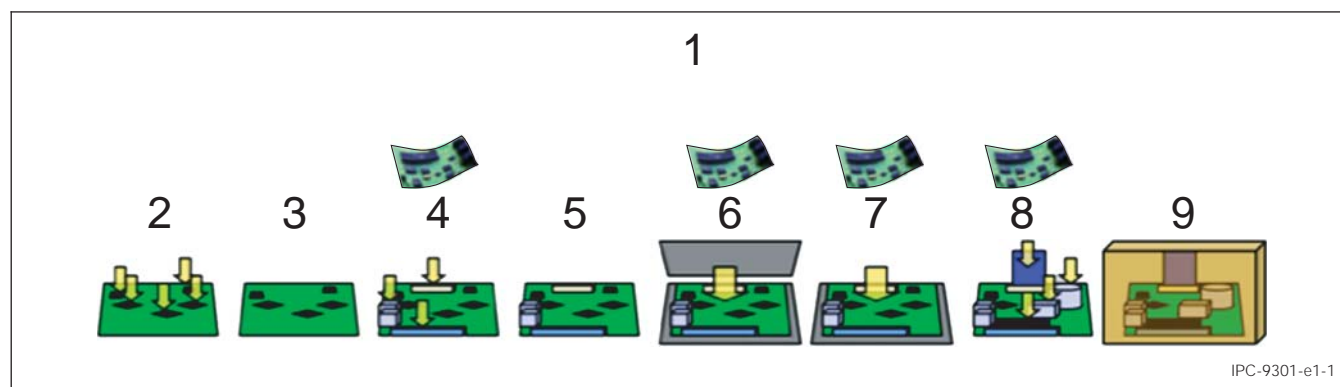


**Figure E-1 Typical System Manufacturing Process Flow**

**Note 1.** Typical Manufacturing Process Flow

**Note 2.** SMT

**Note 3.** Reflow

**Note 4.** Board Assembly

**Note 5.** Wave Solder

**Note 6.** ICT

**Note 7.** Functional Test

**Note 8.** System Assembly

**Note 9.** Packaging

To access the risk and capability of the second level solder joint under these manufacture processes, bending test is performed following the semiconductor industry standard known as IPC/JEDEC-9707: “*Spherical Bend Test Method for Characterization of Board Level Interconnects*” (IPC/JEDEC 9707, 2011). This test is also known by the name “**Transient Bend (TB)**” and this is the terminology adopted in this document. The detailed description of Spherical bend testing methodology can be found in the IPC/JEDEC-9707. Therefore, only a brief description of the test set-up is provided here. A typical test set-up is shown in Figure E1-2a and Figure E1-2b.

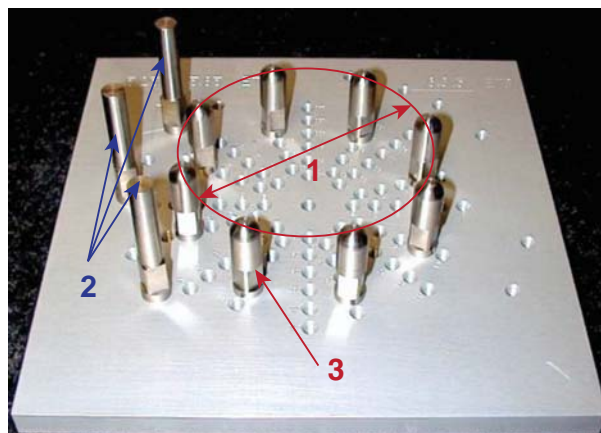


Figure E1-2a

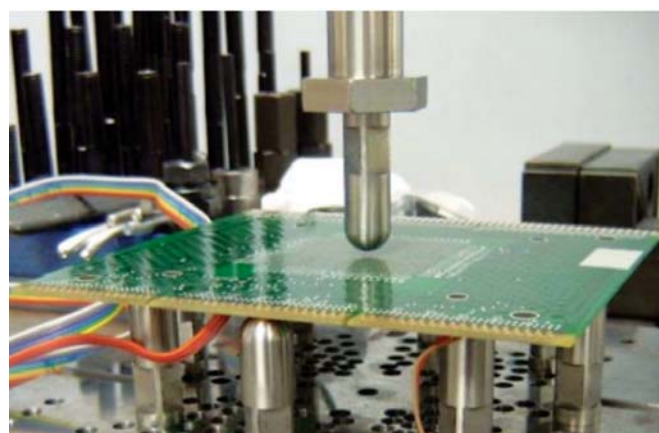


Figure E1-2b

IPC-9301-e1-2a-2b

**Figure E1-2a and Figure E1-2b Typical Spherical Bend Test Set-Up****Note 1.** Support Span**Note 2.** Board Alignment**Note 3.** Reaction Pins (x8)

The test set-up consists of a fixture plate with 8 support/reaction pins placed in a circular pattern of suitable radius (defined by the Support Span), as shown in Figure E1-2a. A BGA package assembled onto an ETB (test boards of 6"x7") is placed on the 8 posts as shown in Figure E1-2b, with the package facing downwards (i.e., facing the fixture plate). The bending of the ETB/board is accomplished by using a loading fixture which is moved into the board at a rate of 5mm/s. Strain gauges are used to measure the board-strains near the package corners (the strain gauges are placed at a distance of 5mm from the package corners along the package diagonal direction) to monitor the board flexure during bending.

The board flexure during the assembly process results in differential bending of the package/board assembly thereby significantly loading the solder-joints (particularly the corner solder joints) until solder-joint failure occurs. Since the solder-joint internal-forces/stresses cannot be measured directly, the board-strains (measured using strain gauges) near the package corners are used to monitor board-flexure. During the test, the package is assumed to have failed the test if a crack in any of the solder-joints is initiated.

**E1.1.2 Scope** A study has been performed to establish the modeling technique for TB aimed at both efficiency and predictability of the risk of BGA packages in TB (Table E1-1). The TB model and modeling methodology are limited to BGA packages. The modeling methodology will work without additional modification for single and dual bare die Multi-Chip Package (MCP) products with and without Board Level Underfill (BLUF).

**Table E1-1 Parameters Defining Scope of Modeling Approach Applicability**

Attribute	Values over which BKM is Applicable
Package dimensions	In plane dimensions limited by board size
Boundary conditions	TB mTPS Boundary Conditions
Pad Type	Circular MD or SMD pads only (no wide trace, oval or spoked pads)
Raw Solder sphere size	Limited by Solder Joint (SJ) pitch, pad size and SRO
Board/Substrate pad size	Limited by SJ pitch and SRO
Board/Substrate SRO	Limited by SJ pitch and pad size
Number of dies	2 (Can add more dies if necessary)
IHS	No (Can add IHS if necessary)

Modeling methodology is currently limited to Metal Defined (MD) and Solder Mask Defined (SMD) pads only. Wide Trace Metal Defined (WTMD), spoked pads and oval pads are not included. Base layer Cu routing (trace orientation) is not included.

This modeling methodology cannot be applied to Socket SJR in TB. Extension to TB SJR models on boards other than Enabling Test Board (ETB) is not described in this document. The TB modeling BKM is currently applicable for performing relative risk assessment for BGA package(s) subjected to TB loading conditions. The board strains can be extracted at any coordinate on the board through appropriate user input of the coordinates.

## E2 MODELING

**E2.1 Modeling Technique** The TB modeling methodology developed in this document is aligned with the TB test and the associated test boundary conditions. A summary of the TB analysis model is given below.

- **Analysis Procedure:** A single static analysis step/procedure is used to model the bending of package/board assembly. *NLGEOM* parameter is used to account for the nonlinear geometric effects during the analysis
- **Boundary Conditions:** The model boundary conditions as per the TB test method. The bending of the package/board assembly is in a spherical bend mode which was determined to be the most severe bend mode through internal work (Hsieh G. et. al.)
- **Loading Fixtures:** The tooling fixtures used to bend the package/board assembly are represented using analysis rigid-surfaces to account for their significantly higher stiffness (therefore less material deformation) compared to the package/board assembly
- **Board Bending/Flexure:** Displacement boundary conditions are used to represent fixture motion and contact-interactions between the fixtures and board is defined
- **Contact Interaction:** The interaction between the rigid fixtures and ETB is modeled using a hard-penalty type contact to model the normal interaction. The tangential interaction is modeled using a Coulombs friction law

The TB model outputs, i.e., board strains and SJ forces can be used to evaluate the strains at certain regions on the board and force-states at the critical (mostly package corner) SJs, respectively. This information can be used to evaluate the relative risk of package designs in TB loading conditions.

**E2.2 Modeling Techniques Overview** Modeling Techniques Overview Commercial FEM software ABAQUS® is used for this study. After the package and board detail is collected, the board and package will be built following the guidelines below. If the package is symmetric, quarter symmetric models can be used, as shown in Figure E2-1. Otherwise, the whole package and board will be modeled.

**E2.2.1 Finite Element Mesh** A detailed mesh sensitivity study is conducted and the results of the study are presented here. A summary of the finite element mesh used in different regions of the model is provided in Table E2-1.

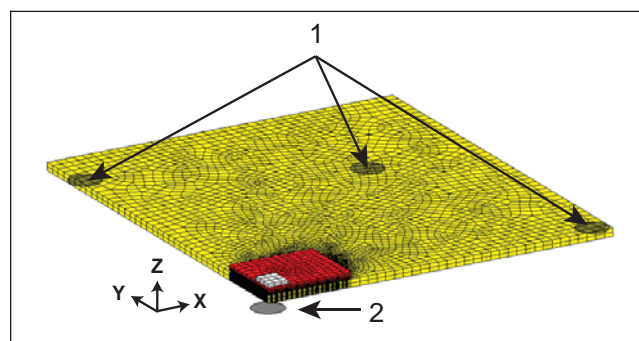


**Figure E2-1 A Typical Quarter Symmetric TB Analysis Model Created in Abaqus® CAE**

**Note 1.** Support Fixtures

**Note 2.** Loading Fixture

**Table E2-1 Summary of the Finite-Element Mesh in the TB Model**

Part	Element Type	Element Density
ETB	C3D20R	2 through thickness. In-plane seed size 2mm.
Substrate	C3D20R	=>3 through thickness
Die	C3D20R	Seed-size = 0.3mm
Fixtures	N/A	N/A Modeled as a analytical rigid surface without discrete finite elements.

- ETB:** The element type used is continuum 20-node three-dimensional reduced integration (C3D20R) elements. The average mesh seed size is 2mm in the plane. Through the board thickness 2 elements are used. The package shadow portion of the board is also represented using two elements through the board thickness.
- Substrate:** Continuum 20-node three-dimensional reduced integration (C3D20R) elements are used. The substrate is divided into two halves' through the thickness, i.e., top and bottom. Through the substrate thickness 2 elements are used for the lower-half of the substrate. However, the top-half is meshed with a seed-size of 0.3mm in the thickness direction. Both the top and bottom half have two elements each through the thickness. The top and bottom halves of the substrate are tied together for all the translation and rotation degrees of freedom.
- Die:** Continuum 20-node three-dimensional reduced integration (C3D20R) elements are used for representing the die. The die is meshed with a seed-size of 0.3mm.

- d. Solder Joints:** Continuum 20-node three-dimensional reduced integration (C3D20R) elements are used to represent all the solder joints. The most critical solder joints (for which force output is required) during TB of the package should be represented using a fine mesh, as shown in Figure E2-2. However, the non-critical solder joints can be represented using a coarse mesh.
- e. Fixtures:** No finite-element mesh is associated with the fixture geometry since the fixture is modeled as an analytical rigid surface instead of representing it as a finite element mesh.

**E2.2.2 Material Properties** Since the overall bending response of the package/board assembly during transient bend will be influenced by the material properties, the user should obtain and use the actual material properties for different sections of the model when it is available. Except for copper and die sections since the properties of these two materials do not have too much variation from supplier to supplier so does not need to be measured or changed.

When the property is not available, default material value can be used for initial risk assessment. The default property for the board modulus is 22GPa for all board thicknesses. The solder material is assumed to have linear-elastic and homogeneous properties.

**E2.2.3 Boundary Conditions** In order to represent the displacements of the fixtures (both supports and loading fixtures) boundary conditions are applied in the model to both the support and loading fixtures. Since the fixture is represented as a rigid analytical surface (i.e., a single reference node controls the motion of the part), the support fixture reference nodes are fixed in all the translational and rotational degrees of freedom. However, the loading fixture reference node is applied with the user supplied Z-displacement moving into the board. All the other translational and rotational degrees of freedom of the loading fixture reference node are constrained. In summary the loading fixture is free to translate only in the Z-direction. In addition to fixture boundary conditions, if the model is a quarter or half symmetric model, appropriate symmetry boundary conditions are applied to the die, substrate and board to enforce the symmetry conditions. As an example, displacement boundary conditions in a quarter symmetry model are displayed in Figure E2-3.

**E2.2.4 Contact Interactions** The board flexure in TB is accomplished by defining contact interactions between the fixtures (support and loading fixtures) and the board/ETB. The contact interactions in the model are defined using the contact pair (\*CONTACT PAIR card) algorithm within Abaqus®. The regions in the model for which contact interaction is defined in the model are summarized in Table E2-2. The contacting regions are defined using element-based surfaces. The interacting pairs are assumed to undergo relatively small amount of sliding relative to each other and therefore **SMALL SLIDING** theory (Abaqus® Analysis User's Manual, Volume II: Analysis. (2008)) is used for contact modeling. Each contact pair requires definition of the slave and master surfaces. It should be noted that the loading fixture surface interacts with the package shadow bottom surface and each individual support fixture surface interacts with the top surface of the board.

The contact pressure resulting from the surfaces contacting each other are modeled using a hard-contact pressure-overclosure model in which the contacting surfaces transmit no contact pressure unless the nodes of the slave surface contact the master surface. Also, there is no limit to the magnitude of contact pressure that can be transmitted when the surfaces are in contact. The enforcement of the contact interactions in the model is accomplished using the penalty method.

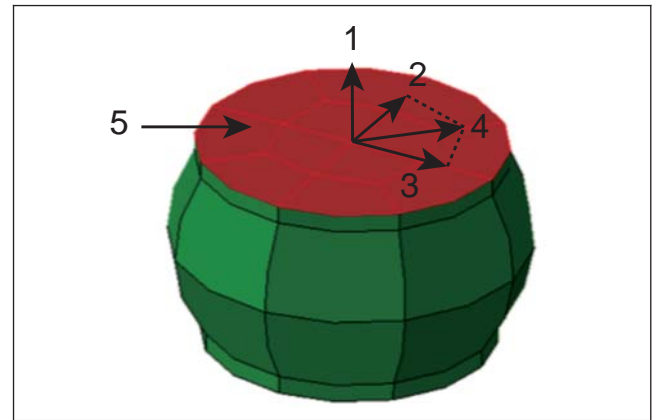


**Figure E2-2 Example of Solder Joint Mesh**

**Note 1.**  $F_N$  = Normal force perpendicular to the solder joint

**Note 2.**  $F_{S2}$  = In-plane Shear Force in the solder joint along y-axis

**Note 3.**  $F_{S1}$  = In-plane Shear Force in the solder joint along x-axis

**Note 4.**  $F_S$  = Resultant in-plane Shear Force

**Note 5.** Board-side Section

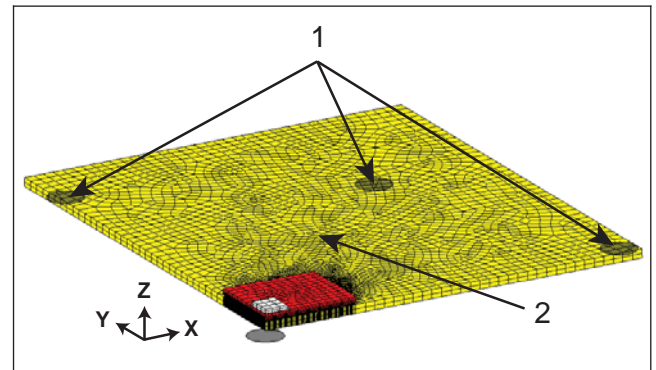


**Figure E2-3 An Example of the Boundary Conditions in a Typical Quarter Symmetric TB Model**

**Note 1.** Support Fixtures:  $U_1=U_2=U_3=U_4=U_5=U_6=0$

**Note 2.** Loading Fixtures:  $U_1=U_2=U_4=U_5=U_6=0$



**Table E2-2 Summary of the Contact Interactions in the TB Model**

Master Surface	Slave Surface	Description
Loading Fixture	Package shadow bottom	One contact pair is defined.
Support Fixtures	Board top surface	Each master surface interacts with the slave surface through a separate contact pair.

The normal component (contact pressure) of the contact force is accounted for as discussed above. The tangential shear force is accounted for in the model using the Coulomb's friction law. The friction coefficient in the model is assumed to be 0.2. The effect of the friction coefficient on the modeling results was found to be negligible and is described in Section E3-0. Regarding contact convergence in the TB analysis model, no issues were found with several model examples with different packages.

**E2.2.5 Analysis Procedure** The transient bending of the package/board assembly is generally a relatively low-displacement rate event. Therefore, the TB problem is analyzed as a single static analysis (\***STATIC**) step within which the loading fixture is displaced by a given displacement magnitude. The TB plug-in creates a single static analysis step. Since the fixture displacement is generally larger than the thickness of the board, geometric nonlinearity (using \***NLGEOM** card) is accounted for during the analysis. A comprehensive comparison of the modeling (using the large displacement theory) and test results is provided later.

**E2.2.6 Analysis Outputs** The TB analysis model requests the nodal displacement (**U**) components, stress (**S**) tensor components and the logarithmic strain (**LE**) components as model outputs. In addition to the default outputs, the internal section forces at predefined SJs defined by the user are available. The section force is the total internal reaction force (SOF) experienced by a section/surface in the selected SJ in the local deformed coordinate system. A summary of the TB model outputs defined by the plug-in is displayed in Table E2-3.

**Table E2-3 Summary of the TB Analysis Model Outputs**

Output Variable	Type	Location
LE, S, U	Field Output	Output Data Base (odb) file
U, RF	History Output	Data (dat) file
SOF	History Output	Data (dat) file

It should be noted that all the above TB model outputs are not required to be post-processed (discussed later).

**E2.2.7 Running Models** ABAQUS® version 6.12 was used when this study is performed. The run-times for a typical full TB analysis model along with half and quarter symmetric models are displayed in Table E2-4. The typical run environment is Intel XEON with 40 cores.

**Table E2-4 Typical TB Analysis Model Run-Times**

Model Type	Run Time (hrs.)
Full Model	7
Half Model	3
Quarter Model	1

**E2.2.8 Post Processing** The post-processing of the TB analysis results consists of the following two discrete steps:

- Extracting board strains
- Extracting solder-joint forces.

A detailed description of the two steps is provided below.

**E2.2.8.1 Extracting Board Strains:** Given the location of a point, ABAQUS® can provide the strain component by interpolation. Taken advantage of this function, board surface strain will be extracted by averaging multiple sampling points in the grid area of a strain gage. To simulate the way strain gage works, only three in plane strain components are output and will be compared with test strain gage data.

**E2.2.8.2 Extracting Solder Joint Forces:** The following solder joint force is extracted from the result file as shown in Figure E2-4:

- (a) For a given SJ set, three force components,  $F_N$ , normal force perpendicular to a SJ section,  $F_S$ , in-plane shear force (effective shear force) and effective SJ force on a SJ section. A schematic of the post-processed forces for a given SJ section/surface is displayed in Figure E2-4. It should be noted that if output force,  $F_N$ , is positive then the SJ is under tension.
- (b) Global reaction force ( $RF_3$ ) vs. Displacement ( $U_3$ ) history during the TB of the package/board assembly.

## E2.3 COMPUTATIONAL MODEL

**E2.3.1 Computational Model Sensitivity Analysis** It is well known that the accuracy of a computational model depends on several analysis model parameters (e.g., mesh type/density, boundary conditions, analysis-type etc.). The objective of this section is to document a comprehensive investigation of the effects of different computational model parameters on the modeling results. The effects of model parameters on the modeling results are described below. All model sensitivity studies are conducted using a 30×30 (mm) package with a regular grid BGA-map assuming quarter symmetry. The results from the model sensitivity analysis are used to define the model parameters in the TB modeling methodology/BKM.

**E2.3.1.1 Mesh Sensitivity** The board and package assembly are modeled using continuum solid brick finite elements (FE). The FE mesh related parameters which affect the results of the computational model are: (a) order of the element, i.e., linear or quadratic; and (b) order of the element integration, i.e., full or reduced integration.

Since, the TB process involves significant bending of the package/board assembly, it is immediately evident that linear/first order elements cannot model the curvature and bending deformation accurately and may become locked or overly stiff under an applied bending moment. This may introduce artificial shear stress even under a pure bending moment. Therefore, second-order quadratic solid brick elements are used to model the board and package. However, to determine the order of element integration, a study was conducted in which quadratic solid brick elements with the following two element integration schemes: (a) full-integration (C3D20); and (b) reduced integration (C3D20R), were used in the entire board/package assembly.

Figure E2-5 shows a comparison of the two element-integration schemes when the mesh density is constant. It is seen that the percentage difference in board strain and SJ force for the two element integration schemes is 0.8% and 0.4%, respectively. There is very little difference in run-time between the two cases considered. Therefore, quadratic reduced integration solid brick elements (C3D20R) are used in the entire model.

Further, to determine an appropriate mesh density for the board and package, a mesh density study was conducted separately for the board and package. The objective of the study is to determine the mesh densities for the board and package assembly which ensure good accuracy as well as computational efficiency. The results of the mesh density study for the board and package are detailed below.

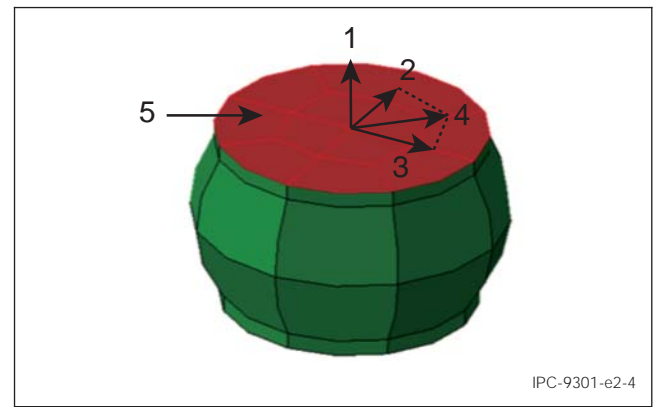


**Figure E2-4 A Schematic of the Post-Processed SJ Forces for a Given SJ Set in the Local Coordinate System**

- Note 1.**  $F_N$  = Normal force perpendicular to the solder joint  
**Note 2.**  $F_{S2}$  = In-plane Shear Force in the solder joint along y-axis  
**Note 3.**  $F_{S1}$  = In-plane Shear Force in the solder joint along x-axis  
**Note 4.**  $F_S$  = Resultant in-plane Shear Force  
**Note 5.** Board-side Section

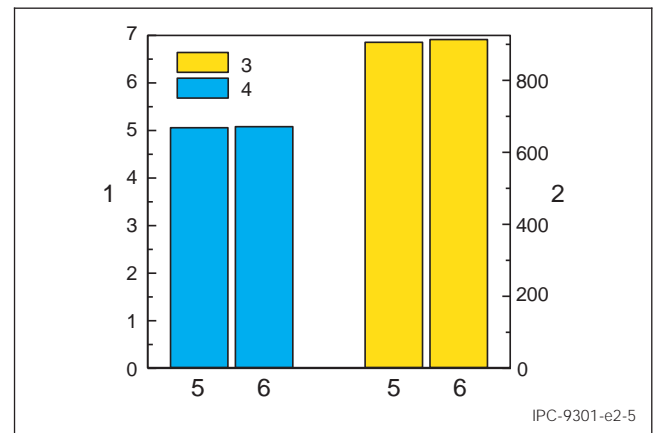


**Figure E2-5 Effect of Computational Model Element Type on the Board Strains and SJ Force**

- Note 1.** SJ Force, N  
**Note 2.** Board Strain,  $\mu e$   
**Note 3.** Board Strain  
**Note 4.** SJ Force  
**Note 5.** C3D20R  
**Note 6.** C3D20



**E2.3.1.2 ETB** A matrix of all the different cases considered for the mesh density study is shown in Table E2-5. Two cases are considered for the mesh densities in the board in-plane and out-of-plane (through the thickness) directions, respectively. The board diagonal strain ( $\epsilon_2$ , radial strain component) at a fixed location on the board and for a fixed applied displacement is used as a measure for comparative purposes. Figure E2-6a and E2-6b display the results of the board mesh density study for the board out-of-plane (through the thickness) and in-plane directions, respectively. It is seen that the percentage difference in board strain and SJ force when the mesh seeding in the ETB thickness direction is varied, is 0.7% and 0.4%, respectively. Considering the ETB in-plane mesh seeding, it is seen that the percentage difference in board strain and SJ force when the mesh seeding in the ETB in-plane directions are varied between medium and fine, is 1.6% and 1.4%, respectively. It is evident that a medium ETB mesh density in the board in-plane direction and two elements through the thickness can accurately represent the overall board deformation. Therefore, the ETB is modeled using an average mesh seed-size of c.a. 2mm in the board plane and 2 elements through the board thickness.

**Table E2-5 Details of the ETB Mesh Size/Seed Study**

	No. of Elements/Seed-Size	Board Strain, ( $\mu\epsilon$ )	SJ Force, (N)
ETB Thickness	2	912.5	5.081
	3	905.3	5.044
ETB In-plane	Coarse (seed-size = 4mm)	835.4	4.630
	Medium (seed-size = 2mm)	912.5	5.081
	Fine (seed-size = 1mm)	927.4	5.156

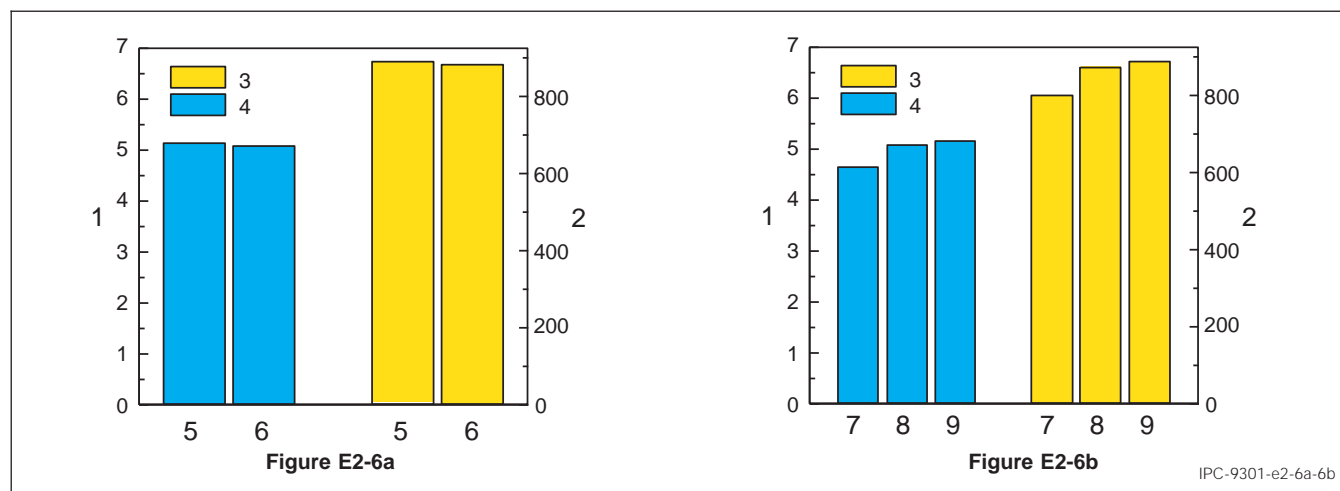


**Figure E2-6a and Figure E2-6b ETB Mesh Size Effect on Board Strains and SJ Force due to Variation in Mesh Size/Seed in the: (a) ETB Thickness Direction; and (b) ETB In-Plane Direction**

**Note 1.** SJ Force, N

**Note 4.** SJ Force

**Note 7.** Coarse

**Note 2.** Board Strain,  $\mu\epsilon$

**Note 5.** 1-ELEM

**Note 8.** Medium

**Note 3.** Board Strain

**Note 6.** 2-ELEM

**Note 9.** Fine

The different cases considered for the mesh size/seed study for the substrate is shown in Table E2-6. The different levels for the mesh size/seed for the following package parameters: (a) package thickness; and (b) critical SJ are shown in the table. The board strain and SJ force are used as a metric for evaluating the sensitivity effects of the above-mentioned parameters. Figure E2-8a and Figure E2-8b display the results of the package mesh density study.

Figure E2-7a, Figure E2-7b, and Figure E2-7c displays the three differently meshed SJs considered in the TB model, i.e., coarse, medium and finely meshed SJs. Results of the sensitivity analysis indicate the following:

- The percentage difference in board strain and SJ force when the package mesh size/seed in the thickness direction is varied is 0.05% and 0.3%, respectively.
- The percentage difference in the SJ force when the critical solder joint mesh size/seed is coarse vs. fine is 16.2%. The percentage difference in the SJ force when the critical solder joint mesh size/seed is medium vs. fine, is 0.6%. No significant difference in board strain was seen.

Considering the above sensitivity results, 2 elements through the lower-half of the package thickness is sufficient in terms of accuracy. While having a medium mesh for the critical SJs is sufficient, a fine mesh for the critical SJs of interest should be used since creating a fine SJ mesh also creates a set for each SJ in the model which is then used for extracting SJ forces.

A study using fine mesh for all the solder-joints and a separate study with medium mesh solder-joints (but fine meshed critical/corner SJs) was also conducted. For the medium mesh solder-joints, no significant difference in result accuracy as well as run-time is seen. However, when the all solder-joints have a fine mesh the run-time was 3 times higher compared to when only coarse solder-joint mesh (but fine meshed critical/corner SJs) is used. There was no significant difference in results. Therefore, using a coarse or medium mesh for the non-critical solder joints is recommended and sufficient.

**Summary:** Critical SJs (generally package corner) should have a fine SJ mesh, while, the non-critical SJs can have either coarse or medium SJ mesh.

**Table E2-6 Details of the Substrate Mesh Size/Seed Study**

	No. of Elements/Seed-Size	Board Strain, ( $\mu\epsilon$ )	SJ Force, (N)
Package Thickness	2	912.5	5.081
	4	912	5.061
Critical SJs	Coarse	917.6	4.286
	Medium	922.2	5.084
	Fine	922	5.119

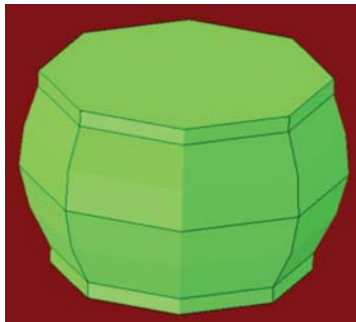


**Figure E2-7a**

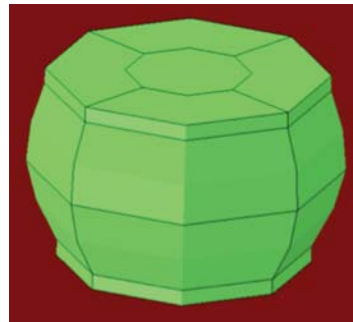


**Figure E2-7b**

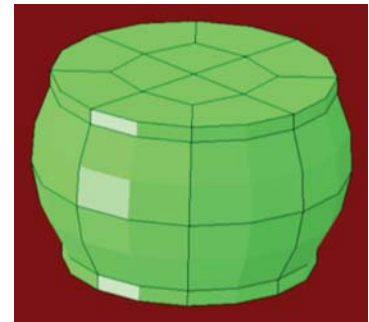


**Figure E2-7c**

IPC-9301-e2-7a-7b-7c

**Figure E2-7a, Figure E2-7b, and Figure E2-7c The Three Types of SJ Mesh Sizes/Seeds: (a) Coarse Mesh; (b) Medium Mesh; and (c) Fine Mesh**

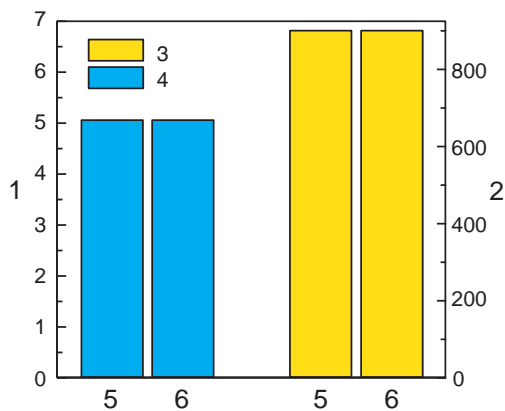


**Figure E2-8a**

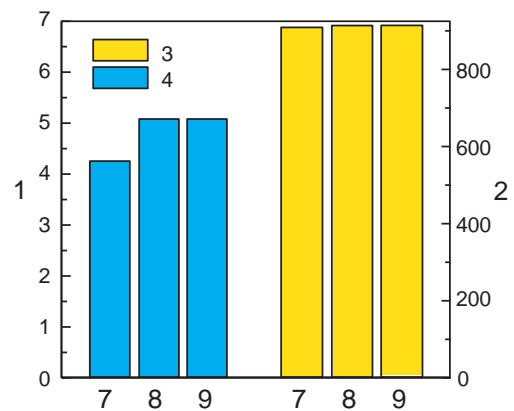


**Figure E2-8b**

IPC-9301-e2-8a-8b

**Figure E2-8a and Figure E2-8b Package Mesh Size/Seed Effect on Board Strains and SJ Force Due to Change in Mesh Size/Seed in the: (a) Package Thickness Direction; and (b) Critical SJs**

**Note 1.** SJ Force, N

**Note 2.** Board Strain,  $\mu\epsilon$

**Note 3.** Board Strain

**Note 4.** SJ Force

**Note 5.** 2-ELEM

**Note 6.** 4-ELEM

**Note 7.** Coarse

**Note 8.** Medium

**Note 9.** Fine

**E2.3.1.3 Fixtures** The loading and support fixtures are generally made of hardened steel. It is reasonable to assume that the fixture deformation is insignificant compared to package/board deformation during transient bend. Therefore, rigid analytical surfaces are used to represent the support and loading fixtures. The analytical surfaces are defined by revolving two-dimensional geometries. Each rigid surface is associated with a rigid body reference node which controls the associated rigid-surface. Comparison of the model and test results in the case of the bare-aluminum boards, as discussed later, shows that assuming the fixtures to be rigid is a very good assumption. Therefore, no sensitivity analysis for fixture modeling was conducted.

**E2.3.1.4 Contact Interaction Behavior** The interaction between the fixtures and the ETB is modeled by allowing the two to come into contact with each other during transient bending. The contact between the ETB and fixtures is modeled as a hard-penalty contact in which a normal contact force is calculated and transmitted across the contacting surfaces. The surfaces in contact transmit no contact pressure unless the nodes of the slave (ETB) surfaces contact the master (rigid fixtures) surface. A coulomb based friction model that defines the force resisting the relative tangential motion of the contacting surfaces is also defined. To define a value for the friction coefficient, a sensitivity analysis involving three different friction coefficients, i.e., 0.0, 0.1 and 0.2 was conducted. The results of the sensitivity analysis are displayed in Figure E2-9. As seen in the figure, no significant difference in the board strain and SJ force is observed. Therefore, a friction coefficient of 0.2 is used within the coulomb model.

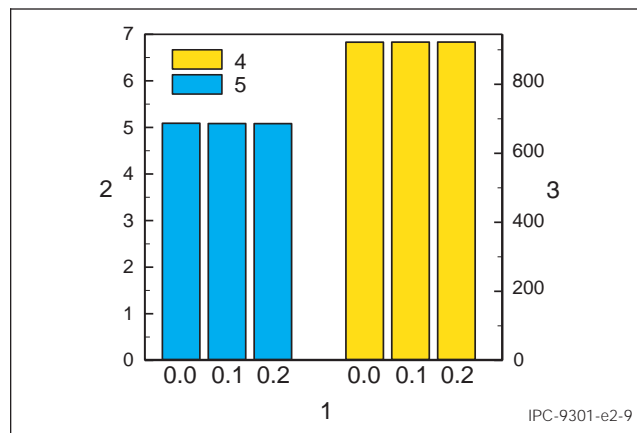


**Figure E2-9 Effect of Friction Coefficient on the Board Strains and SJ Forces**

**Note 1.** Friction Coefficient

**Note 2.** SJ Force, N

**Note 3.** Board Strain, µε

**Note 4.** Board Strain

**Note 5.** SJ Force

**E2.3.1.5 Analysis Procedure** In order to solve the transient bend problem, a single static analysis step is used in the model. The bending of the board generally takes place at low-displacement rates (when compared to shock-type event). Therefore, the effect of inertia on the model response is assumed to be insignificant. The loading fixture displacement is linearly ramped up during the analysis to the value specified in the step. The results from the model validation process show that a single static analysis step can model the bending process very well. Therefore, no sensitivity analysis was conducted.

**E2.3.1.6 Local Instability (STABILIZE Option)** In the presence of local instabilities/rigid-body motion in the model (due to excessive bending due to large displacements or fixture to ETB contact), particularly in the case of full-models, using automatic stabilization (i.e., viscous damping) via the STABILIZE option prevents the model from failing. This will generally help to overcome local instabilities in the model if present. A viscous energy dissipated fraction equal to 0.02% (0.0002) of the total model energy is used in the model. A sensitivity analysis was conducted to assess the effect of the model stabilization on the board strains and critical SJ forces. No significant difference in the board strains or the critical SJ forces was found. However, in the event of any local instability in the model, local stabilization will help progress the analysis.

## E3 MODEL VALIDATION

**E3.1 Transient Bend Testing (Used for Model Validation)** The TB testing conducted as part of the computational model validation process was done in three separate steps. The three different steps are summarized in Table E3-1.

**Table E3-1 Summary of the TB Testing Used for Model Validation Purpose**

Transient Bend Testing	Summary
<b>Step 1</b> Bare-Aluminum Board	Bare-aluminum boards of three thicknesses (32, 40, 62mils) are used for TB testing
<b>Step 2</b> Bare PC Board	Bare PCB board of 62mil thickness is used for TB testing
<b>Step 3</b> PCB with package mounted in the center	A BGA on a 40mil thick board is tested in TB

The TB test set-up and boundary conditions are as per the test BKM.

In the case of the bare-aluminum board testing, as part of the model validation procedure, board-level TB testing in conjunction with DIC (Digital Image Correlation) was conducted for each board-level TB test. The board-level testing involved bare-aluminum boards for which the board-strains at certain points on the board were monitored. The board-strains obtained from the testing were used to compare against those obtained from the TB model. These results are presented later in the section. For every board-level TB test, a DIC was also conducted. The displacement and board-strain results from the DIC were used to compare against those from the model as part of the model validation process.

An example showing a typical TB test set-up with the DIC apparatus under the board is shown in Figure E3-1. A schematic of the bare-aluminum board showing details of the TB set-up and the position of the strain gauges on the primary-side of the board is shown in Figure E3-2a and Figure E3-2b, respectively. It should be noted that a fourth strain gauge is placed on the secondary-side of the board under the SW corner strain gauge. This strain gauge is not shown in the figure.

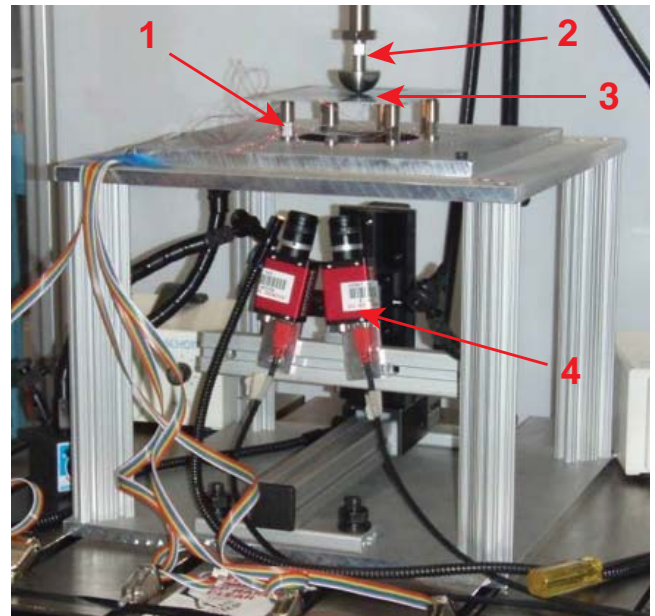


**Figure E3-1 A Typical TB Test Setup (Transient Bend Application of Quasi-Static DIC BKM, 2010) used for the Model Validation Process**

**Note 1.** Support Fixtures  
**Note 2.** Loading Fixtures

**Note 3.** Aluminum Board  
**Note 4.** DIC Apparatus

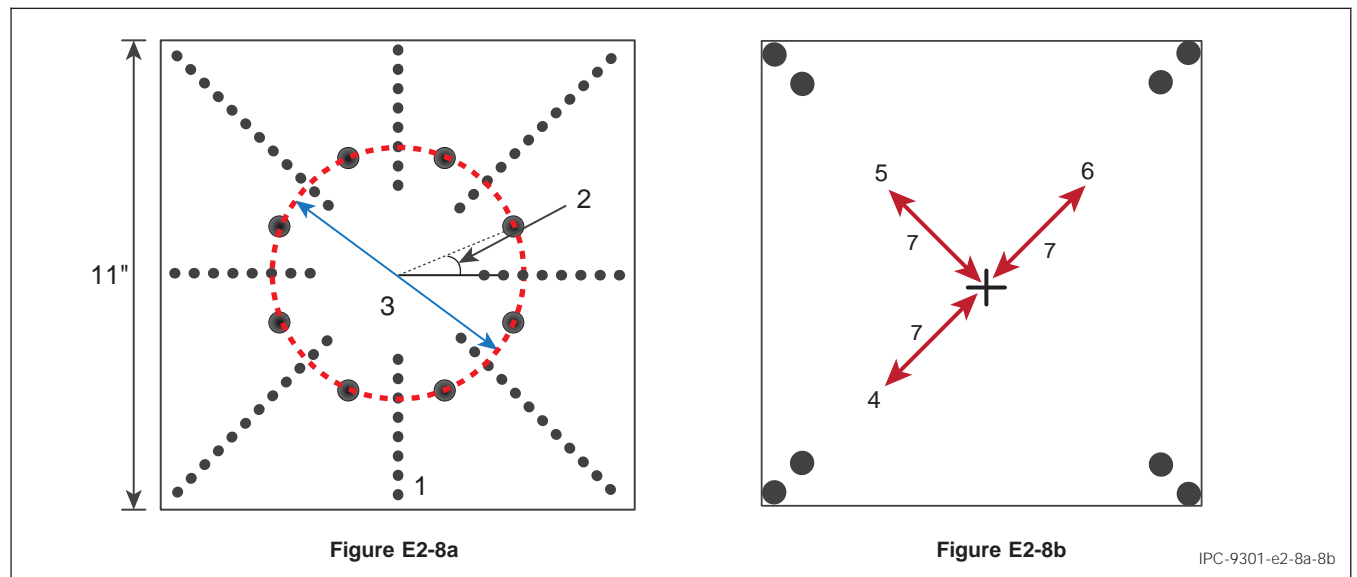


**Figure E3-2a and Figure E3-2b Examples of (a) Schematic of the TB Test Set-up with STB (Shock Test Board); and (b) Position of the Strain-Gauges on the Primary Side of the Board**

**Note 1.** Primary Board Side  
**Note 2.** Angle = 22.5°  
**Note 3.** Span = 155mm  
**Note 4.** SW

**Note 5.** NW  
**Note 6.** NE  
**Note 7.** 25mm

IPC-9301-e2-8a-8b



A typical strain gauge output showing the evolution of the board-strains with the board bending is shown in Figure E3-3. The results from the DIC analysis for the in-plane and out-of-plane displacements for a typical TB test are shown in Figure E3-4a and Figure E3-4b, respectively. It should be noted that only typical examples of the test result(s) are displayed in the figures.

It should be noted that the testing procedure in the case of the bare PCB (Step 2) and package on board (Step 3) is the same as that mentioned above. However, the DIC technique was not used for the last two steps. Some important TB test details for the last two steps are provided in later sections when comparing with modeling results.

**E3.2 Transient Bend Model Validation** The transient bend (TB) model validation was done as a step by step process. It was done in THREE stages: (1) TB model validation for bare-aluminum boards; (2) TB model validation for bare-FR4 boards and (3) Full package-board setup

In the remainder of the section the TB model validation for each of the steps will be provided in detail. The key objectives of the validation procedure are to determine if the model can reproduce well the board strain/deformation signatures (i.e., quantities that can be measured in tests). It should be noted that obtaining consistent and physically meaningful board-level test results are very essential to perform any comparison with models.

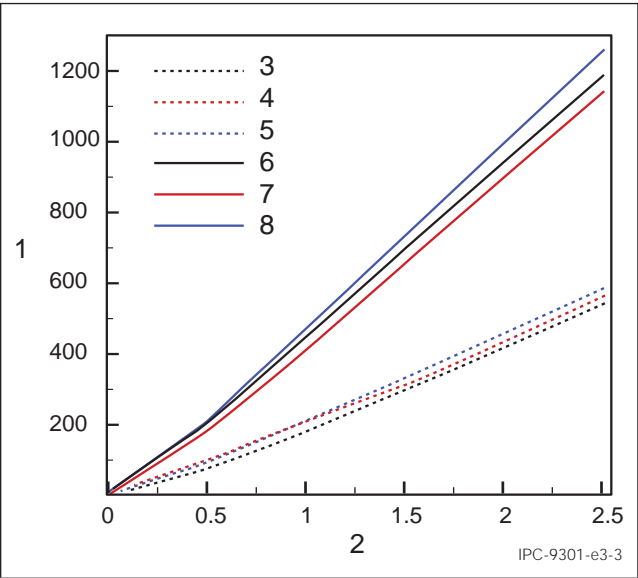


**Figure E3-3 An Example of the Board-Strain Components (e2, e4) at Three of the Strain Gauges from the TB Testing of Bare-Aluminum Boards**

- |  |                               |
|--|-------------------------------|
| <b>Note 1.</b> Board Strain, $\mu\epsilon$ | <b>Note 5.</b> E2 – NE Corner |
| <b>Note 2.</b> Displacement, mm            | <b>Note 6.</b> E4 – SW Corner |
| <b>Note 3.</b> E2 – SW Corner              | <b>Note 7.</b> E4 – NW Corner |
| <b>Note 4.</b> E2 – NW Corner              | <b>Note 8.</b> E4 – NE Corner |

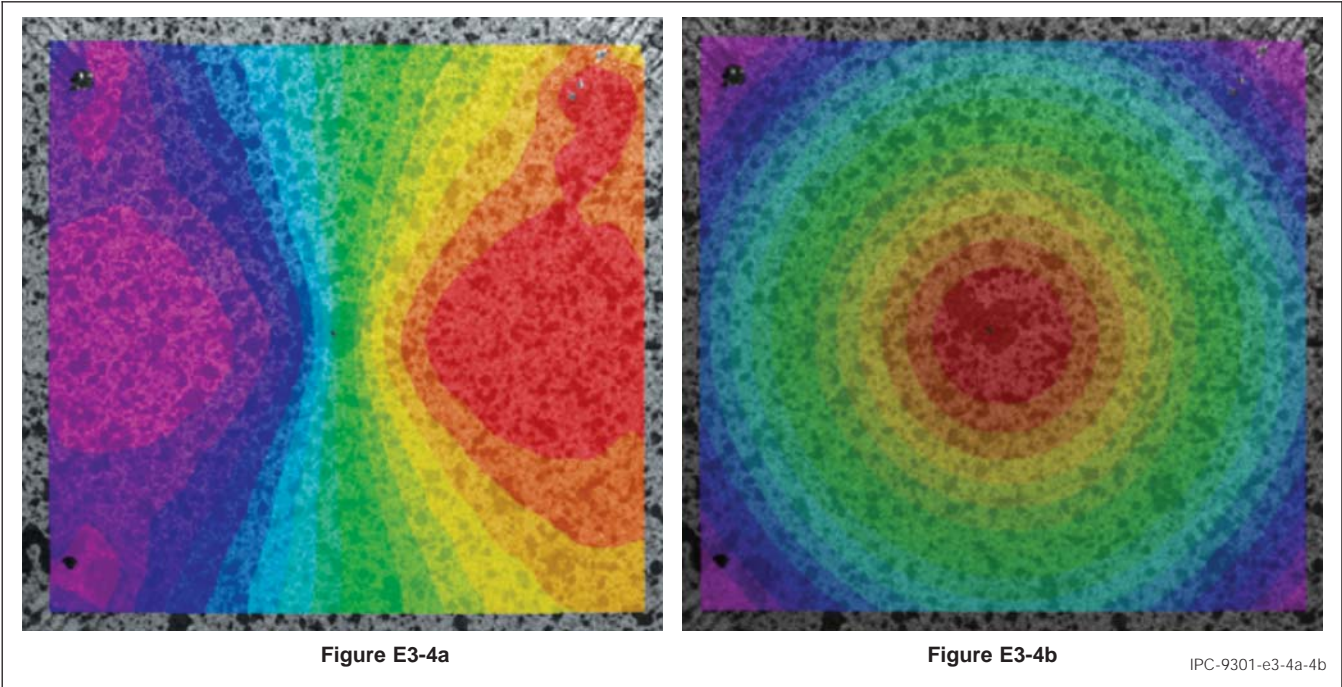


**Figure E3-4a and Figure E3-4b Examples of the DIC Results Showing: (a) In-Plane,  $U_x$ ; and (b) Out-of-Plane,  $U_z$ , Displacement Components During the TB Testing of Bare-Aluminum Boards**

**E3.2.1 Bare-Aluminum Board: Test vs. Model** Preliminary validation of the TB model is conducted using bare-aluminum boards. The advantage of the using bare-aluminum boards within the first validation step is that most of the material property uncertainty present in the case of an actual ETB is absent since aluminum material properties are well-known. The material property for homogeneous and isotropic aluminum (AA6061) material is generally well-known and readily available in literature. The finite-element (FE) computational model of the bare-aluminum board with a spherical bend set-up is displayed in Figure E3-5. The insert in the figure shows the location of the strain gauges placed on the primary side of the board, i.e., the side of the board in contact with the support fixtures. The three strain gauges are placed diagonally at a distance of 25mm from the center of the board. The use of three gauges helps determine if the bending of the board is symmetric. A fourth strain gauge is placed on the secondary side of the board. It noted that for convenience, the board used for this test has the design of a shock test board (STB).

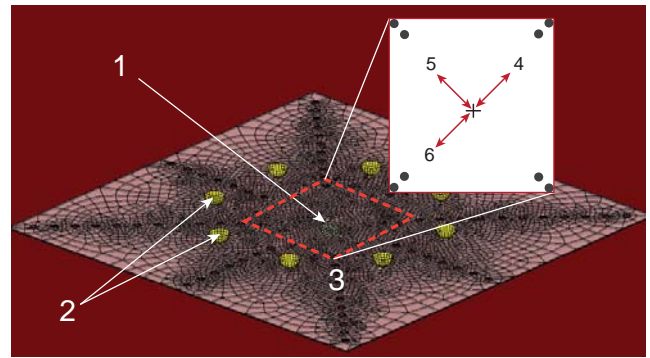


**Figure E3-5 Finite Element TB Model of the Bare-Aluminum Board**

**Note 1.** Loading Fixture

**Note 2.** Support Fixture

**Note 3.** Primary Board Side

**Note 4.** NE

**Note 5.** NW

**Note 6.** SW

**E3.2.2 Summary of Finite-Element (FE) Model** A summary of the FE model (shown in Figure E3-5) for the bare-aluminum board is provided in this section.

**E3.2.2.1 Material:** The aluminum material is modeled as a homogeneous, isotropic, perfectly plastic material. The material young's modulus of 68.9GPa and yield strength of 241MPa is used in the model. Material hardening during plastic deformation is not accounted for in the model. The supports/loading fixtures were assumed to undergo negligible deformation and therefore were modeled as analytical rigid surfaces.

**E3.2.2.2 Element Type:** Meshing of the board was accomplished using quadratic second-order reduced integration elements (C3D20R). In-order to capture the bending of the board effectively during the TB process, second-order elements are employed to mesh the board. A mesh sensitivity analysis was conducted to determine the board mesh-size which accurately captures the strains in the strain-gauge region. A mesh seed size of 2mm is used for the board.

**E3.2.2.3 Fixture and Board Interaction:** The normal contact force developed as a result of the interaction between the supports/loading fixtures and the board is modeled using the hard-penalty type contact within Abaqus® (Abaqus® Analysis User's Manual, Volume II: Analysis, 2008). The tangential force involved in the interaction is also represented using the Coulomb's friction law. A friction coefficient of 0.2 is used as input to the Coulomb's friction model.

**E3.2.2.4 Analysis and Boundary Conditions:** A single geometrically nonlinear static analysis procedure is utilized to solve the TB problem. The reference point for each of the support fixtures are constrained in all the degrees of freedom during the analysis, while, the reference point for the loading fixture is displaced in the direction normal to the board by a known displacement.

**E3.2.2.5 Post-Processing:** The board strains at the strain gauge locations are obtained by averaging the strains interpolated at certain path-points. A grid of path-points at the strain gauge locations is used. The force and displacement responses were directly output from the model. The board-strain post-processing method/script is the same as that discussed in Section E2-0.

**E3.2.3 Model Validation** The TB testing for bare-aluminum boards were conducted for three board thicknesses, i.e., 32mil, 40mil and 62mil. These three thickness aluminum boards have their bending stiffness equivalent to those of 40mil, 62mil and 93mil thick ETB boards, respectively. A comparison of the model and corresponding test results for the 32mil and 62mil thick bare-aluminum boards are provided in this section.

**E3.2.3.1 32mil Board** The results comparing the force-displacement responses from the model and test are shown in Figure E3-6. The model is in very good agreement with the test results suggesting that the overall board deformation during TB is well captured by the model. The maximum difference in force between the model and test results is 5%. It should be noted that the nonlinear force-displacement response as seen in the figure is well captured using a nonlinear geometric analysis.

As mentioned earlier, the board strains experienced during TB are measured using three strain gauges placed at a distance of 25mm from the center of the board on the primary side of the board and one strain gauge on the secondary side. The model strains are extracted at the same locations by averaging the strains over a set of path points (Abaqus® Analysis User's Manual, Volume II: Analysis, 2008). The board strains obtained from the testing along with the corresponding strains from the model are displayed in the Figure E3-7 strains on the primary side of board; and Figure E3-8 strains on the secondary side of the board, respectively. The strains obtained from the model and tests are in very good agreement. The maximum difference in strains between the model and test is 40 $\mu\epsilon$ .

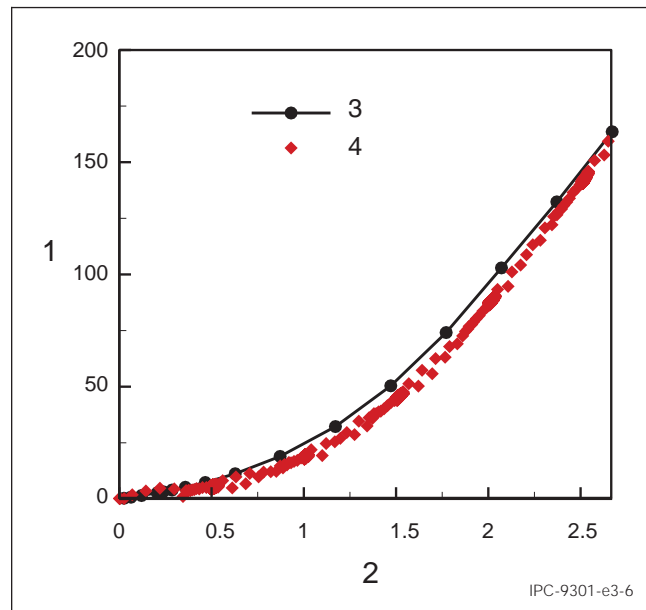


**Figure E3-6 Comparison of the Force vs. Displacement Response from the Model and Experiment for a 32mil Thick Bare-Aluminum Board**

Note 1. Force, N

Note 2. Displacement, mm

Note 3. Computational

Note 4. Experiment

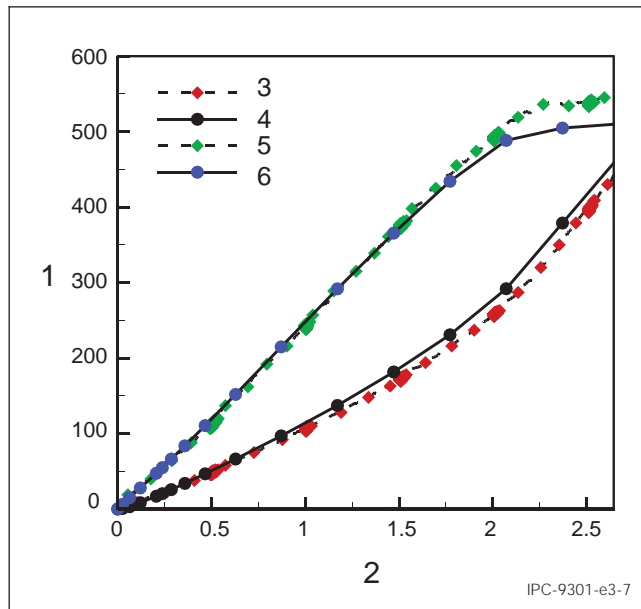


**Figure E3-7 Computational Model vs. Experimental Board Strains Comparison for the Strains on the Primary Board Side in a 32mil Thick Bare-Aluminum Board**

Note 1. Board Strain,  $\mu\epsilon$

Note 2. Displacement, mm

Note 3. Experiment - e2

Note 4. Computational - e2

Note 5. Experiment - e4

Note 6. Computational - e4

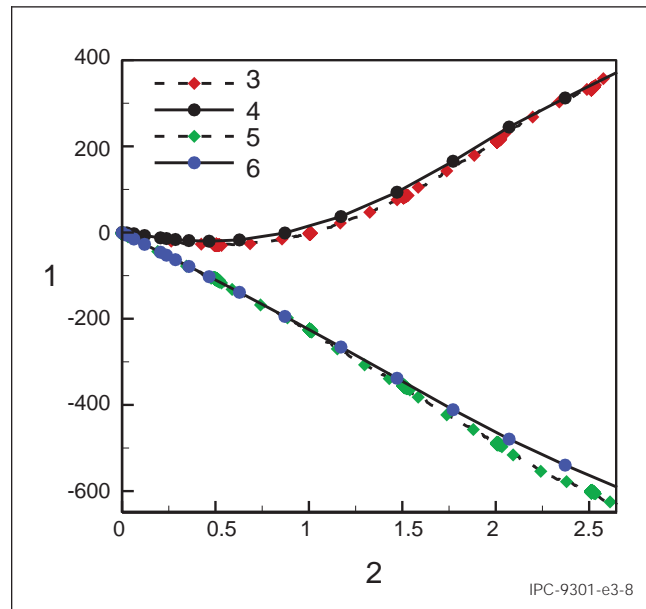


**Figure E3-8 Computational Model vs. Experimental Board Strains Comparison for the Strains on the Secondary Board Side in a 32mil Thick Bare-Aluminum Board**

Note 1. Board Strain,  $\mu\epsilon$

Note 2. Displacement, mm

Note 3. Experiment - e2

Note 4. Computational - e2

Note 5. Experiment - e4

Note 6. Computational - e4



As part of the model validation process, as mentioned earlier, the DIC technique was utilized for every bare-aluminum board TB test conducted. The DIC technique employs high-speed cameras to capture the evolution of the board-deformation by taking images at discrete time steps during the TB process. The images are post-processed to obtain the spatial variation of the in-plane board displacements and strains. A contour plot of the board in-plane U-displacement (x-direction) and out-of-plane W-displacement (z-direction) obtained using the DIC technique and TB model is displayed in Figure E3-9. The model displacements agree very well with the test results. Any variation between the test and model could be due to the inaccuracy in selecting the exact point on the board using the DIC post-processing software.

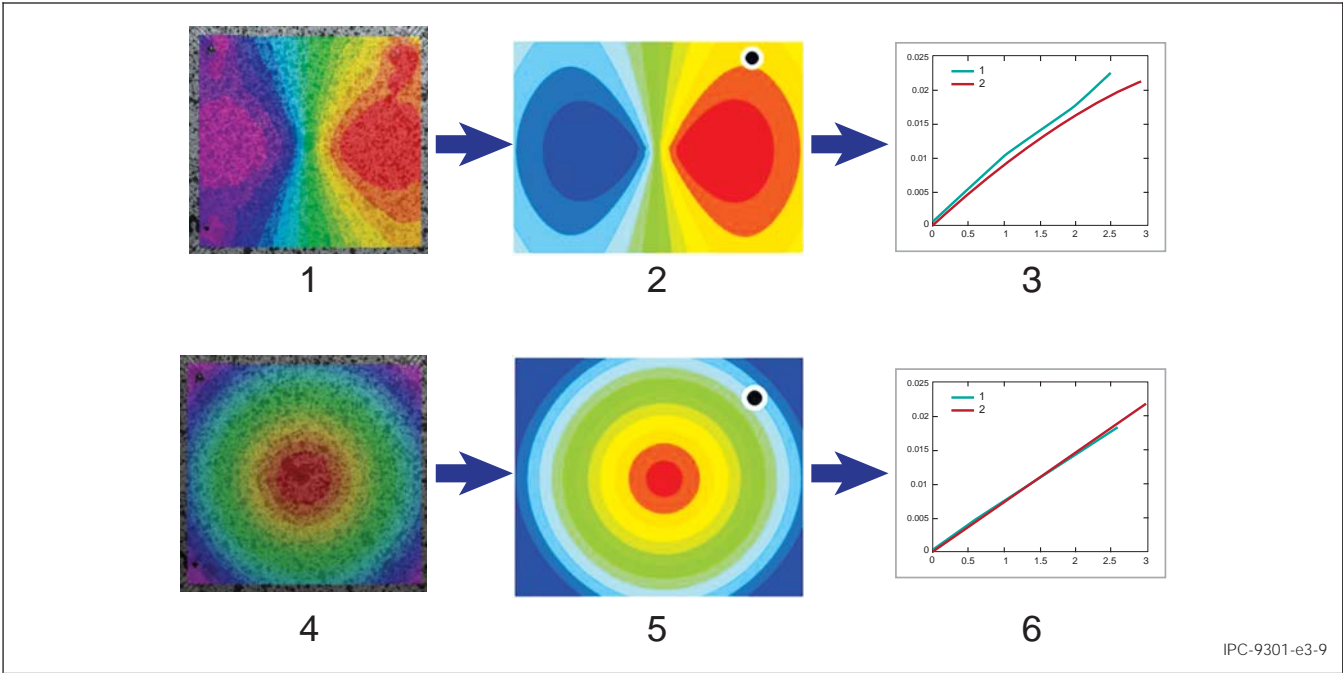


**Figure E3-9 A Comparison of the Computational Model vs. DIC Experimental Results for the Board Displacements for a 32mil Thick Bare-Aluminum Board**

Note 1. Test: U-Disp.

Note 2. Model: U-Disp.

Note 3. Model vs. Test: U-Disp.

Note 4. Test: W-Disp.

Note 5. Model: W-Disp.

Note 6. Model vs. Test: W-Disp.

**E3.2.3.2 62mil Board** The test data used for the computational model validation in the case of a 62mil bare-aluminum are the same as those of the 32mil bare-aluminum board. A comparison of the results obtained from the model and test are provided below. Figure E3-10 shows the force vs. displacement response obtained from the model and test. The modeling results are in very good agreement with the test results. The maximum difference in force between the model and test results is 5%.

The board strains obtained from the board-level testing along with the corresponding strains from the model are displayed in the Figure E3-11a corresponding to strains on the primary side of board; and Figure E3-11b corresponding to strains on the secondary side of the board, respectively. The board strains obtained from the model and test are in very good agreement, with the maximum difference in strains between the model and test being 20 $\mu\epsilon$ .

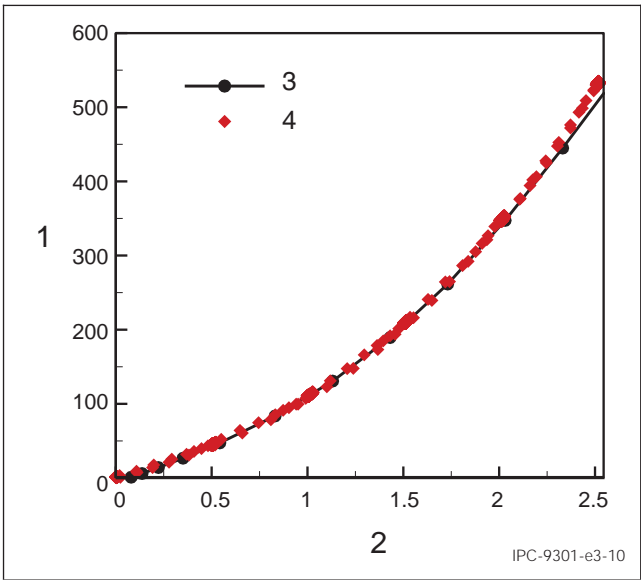


**Figure E3-10 Comparison of the Force vs. Displacement Response from the Model and Experiment for a 62mil Thick Bare-Aluminum Board**

Note 1. Force, N

Note 2. Displacement, mm

Note 3. Computational

Note 4. Experiment

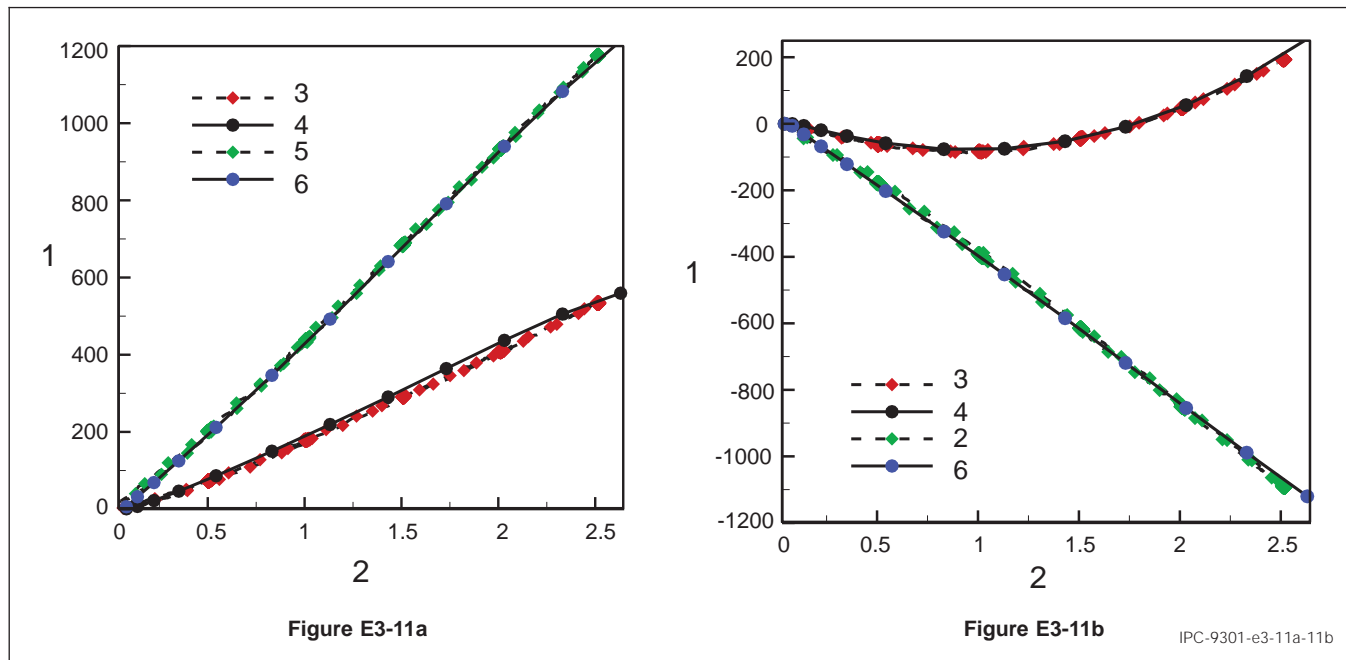


**Figure E3-11a and Figure E3-11b Computational Model vs. Experimental Board Strains Comparison for the Strains on: (a) Primary Board Side; and (b) Secondary Board Side in a 62mil Thick Bare-Aluminum Board**

**Note 1.** Board Strain,  $\mu\epsilon$   
**Note 2.** Displacement, mm

**Note 3.** Experiment – e2  
**Note 4.** Computational – e2

**Note 5.** Experiment – e4  
**Note 6.** Computational – e4

**E3.2.4 Bare FR4 Board** The validation of the TB model in the case of a bare-aluminum board has been discussed in the previous section. The model can predict the board deformation/strains in the case of bare-aluminum board very well. The model validation has been extended for the case of bare-FR4 boards. The board-level testing (Embree T., Daharwal P., 2010) conducted for bare FR-4 boards is used in the model validation process. The bare-FR4 boards are strain gauged at the four locations along the diagonal of the board to monitor the temporal evolution of the board strains with the applied displacement. A comparison of the force vs. displacement response between the experiment and computational model is shown in Figure E3-12. The maximum difference in force between the model and test results is 8%. A comparison of the board strains obtained from the test and model is shown in Figure E3-12 Comparison of the force vs. displacement response from the model and experiment for a 62-mil thick bare FR4 board.

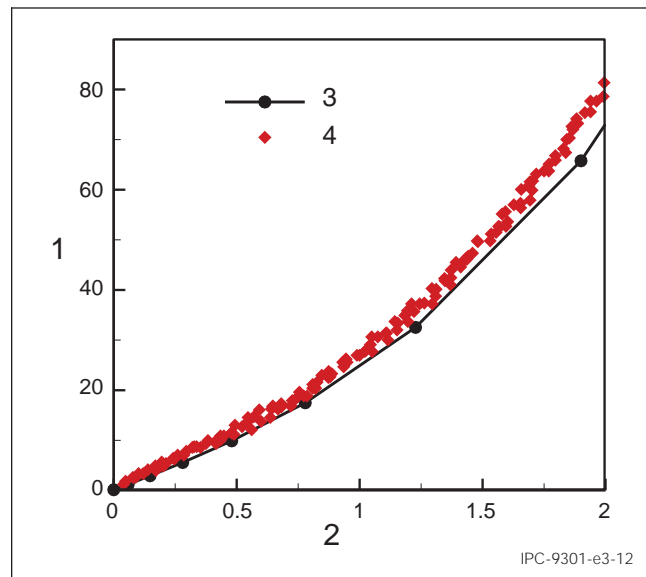


**Figure E3-12 Comparison of the Force vs. Displacement Response from the Model and Experiment for a 62mil Thick Bare FR4 Board**

**Note 1.** Board Strain,  $\mu\epsilon$   
**Note 2.** Displacement, mm

**Note 3.** Computational  
**Note 4.** Experiment

The model, Figure E3-13, is in very good agreement with the test results suggesting that the overall board deformation during TB is well captured by the model. The strains obtained from the model and test is in very good agreement, with the maximum difference in strains between the model and test being 70µε.

The qualitative and quantitative agreement between the TB model and test results is very good. The overall board deformation is well reproduced by the model if accurate material properties are used in the model. Also, it is important to obtain consistent test data for comparison with modeling results. The validation on bare boards ensures that the force, displacements and strain quantities as well as the method of extraction of these quantities from the model are appropriate.

**E3.2.5 Package Board Assembly** The validation of the TB model in the case of an actual package-board assembly is discussed in the section. The package considered in this study is a 37.5×32×0.842mm BGA single-die package. The BGA minimum pitch is 0.7mm. The nominal ETB thickness in this case is 40mil. The TB testing of the package is done according to the test BKM. During the package bending, board strains at all the four package corners (in the North East, South East, South West and North West directions) are monitored. It should be noted that the four package corner locations, i.e., North East, South East, South West and North West are abbreviated as NE, SE, SW and NW, respectively. At each of the four corners, strain gauges are placed on the board at a distance of approximately 5mm from the package corner along the package diagonal direction. The positions of the board strain gauges at the four corners of the BGA TV are displayed in Figure E3-14. The support span in the TB test is 120mm.

The results from the test are then compared with those obtained from the TB computational model developed in this BKM. A comparison of the global force vs. displacement response obtained from the model and test is displayed in Figure E3-15. The overall agreement between the model and test is very good (Figure E3-15). The model can predict the board bending response very well.

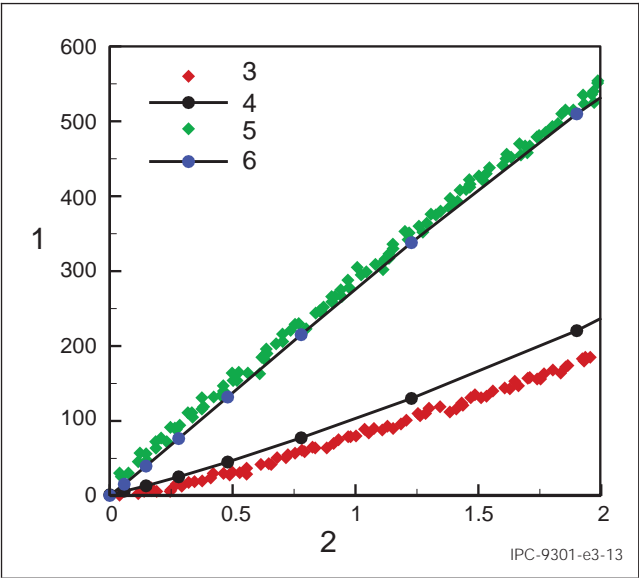


**Figure E3-13 Comparison of the TB Model vs. Experimental Results for the Strains on the Primary Board Side for a 62mil Thick Bare FR4 Board**  
**Note 1.** Board Strain, µε  
**Note 2.** Displacement, mm  
**Note 3.** Experiment – e2  
**Note 4.** Computational – e2  
**Note 5.** Experiment – e4  
**Note 6.** Computational – e4

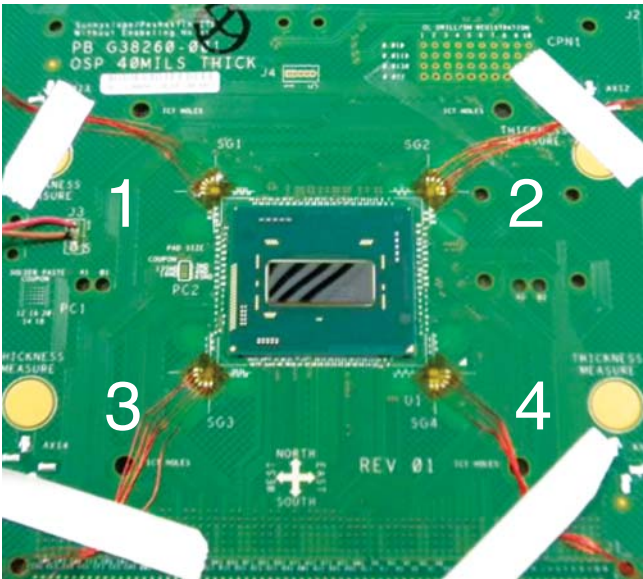


**Figure E3-14 BGA TV with the Board Strain Gauges Attached**  
**Note 1.** NW  
**Note 2.** NE  
**Note 3.** SW  
**Note 4.** SE

## E4 MODEL CALIBRATION

**E4.1 Solder Joint Failure Metric** The solder joint failure metric used is the failure stress at which crack initiates in the solder joints. This failure metric is calculated using the effective solder joint force which is computed in the model. In order to determine the solder joint failure stress, board level test-to-fail data is used. For model calibration, test to fail data for test-vehicle is utilized. From the test to fail data, the board strain at which crack initiation occurs (in the case of a 40mil thick board) is  $\sim 700\mu\epsilon$ , Figure E4-1. This board strain will be referred to as failure strain in this document. The solder joint failure stress for a failure strain of  $\sim 700\mu\epsilon$  is  $\sim 40\text{MPa}$ , Figure E4-2. Therefore, the solder joint failure stress is  $40\text{MPa}$ .

Ideally, the model calibration has to be done for several different BGA-pitches (or ball sizes) in order to obtain a failure stress which captures the differences in solder joint micro-structure which could impact the failure stress.

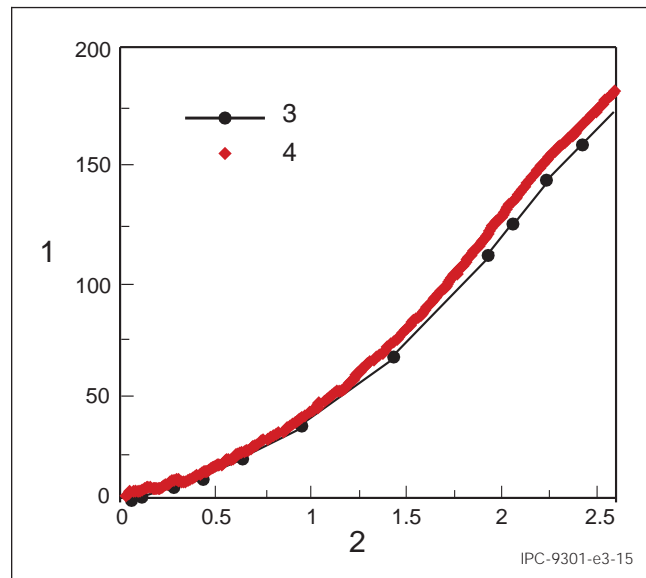


**Figure E3-15 Comparison of the Force vs. Displacement Response from the Model and Experiment for BGA TV on a 40mil Thick ETB**

**Note 1.** Force, N

**Note 2.** Displacement, mm

**Note 3.** Computational

**Note 4.** Experiment

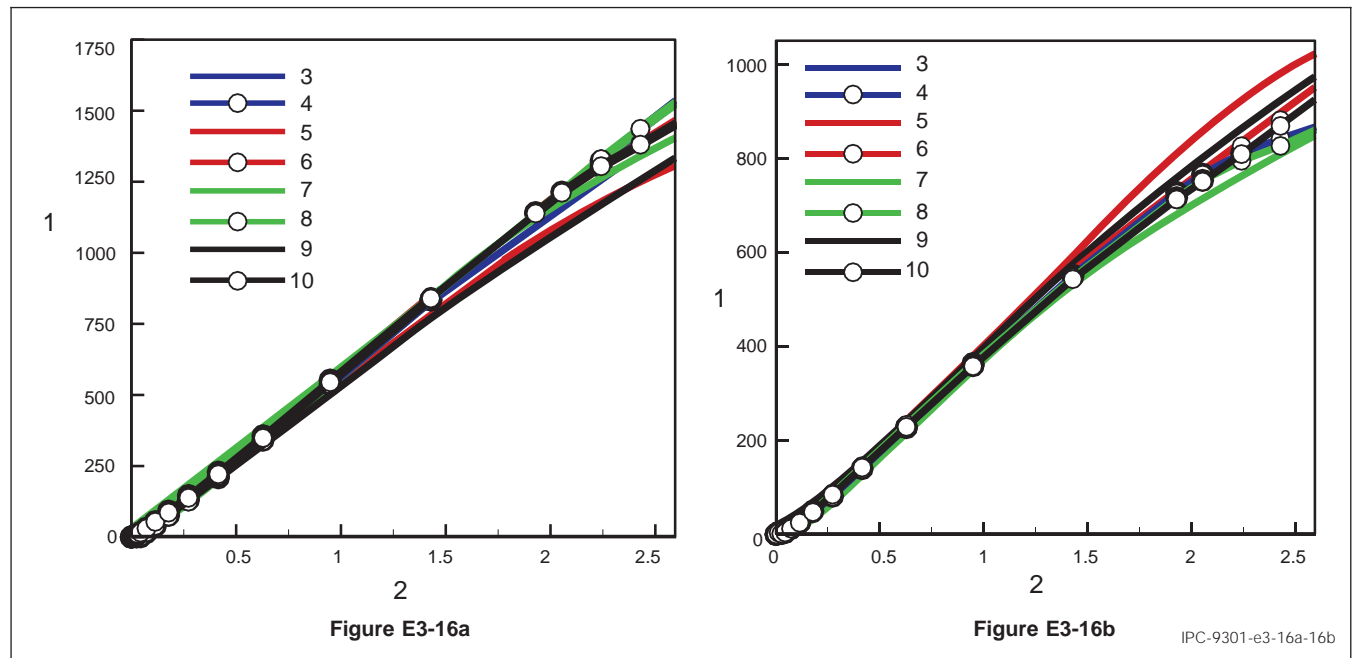


**Figure E3-16a and Figure E3-16b Package Corner-to-Corner (SW, NW, NE and SE) Board Strain Comparison Between the Computational Model and Test Results: (a)  $e_2$  Strain Component; and (b)  $e_4$  Strain Component**

**Note 1.** Board Strain,  $\mu\epsilon$   
**Note 2.** Displacement, mm  
**Note 3.** Test SW  
**Note 4.** Model SW  
**Note 5.** Test NW

**Note 6.** Model NW  
**Note 7.** Test NE  
**Note 8.** Model NE  
**Note 9.** Test SE  
**Note 10.** Model SE

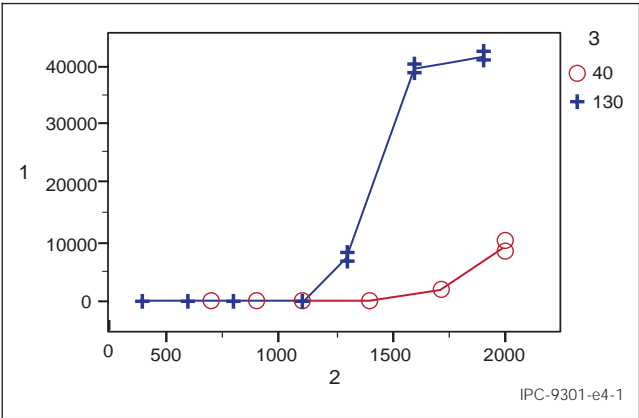


Figure E4-1 Board Level Test to Fail Data

- Note 1.** T4 Cumulative Damage  
**Note 2.** Strain Target (ue)  
**Note 3.** Thickness (mil)

E5 MODEL BENCHMARKING

**E5.1 Predicting Failure Strain** In this section, the calibrated model along with the solder failure stress metric of 40MPa is utilized to predict the failure strain (i.e., at crack initiation) for another TV. The solder joint pitch for this TV is 0.4mm and board thickness is 28mil. The tests to fail results are shown in Table E5-1. The results indicate that the strain at 0% crack is 450µε and the corresponding displacement is 0.4mm. The modeling results are shown in Figure E5-1. A comparison between the model prediction and test data is displayed in Table E5-2. The model prediction error for failure strain and failure displacement is ~16% and 12% respectively.

It should be noted that the model benchmarking in this case is done for a TV which has a different pitch, board thickness and package architecture compared to TV used for model calibration. Model calibration using a BGA package of 0.7mm pitch would be a more suitable comparison to make.

The source for difference between model and test could be due to several reasons: (a) material properties of board/packages; (b) board strength and supplier variation; (c) variations due to test metrology e.g., displacement measurement and strain gauge placement etc.; (d) solder joint microstructure etc. will impact strength. Table E5-3 shows some of the sources for the differences between model and test.

Table E5-1 Summary of Transient Bend Test Data for TV Used for Validation

Transient Bend Data Summary for TV: Pitch=0.4mm, Board Thk=28mil					
# Boards	Displacement Target (mm)	Strain Target (µε)	Failure Analysis		
			FA Type	Pass/Tested	FA Result
8	0.4	450	XS	8/8	Pass
8	0.5	500	XS	7/8	Fail

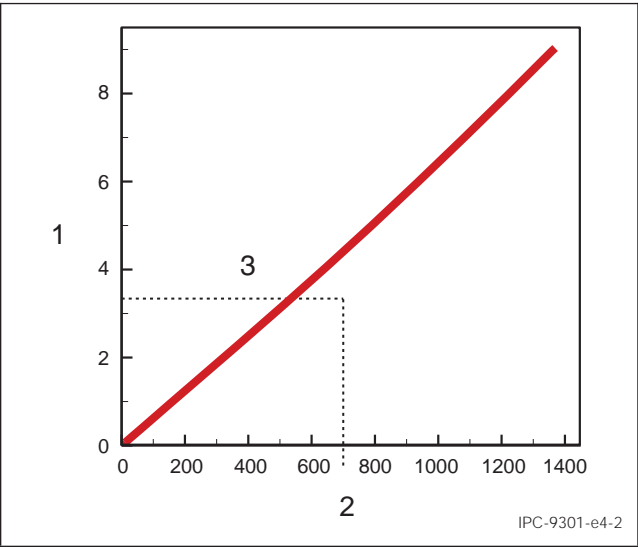
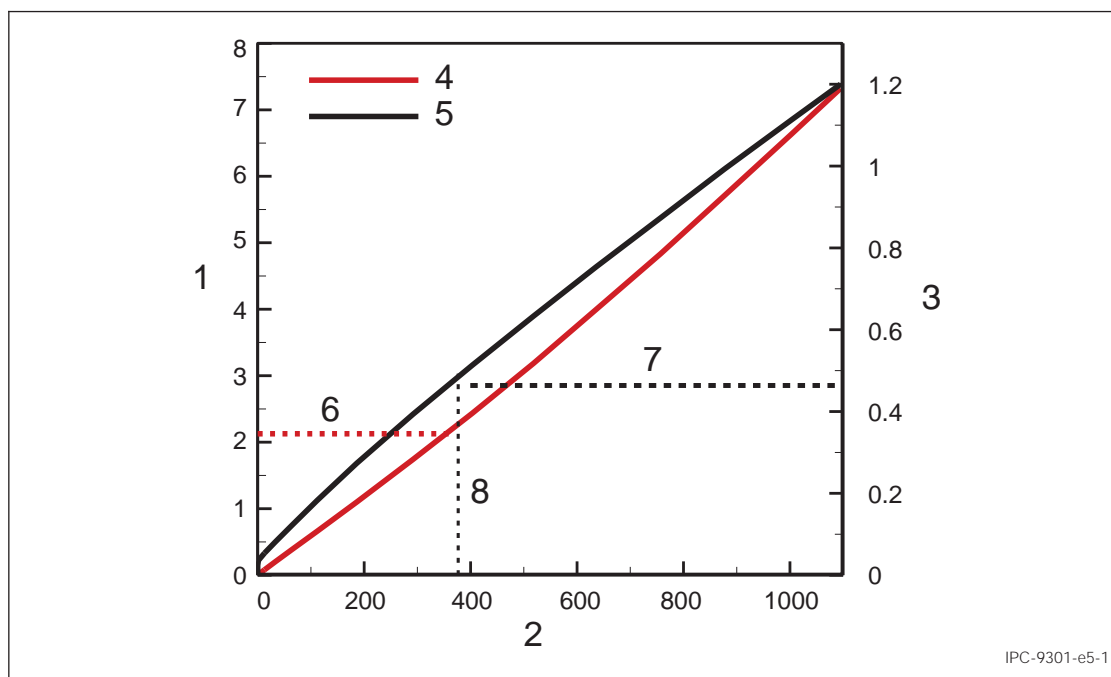


Figure E4-2 Model Calibration Board Level Test Data for 40mil Thick Board

- Note 1.** Solder Joint Effective Force, N  
**Note 2.** Board Strain, µstrain  
**Note 3.** Failure Stress = 40MPa



**Figure E5-1 Model Prediction Results for TV (pitch=0.4mm and board thickness=28mil)**

**Note 1.** Solder Joint Effective Force, N

**Note 2.** Board Strain,  $\mu\epsilon$

**Note 3.** Fixture Displacement, mm

**Note 4.** Solder Joint Force

**Note 5.** Fixture Displacement

**Note 6.** Failure Stress = 40MPa

**Note 7.** Displacement = 0.47mm

**Note 8.** Failure Strain = 370 $\mu\epsilon$

**Table E5-2 Comparison Between Model and Experiment**

Comparison between model and experimental data			
	Experiment	Model	Error
Displacement (mm)	0.4	0.47	12%
Failure Strain ( $\mu\epsilon$ )	450	370	16%

**Table E5-3 General Reasons for Difference Between Model and Test Data**

Parameter	Comments
Package/Board material properties	Variation in material properties will result in differences between model vs test.
Board laminate strength	Will cause differences in failure mode
Variation in test metrology	The displacement and board strain are very sensitive to the metrology. Slight error in placement of strain gauges will cause change in board strain
Microstructural differences for different pitch BGAs	The differences in microstructure between size BGAs could impact their and therefore the failure stress
Board design features	Model does not account for local board design features and in-homogeneity. Model assumes isotropic homogeneous board material. This will cause some differences in strain

## E6 MODEL APPLICATION

**E6.1 Usage of Model Results** The model once calibrated and validated can be utilized in several different ways. It can be used to: (a) predict the board strain limit(s) for a given package and board design; and (b) understand the impact of package and board parameters on the board strain limits. One of those studies can be found in the paper by G. Arakere et. al. (Itherm2016).

## E7 SUMMARY

**E7.1 Development of FEM Modeling** This document demonstrates in detail a systematic approach for development of a FEM modeling methodology that is to be used for risk assessment, design for reliability and to replace time consuming and costly tests.



When a specific problem is identified, the key deformation mechanisms need to be understood in order for adequate mathematical description to be adopted. Right computational scheme for solving the equations as well as mesh sensitivity study needs to be performed in order to assure convergence of the solution.

The measurable properties are used to validate the model with the experimental data. When the uncertainty from the electronic component and boards are hard to control, artificial setup can be used to simplify the test, to ensure the high confidence model validation. In this case, uniform aluminum board was used before bare PCB board or board with component to validate the strain and reaction force from the spherical bend.

After validation, high quality failure data is needed to calibrate the model and determine the parameters that cannot be measured, like stress which is the adopted failure metric in this study. The obtained failure metric values were benchmarked with more test data.

## **E8 BIBLIOGRAPHY**

IPC/JEDEC 9707: "Spherical Bend Test Method for Characterization of Board Level Interconnects," 2011

G. Arakere, M. Vujosevic, T. Embree, "Board Level Interconnect Risk Assessment in Spherical Bend," Itherm 2016, accepted for publication.

## E9 SAMPLE TB MODEL

**E9.1 Example: TB Analysis Model Input File Format** The default material properties used in the TB model is given below.

**E9.1.1 Material Properties (Abaqus® Input Format)** The Abaqus® script for the TB model analysis outlined in this section. This script illustrates the steps and parameters used to perform the TB analysis.

```
** MATERIALS
**
** Generic Board property - Isotropic
*Material, name=BOARD-ISO
*Density
2.15e-09,
*Elastic
22000., 0.36
** Generic Board property - Orthotropic (Eng. Constants)
*Material, name=BOARD-ORTHO
*Density
2.15e-09,
*Elastic, type=ENGINEERING CONSTANTS
24000.,24000.,16000., 0.2, 0.143, 0.143, 8000., 4000.
4000.,
** Bulk Copper Property
*Material, name=COPPER
*Density
8.23e-09,
*Elastic
128700., 0.3435
** Generic Mold Compound property
*Material, name=MOLD
*Density
1.97e-09,
*Elastic
23000., 0.36
** Solder (SAC405) Property - Elastic
*Material, name=SAC405-ELASTIC
*Density
9e-09,
*Elastic
55181.6, 0.3
** Solder (SAC405) Property - Elastic-Plastic
*Material, name=SAC405-ELASTIC-PLASTIC
*Density
7.4e-09,
*Elastic
53000., 0.3425
*Plastic
26., 0.
60., 0.005
80., 0.01
100., 0.02
120., 0.03
200., 0.1
** Bulk Silicon Property
*Material, name=SILICON
*Density
```

```

2.33e-09,
*Elastic
131000., 0.3
** Generic Substrate property (Non-DS region) - Eng. Constants
*Material, name=SUBS_BULK
*Density
1.7e-09,
*Elastic, type=ENGINEERING CONSTANTS
27000.,27000., 3990., 0.24, 0.24, 0.24,10880., 1610.
1610.,
** Generic Substrate property (DieShadow region) - Eng. Constants
*Material, name=SUBS_DS
*Density
1.7e-09,
*Elastic, type=ENGINEERING CONSTANTS
31000.,31000., 4580., 0.24, 0.24, 0.24,12500., 1847.
1847.,
** Generic Underfill Material property
*Material, name=UF_MTL
*Density
1.97e-09,
*Elastic
9900., 0.23

```

The boundary conditions, step and outputs in a typical quarter symmetric model is given below.

```

** INTERACTION PROPERTIES
**
*Surface Interaction, name=INT-FRICTION
1.,
*Friction, slip tolerance=0.005
0.2,
**
** BOUNDARY CONDITIONS
**
** Name: ETB-XYMM Type: Symmetry/Antisymmetry/Encastre
*Boundary
ETB.XSYMM, XSYMM
** Name: ETB-YSYMM Type: Symmetry/Antisymmetry/Encastre
*Boundary
ETB.YSYMM, YSYMM
** Name: LoadingPin Type: Displacement/Rotation
*Boundary
_G18, 1, 1
_G18, 2, 2
_G18, 4, 4
_G18, 5, 5
_G18, 6, 6
** Name: Support_1 Type: Displacement/Rotation
*Boundary
_G15, 1, 1
_G15, 2, 2
_G15, 3, 3
_G15, 4, 4
_G15, 5, 5
_G15, 6, 6

```

```

** Name: Support_2 Type: Displacement/Rotation
*Boundary
_G16, 1, 1
_G16, 2, 2
_G16, 3, 3
_G16, 4, 4
_G16, 5, 5
_G16, 6, 6
** Name: Support_3 Type: Displacement/Rotation
*Boundary
_G17, 1, 1
_G17, 2, 2
_G17, 3, 3
_G17, 4, 4
_G17, 5, 5
_G17, 6, 6
** Name: TB_JITRA_BOT-XYMM Type: Symmetry/Antisymmetry/Encastre
*Boundary
TB_JITRA_BOT.XYMM, XYMM
** Name: TB_JITRA_BOT-YSYMM Type: Symmetry/Antisymmetry/Encastre
*Boundary
TB_JITRA_BOT.YSYMM, YSYMM
** Name: TB_JITRA_TOP-XYMM Type: Symmetry/Antisymmetry/Encastre
*Boundary
TB_JITRA_TOP.XYMM, XYMM
** Name: TB_JITRA_TOP-YSYMM Type: Symmetry/Antisymmetry/Encastre
*Boundary
TB_JITRA_TOP.YSYMM, YSYMM
**
** INTERACTIONS
**
** Interaction: ETB_to>LoadingPin
*Contact Pair, interaction=INT-FRICTION, small sliding, type=SURFACE TO SURFACE,
adjust=0.
TB_JITRA_BOT.ETB-BOT-SURF, LoadingPin.Fixture
** Interaction: ETB_to>Support_1
*Contact Pair, interaction=INT-FRICTION, small sliding, type=SURFACE TO SURFACE,
adjust=0.
ETB.ETB-TOP-SURF, Support_1.Fixture
** Interaction: ETB_to>Support_2
*Contact Pair, interaction=INT-FRICTION, small sliding, type=SURFACE TO SURFACE,
adjust=0.
ETB.ETB-TOP-SURF, Support_2.Fixture
** Interaction: ETB_to>Support_3
*Contact Pair, interaction=INT-FRICTION, small sliding, type=SURFACE TO SURFACE,
adjust=0.
ETB.ETB-TOP-SURF, Support_3.Fixture
**
**
** STEP: TransientBend
**
*Step, name=TransientBend, nlgeom=YES, inc=100000
*Static, stabilize=0.0002, allsdtol=0.05, continue=NO
0.01, 1., 1e-06, 0.1
**

```

```

** BOUNDARY CONDITIONS
**
** Name: LoadingPin2 Type: Displacement/Rotation
*Boundary
_G19, 3, 3, 2.
**
** OUTPUT REQUESTS
**
*Restart, write, frequency=0
**
** FIELD OUTPUT: F-Output-1
**
*NODE PRINT, FREQ=1, NSET>LoadingPin.LoadingPin-RefPt_
U
RF
*SECTION PRINT, FREQ=1, NAME=Ball_6_47, SURFACE=TB_JITRA_BOT.Ball_6_47, AXES=LOCAL,
  UPDATE=YES
SOF
*SECTION PRINT, FREQ=1, NAME=Ball_5_47, SURFACE=TB_JITRA_BOT.Ball_5_47, AXES=LOCAL,
  UPDATE=YES
SOF
*Output, field
*Node Output
U,
*Element Output, directions=YES
LE, S
**
** HISTORY OUTPUT: H-Output-1
**
*Output, history, variable=PRESELECT
*End Step

```

**E9.2 Solder-Joint Resultant Force Metric** For a given solder-joint, the solder joint effective/resultant force component is used for accessing the relative risk of packages in TB. The resultant force is calculated using the normal force component,  $F_N$ , and the in-plane shear force (effective shear force),  $F_S$ , as follows:

$$SJ \text{ Resultant Force Metric} = \sqrt{F_N^2 + F_S^2}$$

The SJ loading angle (i.e., the angle between the normal force and shear force components) as a function of the different package design factors are generally in the range between 30-50 degrees, as shown in Figure E9-1. The SJ resultant force is used as a measure of the force-state by assuming that the force-state in the loading angle range can be represented by an arc with a radius equal to the SJ resultant force. Therefore, the effective stress calculated using this resultant SJ force is used as the SJ failure metric.

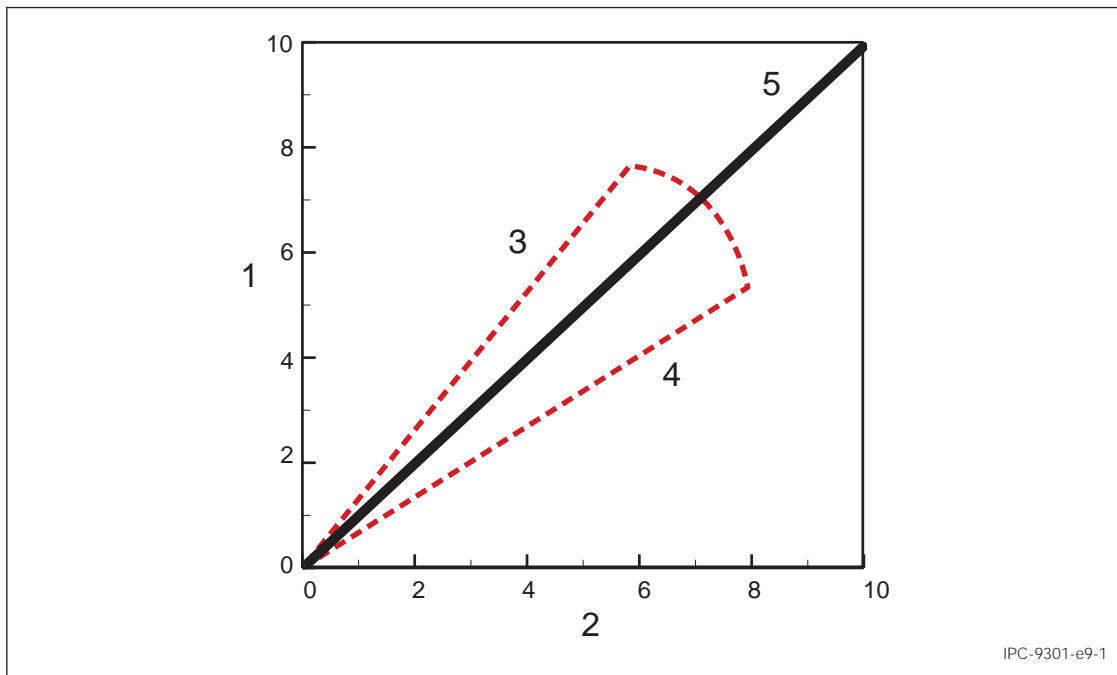


**Figure E9-1 SJ Loading Angle**

**Note 1.** Shear Force

**Note 2.** Normal Force

**Note 3.** 50° Line

**Note 4.** 30° Line

**Note 5.** 45° Line

This Page Intentionally Left Blank





## ANSI/IPC-T-50 Terms and Definitions for Interconnecting and Packaging Electronic Circuits Definition Submission/Approval Sheet

The purpose of this form is to keep current with terms routinely used in the industry and their definitions. Individuals or companies are invited to comment. Please complete this form and return to:

IPC  
3000 Lakeside Drive, Suite 105N  
Bannockburn, IL 60015-1249  
Fax: 847 615.7105

### SUBMITTOR INFORMATION:

Name: \_\_\_\_\_

Company: \_\_\_\_\_

City: \_\_\_\_\_

State/Zip: \_\_\_\_\_

Telephone: \_\_\_\_\_

Date: \_\_\_\_\_

- ☐ This is a **NEW** term and definition being submitted.  
☐ This is an **ADDITION** to an existing term and definition(s).  
☐ This is a **CHANGE** to an existing definition.

Term	Definition

If space not adequate, use reverse side or attach additional sheet(s).

Artwork: ☐ Not Applicable ☐ Required ☐ To be supplied

☐ Included: Electronic File Name: \_\_\_\_\_

Document(s) to which this term applies: \_\_\_\_\_

Committees affected by this term: \_\_\_\_\_

Office Use	
IPC Office	Committee 2-30
Date Received: _____	Date of Initial Review: _____
Comments Collated: _____	Comment Resolution: _____
Returned for Action: _____	Committee Action: <input type="checkbox"/> Accepted <input type="checkbox"/> Rejected
Revision Inclusion: _____	<input type="checkbox"/> Accept Modify
IEC Classification	
Classification Code • Serial Number	
Terms and Definition Committee Final Approval Authorization: Committee 2-30 has approved the above term for release in the next revision.	
Name: _____ Committee: <u>IPC 2-30</u> Date: _____	



## Standard Improvement Form

**IPC/JEDEC-9301**

The purpose of this form is to provide the Technical Committee of IPC with input from the industry regarding usage of the subject standard.

Individuals or companies are invited to submit comments to IPC. All comments will be collected and dispersed to the appropriate committee(s).

If you can provide input, please complete this form and return to:

IPC  
3000 Lakeside Drive, Suite 105N  
Bannockburn, IL 60015-1249  
Fax 847 615.7105  
E-mail: [answers@ipc.org](mailto:answers@ipc.org)

---

1. I recommend changes to the following:

\_\_\_ Requirement, paragraph number \_\_\_\_\_  
\_\_\_ Test Method number \_\_\_\_\_, paragraph number \_\_\_\_\_

The referenced paragraph number has proven to be:

\_\_\_ Unclear \_\_\_ Too Rigid \_\_\_ In Error  
\_\_\_ Other \_\_\_\_\_

---

2. Recommendations for correction:

---

---

---

---

---

3. Other suggestions for document improvement:

---

---

---

---

---

Submitted by:

Name

Telephone

Company

E-mail

Address

City/State/Zip

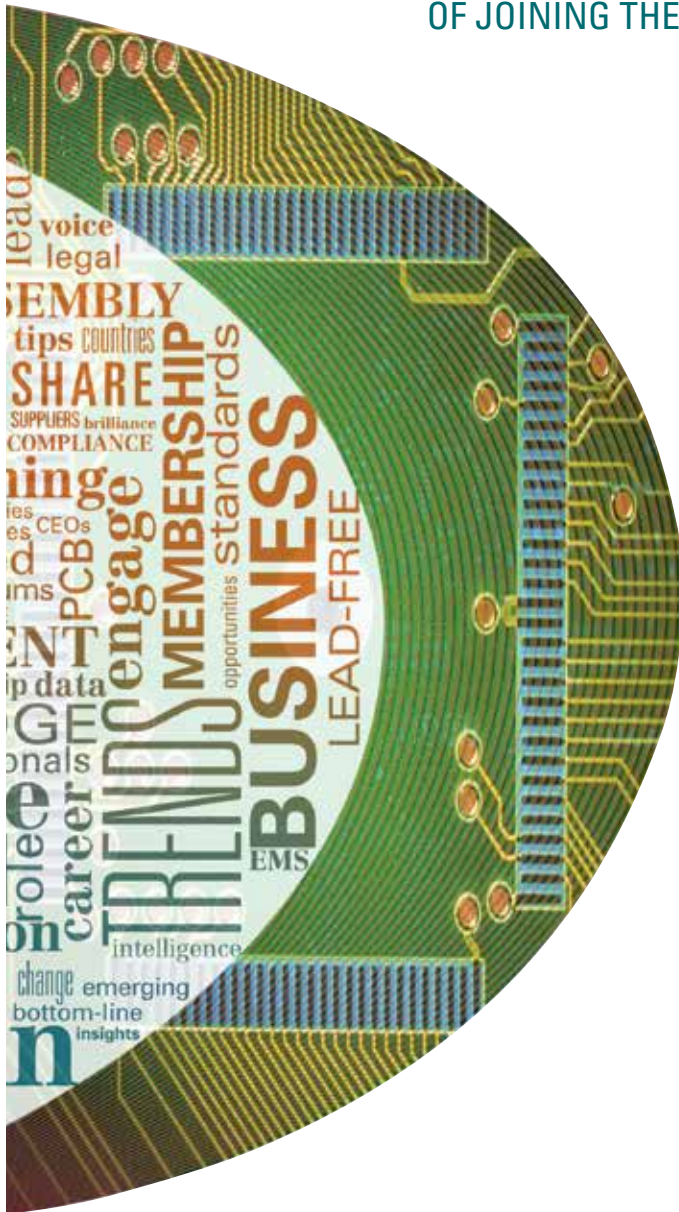
Date

---



# Experience the **BENEFITS**

OF JOINING THE ELECTRONICS INDUSTRY'S PREMIER ASSOCIATION



Expand your company's  
resources and influence in  
the electronics industry.

- Stay Current
- Get Connected
- Shape the Industry
- Train Your Staff
- Contain Costs
- Join the leaders in IPC
- Market Your Business

Learn more about IPC membership and apply online at [www.ipc.org/membership](http://www.ipc.org/membership)  
or contact the Member Success team at [membership@ipc.org](mailto:membership@ipc.org).



*Association Connecting Electronics Industries*



3000 Lakeside Drive, Suite 105 N  
Bannockburn, IL 60015

847-615-7100 **tel**  
847-615-7105 **fax**  
[www.ipc.org](http://www.ipc.org)

ISBN #978-1-61193-434-2